THE UNIVERSITY OF MANITOBA

THE EFFECTS OF BRAZING PARAMETERS ON MICROSTRUCTURE AND PROPERTIES OF DIFFUSION BRAZED JOINT OF IN-738 SUPERALLOY

By

OLANREWAJU A. OJO

A thesis submitted to the faculty of Graduate Studies
in partial fulfillments of the requirements for the degree of
Master of Science

DEPARTMENT OF MECHANICAL AND INDUSTRIAL ENGINEERING
WINNIPEG, MANITOBA

JANUARY 2002

THE UNIVERSITY OF MANITOBA

FACULTY OF GRADUATE STUDIES

*****

COPYRIGHT PERMISSION

The Effects of Brazing Parameters on Microstructure and Properties of Diffusion Brazed Joint of In-738 Superalloy

BY

Olanrewaju A. Ojo

A Thesis/Practicum submitted to the Faculty of Graduate Studies of The University of Manitoba in partial fulfillment of the requirement of the degree

of

MASTER OF SCIENCE

ACKNOWLEDGEMENT

I acknowledge my supervisor Dr M.C. Chaturvedi for granting me the opportunity to work on this project. I am sincerely grateful to him for his valuable guidance and support throughout the duration of the work. I acknowledge Dr N.L Richards, for his unfailing guidance and encouragement. I thank Uttara Prasad for her consistent assistance and discussion, and Mr Brent Junkin of Standard Aero for arranging to have brazed samples prepared.

I acknowledge the financial support provided by Standard Aero Ltd, Bristol Aerospace, Boeing Canada Technologies Ltd, Manitoba Aerospace Association etc in support of this research project and by the University of Manitoba in the form of research assistantship and graduate fellowship. I am grateful to John Van Dorp, Don Mardis and Mike Boskwick for their technical assistance. Finally I am eternally grateful to God, the source of my strength and wisdom and to my wife Sumbo for her love and support.

ABSTRACT

This thesis reports an investigation of the effects of gap width and brazing parameters (temperature and time) on the microstructure and properties of diffusion-brazed joints in IN-738 superalloy, using two commercial filler alloys, Amdry "DF3" and Nicrobraz 150.

Standard metallographic techniques were employed in examining the microstructural features of the diffusion brazed joints, using Optical, Scanning electron and Transmission electron microscopes. Microhardness and tensile properties at 980°C of brazed joint were determined on Lietz microhardness tester and Instron tensile machine, respectively.

Residual liquid present at brazing temperatures, transformed on cooling into centreline ternary eutectic phase in "NB 150" brazement. It consisted of Nickel rich boride, Chromium rich boride and γ austenitic solid solution phase. In "DF3" brazement, MC carbide, Ni_3Ti based intermetallic and Chromium rich boride formed from the residual liquid along the centre of the joint. Precipitation of these second phases was found to increase with increase in gap size at a given brazing temperature and time. In addition to the centreline eutectic in "NB 150" brazement, Chromium rich borides and Nickel rich borides were observed at the substrate – braze interface of samples brazed below quoted eutectic temperature range of Ni-B system (1080°C – 1140°C). Above this temperature range only Chromium rich borides were observed at the interface. Extensively distributed fine globular Chromium rich borides were also observed within the base alloy grains adjacent to the substrate – braze interface in all brazed samples. The hard and brittle

precipitated second phases were found to be deleterious to the brazed joint's strength and ductility. Applying an existing TLP diffusion model to "NB 150" brazement, showed that the eutectic width decreased linearly with increase in square root of the holding time and also, isothermal solidification increased with bonding temperature. The apparent activation energy for diffusion of boron in the IN-738 base alloy was evaluated to be 218KJ/mole. This value was used to formulate an expression for estimating the time needed for complete isothermal solidification of liquid interlayer (required to prevent the formation of deleterious centreline eutectic phase) at a given brazing temperature and joint size. Estimated completion times agreed well with experimental values. It was evident that subsequent to isothermal solidification of liquid insert, the brazed joint should be thermally treated to achieve both microstructural and chemical homogeneity in order to achieve properties comparable to the base alloy.

TABLE OF CONTENTS

LIST OF FIGURES

LIST OF TABLES

Chapter 1

INTRODUCTION

The gamma prime strengthened Ni-base superalloy Inconel 738 is extensively used in hot sections of aero gas turbine engines due to its excellent elevated temperature strength and hot corrosion resistance. Its excellent high temperature mechanical strength is attributed mainly to the presence of precipitates like γ' (Ni_3 Al, Ti), MC and $M_{23}C_6$ carbides present in the austenitic γ matrix and at grain boundaries. The severe operating environment, however, causes the alloy to encounter various forms of damage in service such as fatigue cracking, surface degradation, oxidation, sulphidation and erosion.

Damaged components are replaced not only because of loss of structural integrity but also due to their contribution to loss of operating efficiency of the engine. In most instances, it is more economically effective to carry out a repair to return the degraded parts to a serviceable condition rather than replacement. It is thus a common practice for modern aero engines to undergo major overhauls at regular intervals, when all critical components are inspected and damaged parts are repaired, enabling the engine to return to service.

Unfortunately, opportunities to fusion weld repair a part made of Inconel 738 are limited because, like other precipitation-hardened superalloys that contain a substantial amount of Ti and Al, it is highly susceptible to heat affected zone (HAZ) cracking. Diffusion brazing has consequently evolved as an attractive alternative method for repairing this difficult to weld alloy. This is due mainly to the fact that repairs can be produced without melting the bulk base alloy, which

eliminates the possibility of fusion related cracking and at the same time preserving some of the metallurgical characteristics of the base metal. However, there are applications where superalloy brazement does not possess adequate high temperature strength and corrosion resistance properties. The major cause of these problems is the formation of hard and brittle intermetallic phases in the brazed layer. These phases are undesirable in repaired sections as they provide a continuous low resistance path for crack propagation, reducing the ductility and toughness.

Efforts to prevent the formation of these phases have resulted in the development of Transient Liquid Phase (TLP) bonding, which is achieved by isothermal solidification of the liquid phase, that temporarily exists at the brazing temperature between the substrates. Conventional TLP models for production of second phase-free joint are based on binary alloy systems. In contrast, the phase relationships that are actually encountered when joining complex multicomponent alloys do not always lend themselves to an extrapolation of the binary alloy analysis. In this research, application of principles based on TLP bonding process in producing a reliable joint in IN-738 superalloy using "NB 150" (a ternary filler alloy) and "DF3" filler alloy was investigated.

There are few detailed publications found in open literature about brazing of IN-738 alloy, although it is extensively used in industrial applications due to the difficulty of welding. In this connection, a research project was designed with the intent of studying the influence of filler alloy, gap width and brazing parameters (temperature and time) on microstructure and integrity of diffusion brazed joint in

IN-738 superalloy. This work aimed at correlating the microstructural characteristics of the diffusion-brazed joint with its mechanical properties. This was achieved firstly by examining the microstructure that developed in a variable gap between IN-738 plates, which were brazed by "NB150" and "DF3" fillers. This was followed by investigating the effect of brazing parameters, temperature and time, on the braze microstructure. A diffusion model based on TLP bonding process was applied to "NB 150" brazement to estimate the activation energy for diffusion of boron (the melting point depressant of the filler) into the base alloy, which is considered to be the controlling mechanism of the whole TLP process. This contribution led to the formulation of an expression for estimating the time needed to complete isothermal solidification at a given brazing temperature and gap size. Finally the effect of the intermetallic phases that formed during brazing on mechanical properties of brazed samples was investigated by tensile tests.

The results obtained have provided a better understanding of the fundamental metallurgical characteristics of diffusion-brazed joints of IN-738. This would serve as a basis for developing an optimized commercial repair technique for service-degraded components. In this thesis, the physical metallurgy of IN-738 and brazing as a repair technique for gas turbine alloys made from Nickel base superalloy are first reviewed in depth, the metallurgical investigation conducted by various metallographic and mechanical testing techniques on IN-738 brazed joint are subsequently presented.

Chapter 2

LITERATURE REVIEW

Cast IN-738 is a precipitation hardened Ni base superalloy developed to combine the strength of IN-713 with the oxidation and sulphidation resistance of Udimet 500. The alloy possesses excellent high temperature creep rupture strength and hot corrosion resistance [1]. Components manufactured from IN-738 can be effectively used to a service temperature of 980°C. It has wide applications in manufacturing of major components of aero and industrial gas turbine engines. Typical applications include stator parts such as nozzle guide vanes, blades and integral wheels [1,2]. Modern gas turbine engines are designed for the best possible efficiencies and output, and as such, complicated designed parts are needed to withstand the stringent demands encountered in these engines. This results in higher costs and longer delivery for cast components and thus it becomes worthwhile to repair service damaged components rather than a replacement of the damaged parts. Opportunities for fusion weld repairs are limited for this alloy (IN-738), as it is very sensitive to hot cracking during welding and development of cracks in the weld metal and heat – affected zone, and also during post – weld heat treatment.

Diffusion brazing has consequently evolved as a viable alternative procedure for repairing this difficult to weld alloy due its technological and economic advantages, and it is often superior to other joining techniques in manufacturing and reconditioning of Nickel and Cobalt base superalloys [3]. It has been also found to be a promising approach for new advanced materials that

exhibit excellent properties but are difficult to be assembled by traditional structural joining techniques [4]. Detailed attention, however, needs to be paid to the microstructure of materials repaired by brazing, as there are a number of factors that influence the microstructure and, as a result, the properties of the brazed joint. A careful and intelligent appraisal of the following variables, which are reviewed in this chapter of the thesis, will serve as basis for producing a satisfactory brazed joint, since they all directly affect the resulting microstructure.

- Base metal characteristics
- Filler metal characteristics
- Surface preparation
- Gap design
- Temperature and Time

It is worth clarifying however, that the strength of brazed layer is more dependent on the base metal's characteristics than those of the filler materials [5]. The microstructure of IN-738 is very complex and is influenced by various factors such as composition, fabrication technique, presence of trace element like C, S, P, Si & Boron, heat – treatment, as well as service environment.

2.1 Composition of the base alloy - Inconel 738

The alloy IN-738 is a vacuum melted and cast alloy to which hot isostatic processing (HIP) is usually applied in order to partially eliminate micro porosity formed during solidification. There are basically two types of the cast product, low carbon version (C ~ 0.09 - .13 wt %) designated as IN-738 LC and a high carbon

version (~0.15 – 0.20 wt %) called IN-738C [6]. The low carbon IN-738 LC also has a lower Zr content, which improves the alloy's castability in large section sizes, while tensile and stress rupture properties are not appreciably affected [6]. In critical parts, trace elements such as selenium, thallium, tellurium, lead and bismuth, need to be held to very small (ppm) levels. This is accomplished by careful selection of raw materials coupled with optimum melting practise. Table 2.1 [6] shows nominal composition of the cast IN-738LC, while Table 2.2 [6] lists its mechanical & physical properties. It is important to note, however, that, exposure to high temperature has significant effect on the alloy properties. Figure 2.1 demonstrates the effects of long time exposure on hardness and variation of the alloy's thermal conductivity with temperature [7].

2.2 Microstructure of As- cast IN 738

As – cast IN 738 alloy has a coarse grain structure (average size 1 - 3mm) that either directly or indirectly affects the nature of precipitates on its grain boundaries and, the mechanical properties of the alloy. The strength of superalloys is very dependent on grain size and its relation to component thickness. In addition, serrated grain boundaries in IN-738, which can be produced by slow cooling from solution treatment temperature, are known to provide a favourable balance between the intragranular and grain boundary strength [8]. The following major phases present in cast IN-738 contribute largely to its excellent high temperature strength.

Table 2.1

Nominal Composition of IN-738 Superalloy [6]

Element	High Carbon IN-738C (Wt%)	Low Carbon IN-738LC (Wt%)
Carbon	0.17	0.11
Cobalt	8.50	8.50
Chromium	16.00	16.00
Molybdenum	1.75	1.75
Tungsten	2.60	2.60
Tantalum	1.75	1.75
Niobium	0.90	0.90
Aluminium	3.40	3.40
Titanium	3.40	3.40
Boron	0.010	0.010
Zirconium	0.10	0.05
Iron	LAP*	LAP*
Manganese	LAP	LAP
Silicon	LAP	LAP
Sulphur	LAP	LAP
Nickel	Balance (61)	Balance (61)

*Low As Possible

Table 2.2

Mechanical and Physical Properties of Alloy IN-738 [6]

Temperature (°C)	Yield Strength (MPa)	Ultimate Tensile Strength (MPa)	Elongation (%)
21	951	1096	5.5
649	910	1055	7
760	793	965	6.5
871	552	772	11
982	345	455	13

Melting Range	1232 – 1315°C
Density	8.11gm/cm^3
Coefficient of Thermal Expansion	15.36 x 10^{-6} / °C
Young Modulus	200.2 GPa
Shear Modulus	78 GPa
Poisson's Ratio	0.29

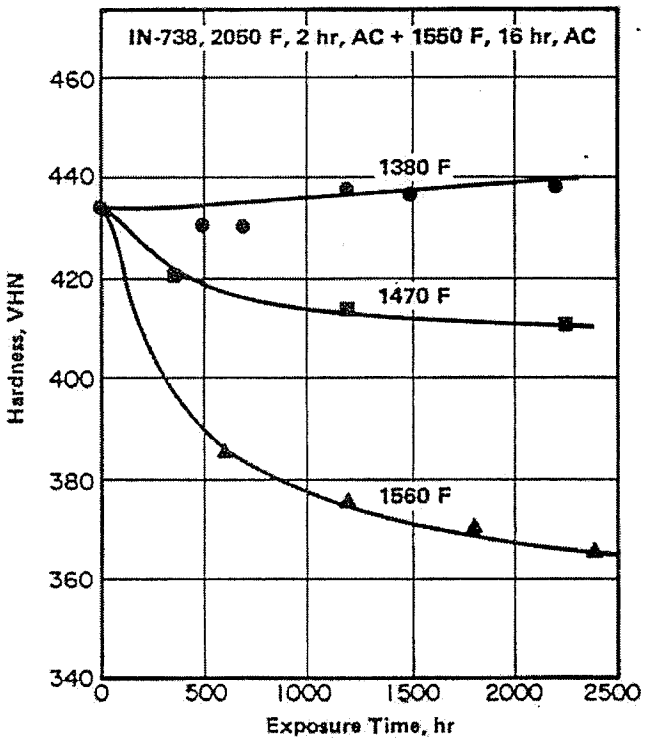

a

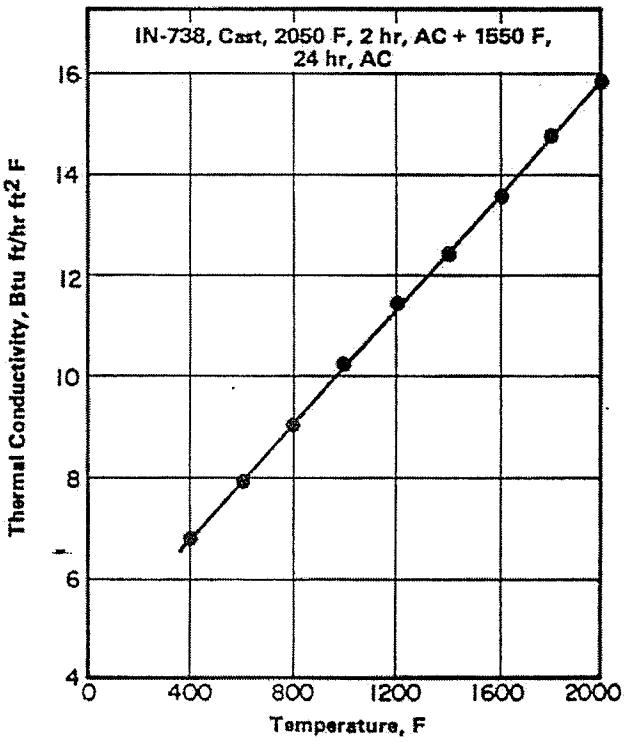

b

Figure 2.1 (a) Effects Of Long –Time Exposures To Temperature on Hardness at Room Temperature (b) Variation of Thermal Conductivity with Temperature [7]

1) Gamma Matrix (γ): This is the FCC Nickel base austenitic matrix that contains high percentage of solid solution elements such as Co, Cr, Mo, W, Al & Ti. These elements, which differ from Ni in atomic diameter by 1 – 15 %, normally occupy substitutional atomic position in Ni crystal, producing a distorted lattice with spherical symmetrical stress field. This field can interact with the stress field around a dislocation, producing an elastic dislocation – solute atom interaction and provides solid solution strengthening.

2) Gamma Prime (γ'): The major contribution to the high strength of IN-738 is from the γ' precipitates, consisting of $Ni_3(Al,Ti)$. It is an $L1_2$ - type phase, with ordered FCC crystal structure. It forms in alloys containing Ti & Al in amounts exceeding their solubility in Ni. It has been suggested [9], that composition of γ' in IN-738 is:

$(Ni_{.922}Co_{.058}Cr_{.017}Mo_{.002}W_{.002})(Al_{.518}Ti_{.352}Ta_{.046}Nb_{.41}W_{.014}Cr_{.020})$

The similarity between its crystal structure and that of the γ matrix causes a rapid aging response, with precipitates' growth occurring largely by the growth of large particles at the expense of small ones, known as Ostwald ripening, rendering the precipitates to be very stable at elevated temperature. Ardell [10] in his review on precipitation hardening, concluded that for Ni base superalloy, the γ' precipitation occurs by homogeneous nucleation followed by growth and coarsening, during which, the volume fraction of precipitates remains constant. Footner & Richards [11] discovered that the variation of γ' particle size with exposure

time was complex, owing to the initial partial solution treatment and subsequent aging which resulted in the presence of two distinct γ' population, a 'bimodal distribution' of cuboidal & spheroidal γ' precipitates. The larger population (primary γ') are found to maintain a constant mean size on aging. Thakur [12] in his work measured and reported variation of γ' size with heat treatment, Table 2.3. Figures 2.2 & 2.3 show primary and secondary γ' phases in as-received and solution heat-treated IN-738LC alloy.

3) Carbides: Carbon content is an important parameter in determining the amount of carbides in the alloy IN-738. Carbides are formed, when the level of carbon concentrations is above 0.05% [13]. It combines with reactive and refractory elements such as Ti, Ta and Nb to form MC carbides, which usually form in cast product during cooling and occur as discrete particles distributed heterogeneously both in intergranular and transgranular positions. The primary FCC carbides are generally strong and stable with size ranging from one micron to a hundred micron, Figure 2.4. It has been suggested [9] that MC carbides have the formula: $(Ti_{.5},Ta_{.2},Nb_{.2},W_{.04},Mo_{.03},Cr_{.02})C$. During heat treatment and service, it decomposes and generates lower carbides such as M_6C and $M_{23}C_6$ (MC + $\gamma' \rightarrow M_{23}C_6 + \gamma$). $M_{23}C_6$ also forms from unused free carbon, when cast ingot cools through its solvus range (1000°C – 1050°C).

Table 2.3

Variation of γ' Size with Heat Treatment [13]

HEAT-TREATMENTS		γ' Primary Cuboids		γ' Secondary Spheroids	
No.	Heat-Treatment Schedule, time in hrs.	Range(nm)	Average Size(nm)	Range(nm)	Average Size(nm)
1	1120^0C/2/S.T.	300-419	347	---	---
2	1120^0C/2/845^0C/08	371-420	392	25-65	65
3	1120^0C/2/845^0C/12	375-456	412.5	52-115	87.5
4	1120^0C/2/845^0C/16	404-457	425	46-147	90
5	1120^0C/2/845^0C/24	381-500	425	32-162	96
6	1120^0C/2/845^0C/72	403-520	450	92-120	102
7	1120^0/2/845^0/120	404-620	482	82-145	112
8	1150^0C/2/S.T.	357-480	432	---	---
9	1175^0C/2/S.T.	184-236	184	---	---
10	1175^0C/2/845^0C/2	179-213	190	---	---
11	1175^0C/2/845^0C/12	130-229	210	---	---
12	1175^0C/2/845^0C/24	175-267	226	---	---
13	1175^0C/2/845^0C/72	222-318	267	---	---
14	1225^0C/2/S.T.	60-150	102	---	---
15	1225^0C/2/845^0C/2	76-145	110		
16	1225^0C/2/845^0C/12	104-129	135	---	---
17	1225^0C/2/845^0C/24	128-184	140	---	---
18	1225^0C/2/845^0C/72	133-248	178	---	---
19	AS RECD.	209-328	248	---	---
20	1200^0C/3-OQ/845C/24	81-132	108	---	---

S.T. = Solution Treated and Air Cooled, O.Q.= Oil -Quenched

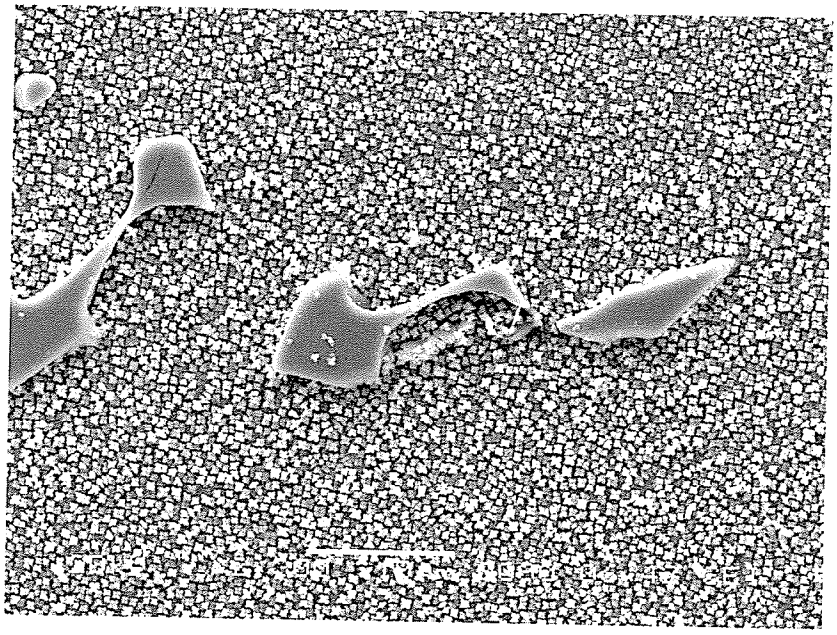

a

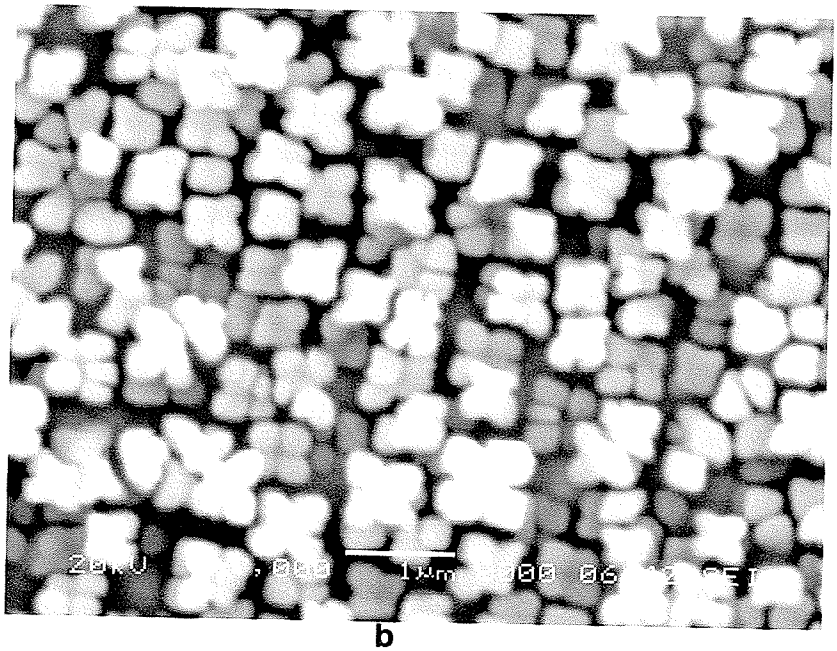

b

Figure 2.2 SCM Secondary Electron Image of Primary γ' Precipitate Morphology in As-Received IN-738LC at (a) 300X (b) 17,000X.

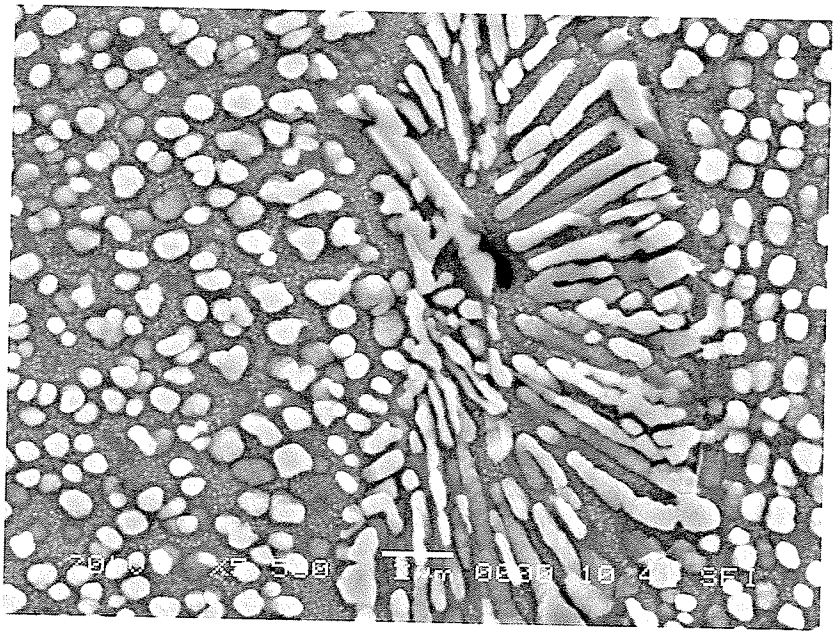

a

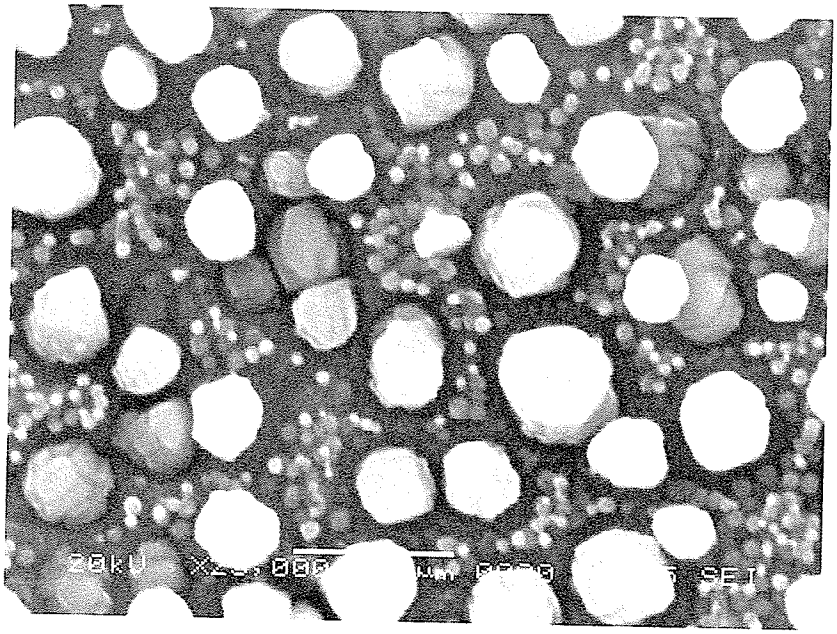

b

Figure 2.3 Primary and Secondary γ' Precipitates in 1120°C Solution Heat Treated and 845°C Aged IN-738LC at (a) 5.5KX (b) 23KX.

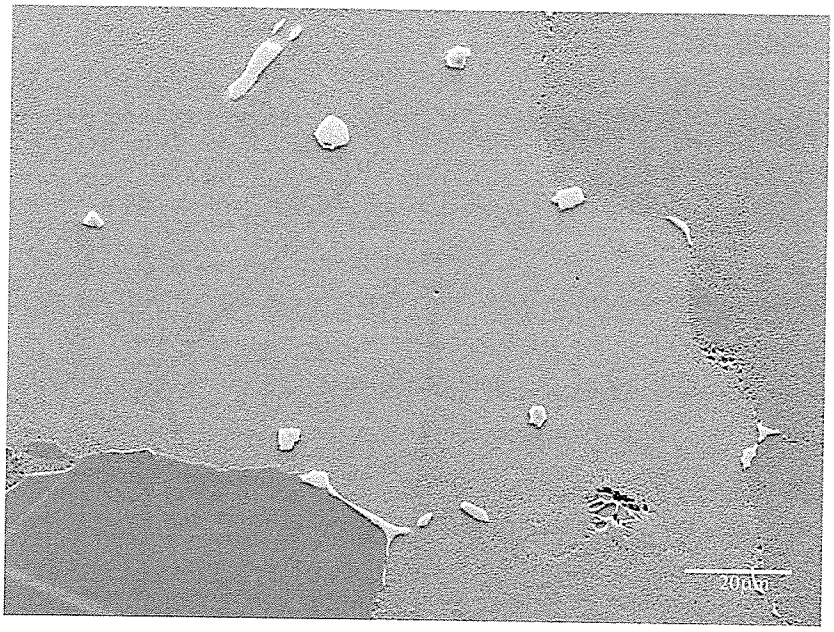

Figure 2.4 MC Carbide Particles at Grain Boundaries and Within The Grains of As-Received IN-738 Alloy.

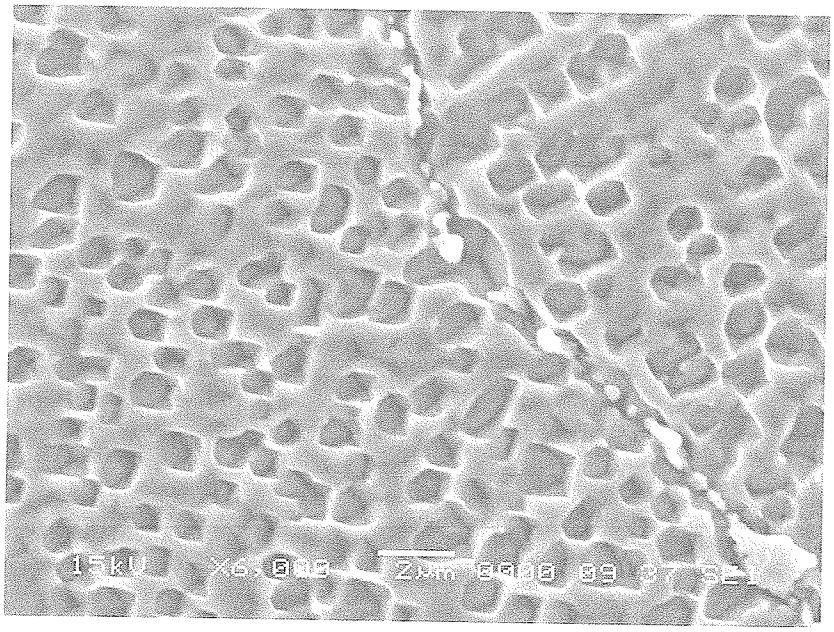

Figure 2.5 Intergranular $M_{23}C_6$ Carbide Particles in 1120°C Solution Heat-Treated and 1025°C Aged IN-738LC. 738.

In situation of high super saturation of carbon, there is a tendency for it to form a cellular grain boundary particle, which is continuous in nature. It however tends to form as globules along grain boundaries at aging temperature of 950°C - 1025°C [14]. Grain boundary $M_{23}C_6$ are known to have either a positive or negative effect on the creep properties of the alloy depending on its morphology, size and distribution. Heavy and/or continuous network of grain boundary $M_{23}C_6$ particles enhance grain boundary sliding and crack propagation by boundary – matrix decohesion. Discrete particles on the other hand are known to improve the creep life and ductility. Figure 2.5 shows Scanning electron microscope image of $M_{23}C_6$ along the grain boundaries of solution heat-treated IN-738 at 1120°C, followed by 1025°C aging. Rong et al [15], by high-resolution transmission electron microscopy, also observed the grain boundary $M_{23}C_6$ in IN-738 to be discontinuous irregular shaped precipitates.

4) Topologically Closed Packed (TCP) Phases: Plate-like phases such as σ, μ and Laves, form under certain conditions in IN-738 alloy. They can be formed during heat treatment or more commonly during service. They are characterized as composed of close – packed layers of atoms aligned with the octahedral planes of the FCC matrix and are known as topologically closed packed or TCP phases. These are known to have detrimental effect on alloy properties, mainly lowered rupture strength and ductility.

2.3 Repair of Turbine Parts made from Nickel Base Superalloy

Gas turbine components are designed to withstand high stresses and corrosive environment at high temperatures. In order to meet the strength demand, they are generally constructed of high strength, heat resistant nickel base and cobalt base alloys such as IN-738. In addition to the harsh operating environment, they experience various forms of loading, such as thermal fatigue, low cycle fatigue and creep, which cumulatively produce cracks, damaged surface, oxidation and erosion of the service parts. Refurbishment of these hot sections is a very complex process including cleaning, rejuvenation heat treatment, welding, brazing, reprofilling, coating and finally diffusion and precipitation heat treatment. The overall economics of operation of turbines is dependent upon the ability to maintain and repair these cost intensive engine parts. Generally, welding and brazing are the most often used repair techniques in practise.

2.3.1 Welding

Weld repair is an essential element in the overhaul of gas turbine blades and vanes. Repair of service generated thermal fatigue cracks is actually the prime object of concern. As far as the cobalt base alloys are concerned, the major welding problems are due to the composition, microstructure and part geometry. In γ' precipitation hardened Nickel base superalloy like IN-738, fusion welding is

usually accompanied by micro-fissuring in heat affected zone [16] and is difficult to control. The cracking probability has been discovered to be proportional to the volume fraction of γ'phase [17]. This is attributed to a number of reasons such as:

a) The degree of supersaturation of γ' following weld induced solution treatment and cooling increases as the solute content increase.

b) The volumetric change and residual stresses due to dissolution and re-precipitation of γ' increases with its volume fraction.

c) The strength of the alloy increases with the γ' volume fraction, and it becomes more difficult for residual stresses to be relaxed by plastic deformation.

Moreover grain boundary liquation of carbides and internal stresses set up by mechanical constraints and thermal gradients, due to complex part geometry, promote microcracking within the weld and the heat-affected zone. Heat resistant nickel base alloys vary from being fully weldable to being completely unweldable and this is chiefly dependent on the composition. IN-738 is considered to be a very difficult to weld superalloy.

2.3.2 Brazing

The need for alternative repair technique suitable for more wide ranging applications including Nickel & Cobalt base superalloys has led to the practice of diffusion brazing. The process has proved to be a promising approach for new advanced materials that exhibit excellent properties, but are hard to be assembled by traditional structural joining techniques [4]. It offers the possibility

of overcoming the shortcoming of welding process, with respect to part geometry, cracking and distortion. Diffusion brazing is a process that joins metals by pre-placing a filler alloy between the substrates and heating the assembly to a suitable brazing temperature (lower than the fusion temperature of the base alloy) at which either the filler metal melts or a liquid phase is formed in-situ by chemical reaction and thus flow by capillary action between the joining surfaces. The filler alloy elements diffuse into the base metal and vice versa resulting in a metallurgical bond between the two metal pieces at the joint.

Advanced diffusion brazing techniques is used in the aerospace industry for joining Ti, Ni, Co and Al alloy. In addition it can be used to join cast, wrought or powder – processed metals, dissimilar metals, oxide and non – oxide ceramics, metals to ceramics and fiber or dispersion strengthened composites with metallic or ceramic matrices. It is adaptable for joining single crystal alloy parts without destroying their crystalline nature. Due to the high affinity of superalloy and brazes for oxygen, brazing can be only done effectively in vacuum [18] using pressure of the order of $10^{-4} - 10^{-6}$ torr. Vacuum brazing produces clean, superior product with high strength, ductility and uniformity. A schematic of diffusion braze repair process is shown in figure 2.6 [19].

2.4 Brazing Process Variables

In addition to the base alloy characteristics which have been discussed previously, the other process variables that contribute to the structure and properties of a diffusion brazed joint are discussed as follows:

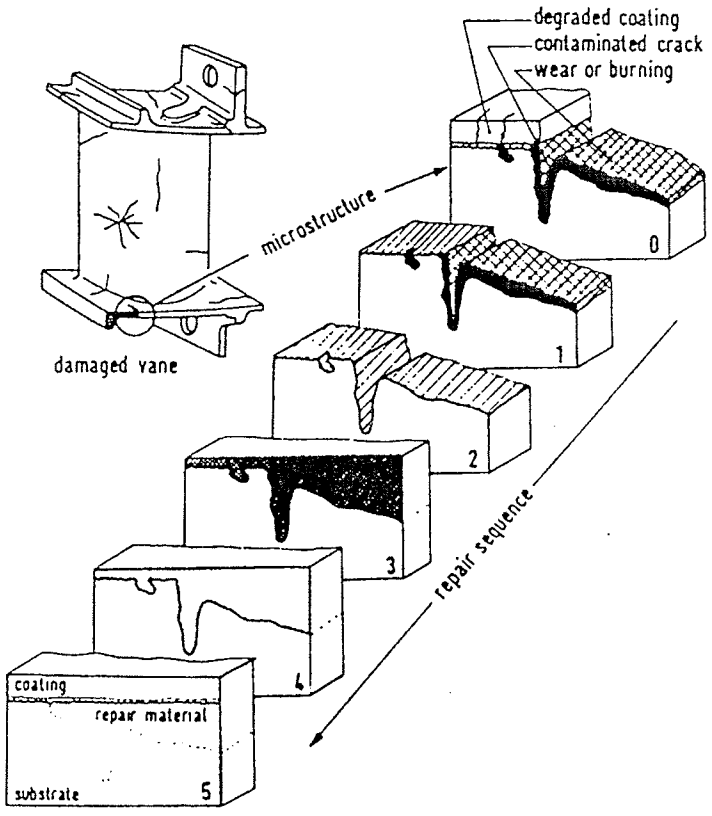

Figure 2.6 Schematic of Diffusion Braze Repair; 1 Coating Stripped, 2 Thermochemically Cleaned, 3 Filler Alloy Applied, 4 Diffusion Brazed, 5 Coated [19].

2.4.1 Surface Preparation

High surface tension, low contact angle (wetability) and viscosity of the liquid braze are required for its flow on base alloy surface. Braze flow is facilitated by capillary attraction, which in turn results from surface energy effect. A clean surface is consequently a prerequisite, for wetting, flow and filling of cracks and small cavities by the liquid filler alloy during brazing cycle. A clean surface is usually obtained by either or combination of the following treatment:

(i) Grinding

(ii) Grit blasting

(iii) Hydrogen gas cleaning

(iv) Vacuum cleaning

(v) Fluoride ion cleaning

Grinding is employed in cases where the surface oxides are easily accessible. Intergranular oxides and those along narrow crack walls require reduction treatment in hydrogen or HF atmosphere. Nickel and Cobalt base alloys with low Al & Ti contents (< ~ 1% total) are usually cleaned by hydrogen cleaning. Those containing considerable quantities of Ti, Al, Zr & Nb can be successfully cleaned only by using reducing halogenate atmosphere. There are several treatments that have been developed, which rely on HF, HCl or C_2F_4 (fluorocarbon) cleaning of Ni base superalloys [20-22]. The most common thermo-chemical cleaning process relies on production of HF gas by heating CrF_2 in a Hydrogen atmosphere by the following reaction:

$$CrF_2 + H_2 \rightarrow Cr + 2HF$$

Oxide reduction by HF takes place as follows:

$$M_2O_3 + 6HF \rightarrow 2MF_3 + 3H_2O$$

However, alloy depletion occurs by treatment in halide atmosphere by the following reaction:

$$2(Al,Ti,Nb,Zr) + 6HF \rightarrow 2(Al,Ti,Nb,Zr)F_3 + 3H_2$$

In order to restore the cracks' surface integrity, the depleted layer is removed by grinding and grit blasting. The HF gas, fluoride ion processing route is specially designed (by Ti Coatings Inc.) to use HF gas directly, as opposed to use of chromium fluoride (CrF_2) as the source of HF. The process involves subjecting oxidized or sulphurdized components to a highly reducing gaseous atmosphere of H_2 and HF at high temperature ranging from 900°C – 1000°C depending on the substrate material being cleaned. The gas is directed uniformly over the section to be processed, using a unique gas distribution system. The end product gas containing H_2 & fluoride reaction products are scrubbed and neutralized. The typical chemical reactions that take place in the reactor chamber are:

$3HF + Al_2O_3$ (on substrate) $\rightarrow 2AlF_3 + 3/2\ H_2O$

$3HF + Al \rightarrow AlF_2 + 3/2\ H_2$ (depletes Al from surface)

$4HF + TiO_2$ (on substrate) $\rightarrow TiF_4 + 2H_2O$

$4HF + Ti \rightarrow TiF_4 + 2H_2$ (depletes Ti from surface)

The typical chemical reactions in the scrubber are:

$HF + NaOH \rightarrow NaF$ (soluble) $+ H_2O$ (neutralize HF)

$H_2 + NaOH \rightarrow H_2$ (spent gas which is discharged to atmosphere)

$AlF_3 + TiF_4 + NaOH \rightarrow$ soluble fluorides

The fluoride ion cleaning (FIC) process results in an effective removal of deeply embedded oxides in wide & narrow cracks typically found in aircraft engine's hot – section parts. It has an added advantage in that when Al & Ti are present in the base metal, it depletes these elements from the surface, thereby improving braze flow and repair of cracked components.

2.4.2 Nature of Filler alloy

The physical and compositional characteristics of a filler alloy are very important factors in producing a sound diffusion brazed joint. The filler alloy must melt at temperature below the melting point of the base alloy and to which it can be exposed without causing any degradation. More so, its composition and amount must be such that a chemically and microstructurally homogeneous bond with the base alloy can be achieved in practical annealing times. To attain bond homogeneity, the braze alloy composition must be reasonably close to that of the base metal being joined. Superalloys are normally brazed with Ni & Co base braze materials. In order to produce necessary filler melting point, a melting point depressing element is normally added to the basic composition of the filler alloy. However certain elements in the base alloy could have deleterious effect, if present in the filler alloy. Common melting point depressant used in the filler materials for brazing superalloys include boron, silicon, phosphorus and hafnium, while Al, Ti & C are either deliberately excluded or restricted in amount because they are found to form very stable phases during bonding [23]. Composition of the brazing filler metal does become important as well when the brazement is to

be subjected to chemically corrosive or high temperature service conditions. The filler alloy must be able to resist oxidation or chemical corrosion and must not remelt in service. Other characteristics that brazing filler alloy must posses include:

(i) Ability to wet the base metal joint surface.

(ii) Adequate fluidity at brazing temperature to assure flow by capillary action.

(iii) Alloying with the base metal to form a brazement with higher melting temperature.

(iv) Controllable erosion of the parent metal within the limits required for the brazing operation.

When B, Si or P is alloyed with Ni alone, the resulting binary alloy exhibit low tensile strength, higher hardness, lower corrosion resistance and excessive fluidity when molten. As a result, commercial Ni base filler alloy containing these elements usually have additional elements to enhance their physical properties. Ni-Hf brazing filler was found to shorten the brazing time for some Ni base superalloy; the mechanical properties of the bond layer, however, were quite inadequate [24]. Chromium is often present in the Ni base filler alloy to provide oxidation and corrosion resistance. In the case of Co base alloy, Cr, W & Ni are added to improve strength and oxidation resistance. Most of these brazing alloys are commercially available in a variety of forms i.e. foil, paste, powder and tape. Brazing foils are commonly made by melt spinning and are available in thickness 0.025 – 0.6 mm and in width up to 50mm. They are generally used for joints with

a large area. Powder filler is produced by inert gas atomization and sieved to a narrow range of particle sizes so as to ensure consistent melting during brazing cycle. Flex tape and shrink – free brazing tape have been recently developed for braze repair of aircraft components [25]. Flex tape is simply a mixture of superalloys and braze alloy powder with an organic binder.

Filler alloys containing elements with high diffusivity in the base metal are generally specified for applications requiring strong joints for high temperature and stress service conditions, such as gas turbine hot sections. Dissolution of the base alloy by filler alloy occurs to some degree in every brazed joint, but it is undesirable when the extent is sufficient to cause erosion, especially in extremely thin sections such honeycomb and heat exchanger structures. The amount of dissolution of the base metal is affected by factors such as composition of the filler, quantity applied to the joint, and the brazing temperature and time. The most important factor affecting degree of erosion for a given filler- base metal combination is the brazing technique, which encompasses assembly & fixture practices, alloy application and the brazing cycle itself [26]. Boron is the most significant melting point depressor element commonly incorporated into braze filler alloys for diffusion brazing of Ni base heat resistant alloys. Silicon being a larger atom, diffuses less readily and forms compounds, which are not quite as stable as borides. However it is not as effective as boron when used as a melting point depressant in Nickel and Cobalt base alloys.

2.4.3 Gap Size

The size of gap to be joined by brazing process influences the joint microstructure in that it determines the amount of braze alloy (containing a melting point depressant element), needed to fabricate the joint. This invariably affects the time required to diffuse the melting point depressing element into the base alloy to produce a chemically and microstructurally homogeneous bond. The wider the gap, the more time will be required to produce a bond free of deleterious second phases, since it will take longer time for the melting point depressant to be fully diffused away from the joint.

2.4.4 Brazing Parameters (Temperature & Time)

Brazing temperature has a direct influence on the wetting action, braze flow, erosion and diffusion during the joining process. The brazing temperature must be above braze alloy melting temperature and below that of the parent alloy. Generally, the lowest brazing temperatures are usually preferred to (a) minimize the heat effects on base metal (b) economize the heat energy expenses (c) minimize filler alloy – base metal interaction. However, higher temperatures could be desirable to, (a) combine annealing, stress relief or heat treatment of the base metal with brazing (b) remove surface impurities & oxides by vacuum brazing (c) enable the use of higher melting but more economical and efficient brazing alloy and (d) promote base metal – filler interactions in order to modify the composition and microstructure of the brazed joint. Since diffusivity increases with temperature, the diffusion of melting point depressant into the

base alloy occurs at a faster rate at higher temperatures, and this in effect reduces the time required for isothermal solidification of the liquid braze and, in effect, to achieve a reliable sound joint. The holding time has a prominent influence on brazement integrity in the sense that, it determines the extent of inter- diffusion between the base metal and the braze alloy. In most cases the strength of a brazed joint depends on diffusion of base alloy strengthening elements into the joint area. To achieve a joint that is chemically and structurally similar to the base alloy, sufficient interdiffusion must take place between the substrate and the filler, which is a function of holding time. The brazing parameters (temperature and time) need to be selected with a true understanding of both the physical metallurgy of the base material and the interaction of the base metal with the filler alloy.

2.5 Wide Gap Brazing

Considerable erosion of superalloy during brazing inhibits braze flow and, thus, makes it virtually impossible to rebuild a damaged surface by conventional brazing process. A pure braze can be used only on cracks of suitable width – neither too narrow nor wide, ideally about (0.1 – 0.3mm). Modification must be made to the brazing process for the repair of dents, pits and wide cracks with sizes above 0.3mm. Wide gap brazing is generally used for reprofilling part areas that have been subjected to hot corrosion and/or foreign object damage (FOD). A wide gap braze is performed by a mixture of braze alloy (which melts) and superalloy powder (which does not melt). It is intended that the powder should

not melt during the brazing process and that the braze will fill the cavities between the powder particles. The mixture is expected to act like slurry and wet the surface of the substrate but does not have to flow during the bonding process. Thus, it is possible to repair wide cracks, large defects and rebuild a large surface area of aerofoil. During a typical wide gap brazing process, the binding agent between the braze and superalloy powder particles disintegrates at about 200°C, sinters and adheres to the surface of the base metal. On reaching the brazing temperature, the braze alloy melts and as a result of capillary and adhesive forces, the mixture shrink and become completely dense. The shrinkage of the braze mixture limits the maximum thickness of braze layer to ~ 1mm in order to prevent the formation of cracks in it. The maximum temperature for wide gap brazing is strongly dependent on the type of braze alloy and must be controlled to within ± 5°C throughout the process. Wide gap braze alloy need to posses the following properties:

1) Their composition should be similar to the base alloy.
2) The melting point should be lower than the base alloy but high enough for post repair coating process and heat treatment.
3) As high a ductility as possible with minimum formation of brittle phases.

Oxidation of wide gap brazes during application only takes place at the surface of the mixture. Therefore it is possible to apply these brazes to very reactive superalloys such as Inconel 100, 738 or Mar-M-200. A good wide gap braze joint has good resistance to corrosion and creep deformation at high operating temperatures.

2.6 Limitations of Brazing Technique

Following are the common problems encountered when diffusion-brazing superalloys:

1) **Melt-Back**: As the melting point depressing element diffuses into the base alloy, it reaches a high enough concentration near the interface to cause melting of the base alloy, known as melt back. This reaction reduces the effective thickness of ductile base metal, and is of great concern when thin material is brazed or when brazed joint must withstand vibration or impact load.
2) **Porosity**: Pores and partially filled cracks often form in brazed joints as a result of oxide residues and contaminants not completely eliminated by thermochemical cleaning. These obviously have detrimental effect on the integrity of the brazement. Apart from non-wetting due to poor cleanliness and improper mating of the surfaces, shrinkage of the braze on solidification often lead to the formation of porosity [27]. A difference in chromium level between the braze filler and the parent metal can lead to Kirkendal porosity after post – brazing annealing treatment [28]. It can also result from the evolution of gas from the base metal.
3) **Grain Size**: The optimum grain size structure of a brazed joint is often one of large grains filling complete width of the joint area. Solidification may also result in a continuous grain boundary running along the centre of the braze. This however is undesirable for high temperature applications.

4) **Second Phase Precipitates**: The major detrimental feature of Nickel base brazes for high temperature applications is their low ductility, which is caused by the formation of second phase precipitates (borides, phosphides & silicides) during brazing process. Insufficient diffusion of melting point suppressing element in the braze alloy causes these elements to form hard and brittle phases on solidification. These phases when formed in a continuous manner, could provide an easy path for crack propagation, thereby reducing the ductility and toughness of the joint. The amount of precipitation will depend on the size of the gap, brazing temperature & time. Efforts have been made over the years in developing a process of producing high strength brazed bond in heat resistant materials that are devoid of deleterious second phases. Duvall et al [23] developed a process for joining heat resistant alloys, initially for Ni base superalloy, which they called "Transient Liquid Phase Bonding". Since its development and application, the TLP bonding process has shown broader applicability covering almost all kind of heat resistant alloys, especially in the alloy system which are susceptible to hot cracking during fusion welding. The process is described in the following section and the research project of this dissertation was conducted based on the principle of TLP bonding process.

2.7 Transient Liquid Phase Bonding

In transient liquid phase bonding, a filler metal of a specific composition and melting point is placed between the metal surfaces to be joined, and the entire assembly is heated to the bonding temperature. The insert alloy will, at the bonding temperature, melt or react with the base metal to form a liquid zone, which is gradually removed by interdiffusion with the substrate until it solidifies isothermally. To better understand the mechanism of producing second phase free joints, models of TLP bonding process have been proposed. Conventional models [29,30,31] are however, based on binary alloy liquid system. According to the models, isothermal solidification process is completed without the precipitation of second phases during holding at the brazing temperature. The remaining melting point suppressor can then be diluted in the substrate by prolonged homogenization treatment. Hence, the precipitation of second phases on cooling can be largely or even entirely avoided.

However, in contrast to the binary alloy fillers, commercial TLP insert alloys usually consist of ternary systems such as Ni-Cr-B. It is suggested that this modification can result in the precipitation of undesired second phases at the bonding temperature during the initial stages of joint formation [32]. Duvall et al [23], when joining Ni-Cr-Co alloys using Ni-B binary filler metal, considered that TLP bonding comprised three different steps, namely, base metal dissolution, isothermal solidification of liquid phase and homogenization. Tuah -Poku et al [31] defined four stages during TLP bonding of silver using pure copper insert. These stages are, melting of the filler metal, base alloy dissolution,

homogenization of the liquid, isothermal solidification and homogenisation of the joint. In order to account for the effect of solute diffusion during heating cycle to the bonding temperature, Macdonald & Eagar [33] suggested that a further stage should be included. It was found that, the heating cycle between the filler metal melting point and the bonding temperature affects the progress of TLP bond. When a eutectic composition filler metal Ni-19at. %P is employed during TLP bonding, solute diffusion when heating from the melting point of the filler (T_M) to the bonding temperature (T_B) can allow solidification to begin before the bonding temperature is reached. Nakagawa et al [34] reported that when the heating rate around 1K/s is used in bonding with thin (5μm) filler metal, isothermal solidification could occur between T_M and T_B. The higher the diffusivity of the melting point depressant, the more likely for solidification to occur prior to reaching the bonding temperature. The principal stages of TLP bonding, can be classified by considering a model for binary eutectic alloy system [35] illustrated by hypothetical phase diagram in figure 2.7 [35] and temperature / time profile of figure 2.8 [35].

2.7.1 Stage I

This stage is represented by stage o to a in figure 2.8 [35]. Here the sample is heated from room temperature to the melting temperature of the filler alloy T_M, during which interdiffusion takes place between the insert metal and the base alloy, so that the solute concentration $C_{\alpha s}$ at the base metal/filler metal

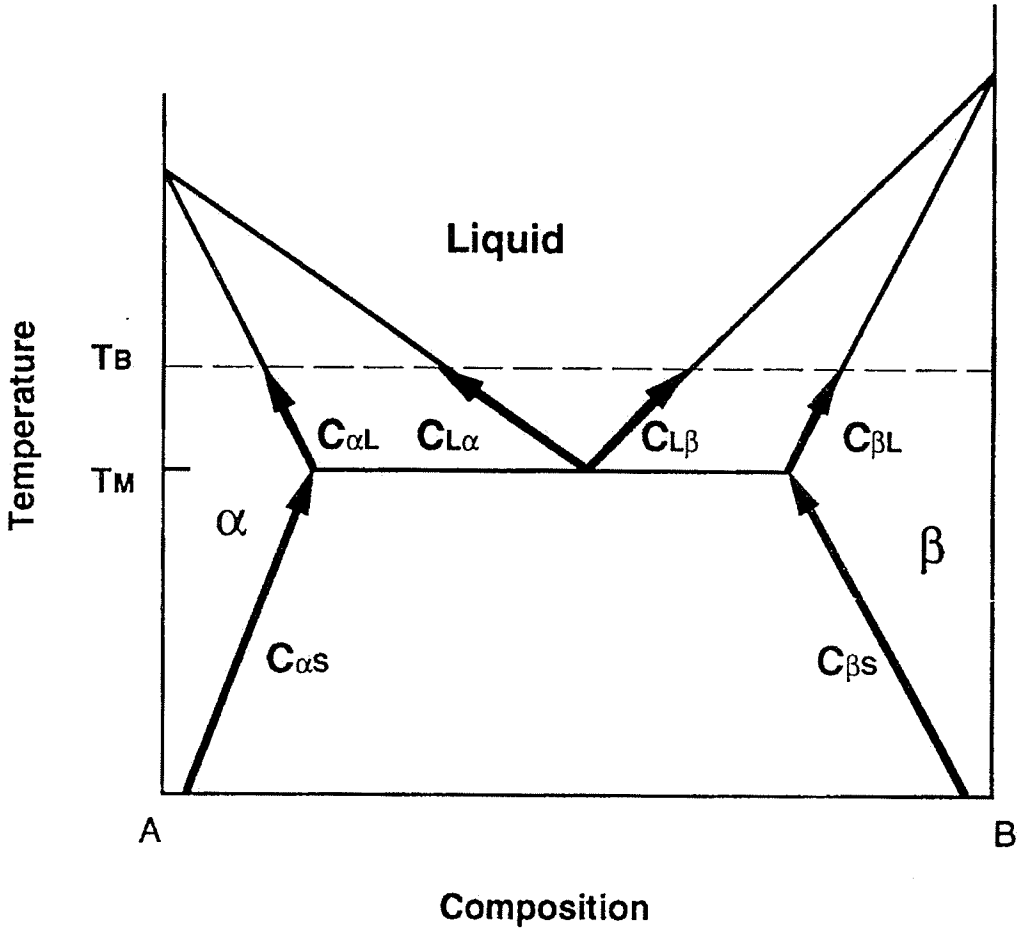

Figure 2.7 Hypothetical Binary Eutectic Phase Diagram [35].

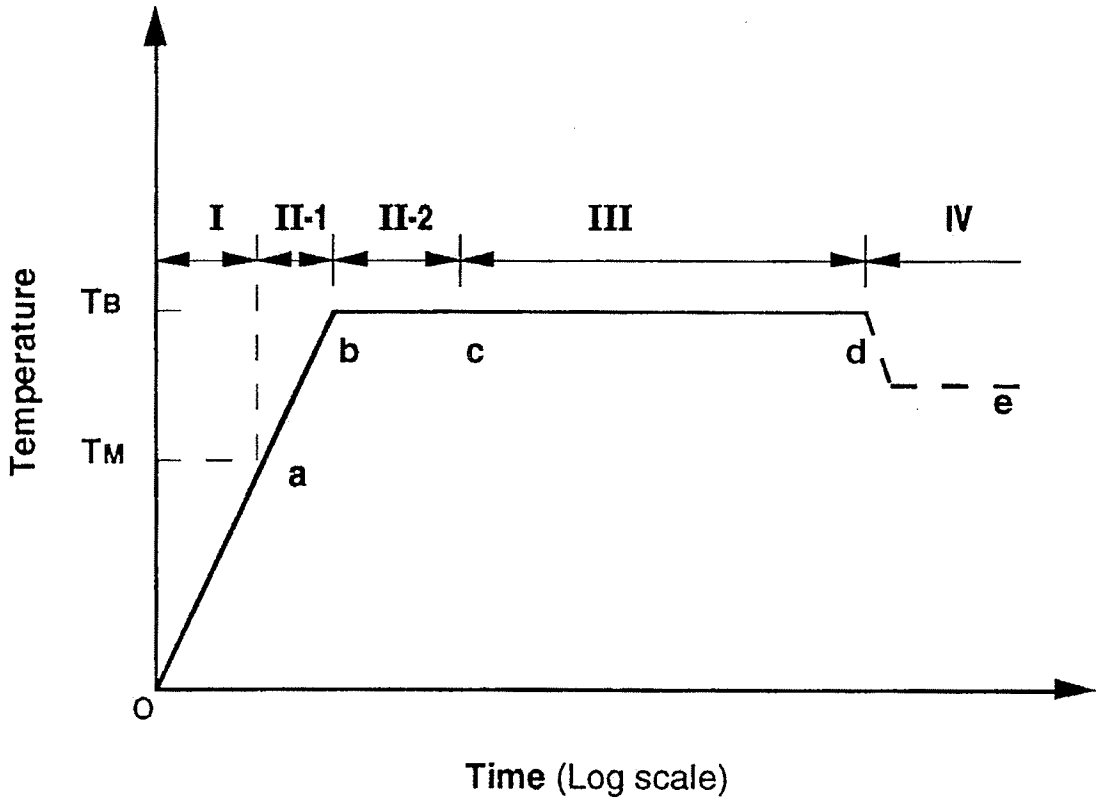

Figure 2.8 Schematic of TLP Bonding Stages with T_B Representing the Bonding Temperature and T_M the Melting Point of the Filler Alloy [35].

interface changes with temperature, following the solvus line in the binary phase diagram figure 2.7 [35]. This stage is said to be of particular importance when the filler metal is very thin, since all of it could be consumed during this stage [36]. In this regard Li et al [37] investigated TLP bonding of alumina bearing metal matrix composite using thin copper foils, and reported that the minimum interlayer thickness for satisfactory joint formation increased from 0.6 to 2μm, when the heating rate decreased from 5 to 1 K/s.

2.7.2 Stage II

Stage II (a to b of figure 2.8 [36]) is the dissolution stage. The base alloy dissolves into the liquid interlayer, increasing the width of the liquid zone. This stage can be further subdivided into two stages as follows:

Stage II – 1

As the temperature increases from $T_{M\ to}\ T_B$ (a to b of figure 2.8 [36]), the solute concentrations $C_{L\alpha}$ and $C_{\alpha L,}$ and $C_{L\beta}$ and $C_{\beta L}$ at the solid / Liquid interface changes with temperature following the solidus & liquid lines in binary phase diagram.

Stage II – 2

This stage, represented by b to c in figure 2.8 [36], involves the isothermal dissolution of the base metal, at the end of which the liquid zone reaches its maximum width. However, the stage may not exist if thin filler metal containing high diffusivity melting point depressant is utilized. Rather the filler metal melting will be immediately followed by solidification [34].

2.7.3 Stage III

This is the isothermal solidification stage. As the solute diffuses continuously into the base metal, the volume of existing liquid gradually decreases and solidification occurs inward from both the mating surfaces (figure 2.9 [23]). The solute concentration at the solid / liquid interface remains constant and, is uniformly distributed in the liquid throughout this stage [34,38]. Since solidification takes place slowly under equilibrium conditions, the only solid phase formed is the solid solution phase. Formation of second phase precipitates is basically prevented because there is an absence of solute rejection into the liquid at the solid / liquid interface. This stage is generally considered to be the most important, since the completion time for the entire TLP process is largely determined by the time for isothermal solidification of the liquid [31,39]. The use of single element filler metal markedly increases the maximum liquid width and joint completion time, compared with the use of equivalent thickness eutectic composition filler metal [31].

2.7.4 Stage IV

This is the homogenization stage, (d to e in figure 2.8 [35]) where solid – state solute redistribution occurs. The homogenization temperature need not be the same as that of stage I & II and it is generally considered completed when the maximum solute concentration at the joint centreline reaches some predetermined value, figure 2.10 [40]. The mechanical properties of a diffusion-brazed joint should advance up to that of base material since chemical

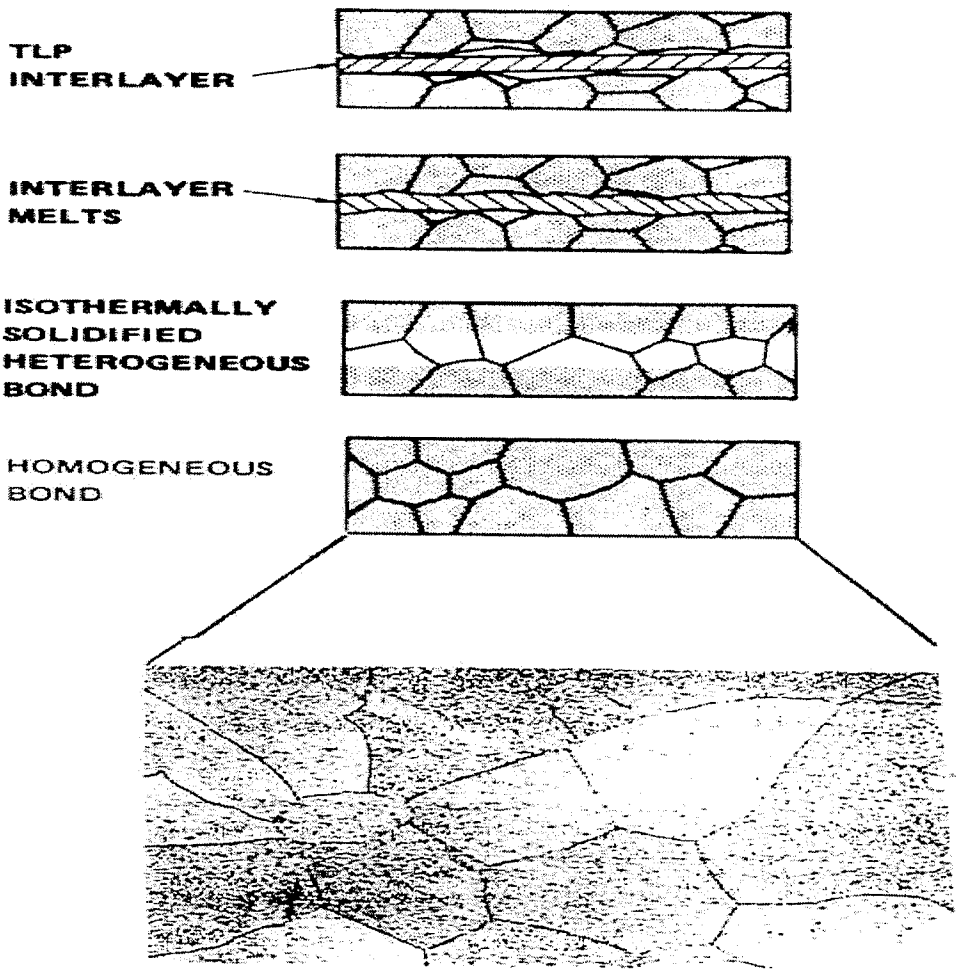

Figure 2.9Schematic of TLP Bonding Process Showing the Isothermal Solidification Stage [23].

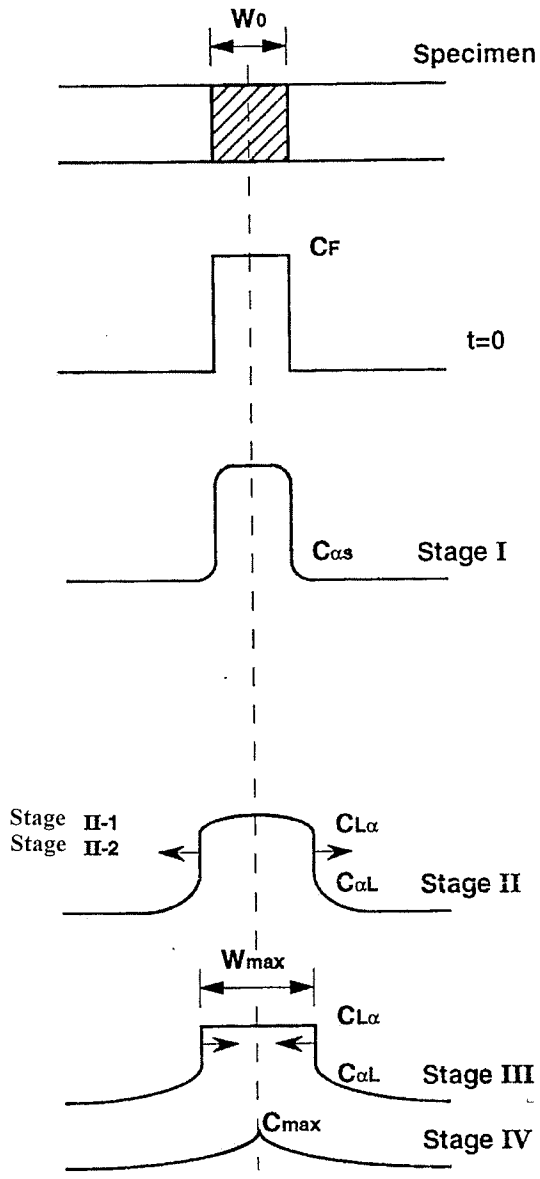

Figure 2.10 Schematic of Concentration Profiles during TLP Bonding Process [40].

composition at the joining zone can be equalized to that in the base alloy after the homogenising process.

2.8 Modelling of TLP Bonding

A great deal of modelling of TLP bonding process has involved analytical methods [31,41,42,43], which treat the joining process as a number of discrete steps, namely, base metal dissolution, isothermal solidification and homogenization. Local equilibrium at the migrating interface is generally assumed when modelling two-phase diffusion controlled problems. This however is an approximation, since it is generally not attained at the solid/liquid interface in practise [44]. It is tactically assumed that the output of any stage does not affect the operating conditions that apply in subsequent stages of the process. Analytical modelling of TLP bonding process depends on classical solutions for Fick's diffusion equations. Diffusion of a solute out of a finite interlayer into semi-infinite solid substrates initially free of the solute, may be represented by the following expression [45]:

$$C_{(x,\,t)} = 1/2C_o[\text{erf}\,(h - x) / 2Dt^{1/2} + \text{erf}\,(h + x) / 2Dt^{1/2}]$$

where $C_{(x,\,t)}$ = concentration of the solute as a function of distance from the centre of the interlayer (x) and time (t).

$2h$ = width of the interlayer

D = Diffusivity of the solute in the substrate

C_o = initial solute concentration in the filler alloy

2.8.1 Base Metal Dissolution

Base metal dissolution during TLP – bonding was examined by Nakao et al [46] based on a derivation of the Nernst – Brunner theory [38]:

$$C = C_{sat} [1 - \exp \{-k (A/V) t\}] \quad \ldots\ldots\ldots (1)$$

where, C is the solute concentration in the liquid, C_{sat} is the saturated solute concentration, k is the dissolution rate, V is the volume of liquid and A is the area of the solid – liquid interface. Differentiating equation (1) above and assuming that the total amount of solute in the liquid remains constant, they developed a dissolution parameter P, which is given as:

$$P = kt = h \ln [\{W_o (W_t + \rho h)\} / \rho h (W_o - W_t)] \quad \ldots\ldots\ldots (2)$$

where, W_t is the width of the base metal dissolved at time t, W_o the equilibrium (saturated) dissolution width, ρ the ratio of the densities of the liquid and solid phases, h half of the initial liquid width and k a constant. Nakao et al [46] used equation (2) to compute the dissolution parameter and showed that it varied linearly with holding time, demonstrating that the Nernst - Brunner theory could be used to explain dissolution during TLP bonding. Liu et al. [47] developed a model that accounts for base metal dissolution during liquid formation. They used a general error function solution to describe the solute distribution in the liquid zone when modelling the dissolution stage. However they assumed that there is no solute diffusion into the base metal, which is not the case in actual practise, as solute diffusion can affect the process kinetics during the base alloy dissolution. Analytical methods so far developed are all based on assumptions that are difficult to apply in modelling the dissolution stage of TLP bonding.

2.8.2 Isothermal Solidification

Several models of isothermal solidification process have been developed and proposed [31,48,49,50]. During this stage of TLP bonding process, solute distribution in the liquid can be considered to be uniform [35], and therefore, solute diffusion in the liquid can be ignored. In addition, the base metal can be assumed to be semi- infinite because solute diffusion in the solid is generally slow. Thus, the isothermal solidification stage can be analytically modelled as a single-phase diffusion controlled moving interface problem figure 2.11 [40].

Tuah – Poku et al [31] proposed a method for estimating the completion time for isothermal solidification during TLP bonding. In this approach an error function solution was used to describe the solute distribution in the base metal, by:

$$C_{(y,\,t)} = C_{\alpha L} + C_{\alpha L}\ \mathrm{erf}\,[y / (4D_s t)^{1/2}] \quad \ldots\ldots\ldots\ldots\ldots (3)$$

Where $C_{\alpha L}$ is the solute concentration in solid at the interface and y is the distance from the solid surface. The total solute amount M_t that has entered the base metal at time t can be calculated from the relation:

$$M_t = 2\, C_{\alpha L}\, (D_s\, t / \Pi)^{1/2} \quad \ldots\ldots\ldots\ldots\ldots\ldots\ldots (4)$$

The total amount of solute diffused into the base metal can be considered to be equal to the original solute content of the filler metal, if the amount of solute diffused into the base metal during heating and dissolution stages is ignored, i.e.

$$C_F W_o = 4\, C_{\alpha L}\, (D_s\, t / \Pi)^{½} \quad \ldots\ldots\ldots\ldots\ldots\ldots\ldots\ldots\ldots\ldots (5)$$

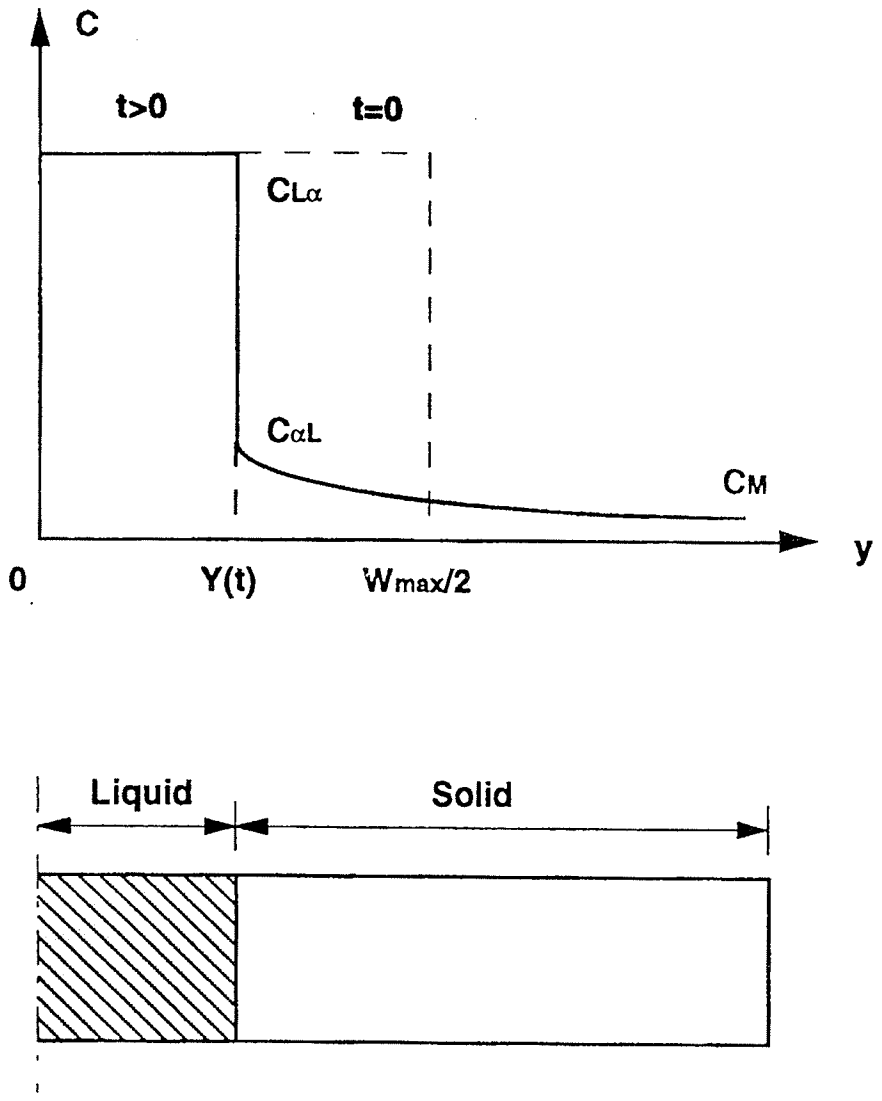

Figure 2.11 Concentration Profile along the Length of TLP Bonding Specimen [40].

where C_F is the solute content in the filler metal and W_o the initial width of the filler metal. The completion time for isothermal solidification can therefore be calculated using the relation:

$$Ts = \Pi / (16\ D_s)\ [C_F W_o / C_{\alpha L}]^2 \quad \ldots\ldots\ldots\ldots\ldots\ldots\ldots\ldots\ldots\ldots (6)$$

Similar treatments of this problem were reported by Ikawa et al [49], Nakao et al [48] and Onzawa et al [50]. Nakao et al [48] showed that the width of the eutectic phase of the joint layer decreased linearly with increase in the square root of holding time at the bonding temperature. Assuming that the isothermal solidification process depends on diffusion of the melting point depressant (boron), the slope of eutectic phase width against holding time (m) was obtained from the equation:

$$\ln m = \ln [\{4C_s / (V_s P^{1/2})\}\ (C_l/V_l - C_s/V_s)^{-1}] + \tfrac{1}{2} \ln D_o - Q / 2RT \quad \ldots\ldots\ldots (7)$$

where C_s and C_l are the molar ratios of the melting point depressant in solid & liquid base alloy respectively. V_s and V_l are the molar volumes of the solid & liquid phases, respectively, Q is the activation energy for diffusion, T is the absolute temperature, and D_o & R are constants. Considering a multicomponent system, the first and second term in the equation (7) above were assumed to be constant, making it possible to rewrite the equation as an Arrhenius – type equation:

$$\ln m = A - Q / 2RT \quad \ldots\ldots\ldots\ldots\ldots\ldots\ldots\ldots\ldots\ldots (8)$$

From this linear relation, the apparent activation energy for diffusion of melting point depressant in the base alloy, which corresponds to the activation energy for isothermal solidification, can be estimated from the graph of ln m against 1/T. Based on their experimental results, Nakao et al [48] demonstrated that the

isothermal solidification process of liquid film during diffusion brazing was controlled by the diffusion process of melting point depressant element in the base material.

2.8.3 Homogenization Stage

According to Fick's diffusion equation, when the initial thickness (2h) of the source of the diffusing species (C_o) is of the order of the diffusion distance $(Dt)^{1/2}$ i.e.

$$C_{(y,\,o)} = C_o \quad h \geq y \geq 0$$

$$C_{(y,\,o)} = C_m \quad y > h$$

where C_m is the initial concentration of diffusant in the substrate, the solute concentration in the substrate with time, is given by:

$$C_{(y,\,o)} = C_m + \tfrac{1}{2}(C_o - C_m) \times [\text{erf}\{(h + y) / 2Dt^{1/2}\}] + \text{erf}[(h - y) / 2Dt^{1/2}] \quad \ldots(9)$$

Ikawa et al [49] used equation (9) to model the solute distribution during homogenization of TLP bonded Nickel base superalloy. In their formulation, h was half the maximum liquid width at the end of the base metal dissolution and C_o equalled $C_{L\alpha}$. The solute concentration attained its maximum value at the centre of the specimen (x=0) when:

$$C_{max} = C_{(0,t)} = C_m + (C_o - C_m) \times \text{erf}[h / 4(D_s t)^{1/2}] \quad \ldots\ldots\ldots\ldots\ldots\ldots\ldots (10)$$

Zhou [40] using h as half the filler metal thickness and C_o the initial solute concentration in the filler metal, also used equation (10) to model homogenization stage during TLP bonding. Nakao et al [46] observed close agreement between evaluated results using equation (10) and the experimental

values of aluminium redistribution during homogenisation of nickel base superalloy.

2.9 Boron Diffusion in Nickel Base Alloy

Boron is a very effective melting point depressant and rapid diffuser in nickel base alloy. Essentially 1 wt% of boron is reported to lower the melting point of nickel by more than 280°C [51]. The size difference between the boron and nickel atoms is greater than 25% [52]. Due to its small size, it has been always believed that boron will diffuse rapidly in nickel by an interstitial mechanism. Jena and Chaturvedi [52] suggested that its presence in nickel alloy in large amounts would be harmful due to the formation of borides. Earlier empirical studies showed that addition of 0.01wt% boron improved hot ductility and rupture life but this marked improvement in properties was lost with increase in boron level to 0.5wt % [51]. The M_3B_2 boride particles found in nickel base superalloys have a tetragonal crystal structure [53]. The precise composition of these boride phases varies with composition of the base alloy but generally seem to be of the form MM'_2B_2 or $M_2M'B_2$ with M being molybdenum or titanium and M' chromium, nickel or cobalt [54]. $M_{23}B_6$ and Cr_5B_3 has been detected with very high levels of boron (1-3.wt%) [55]. Direct evidence of boron segregation has been produced using secondary ion mass spectrometry (SIMS), which clearly shows boron enrichment on grain boundaries. There have been measurements of the diffusion of boron in amorphous nickel base systems by radiotracer and SIMS techniques. However, due to the fact that high temperature data must be

extrapolated from the low temperature amorphous data, the approach is particularly not useful for predicting boron diffusion in nickel base alloys at temperatures around 1100°C. It was suggested that boron acts as a getter of embrittling impurities such as sulphur and "fills" grain boundaries preventing the precipitation of carbides and other boundary reactions [51].

A more theoretical approach was adopted to explain the role of boron at grain boundaries [56]. Calculations of chemical bonding at a boundary show that, unlike embrittling segregants, boron does not draw charge from nearby metal-metal bonds, which would reduce the grain boundary strength. It was suggested that it forms bonds of a more covalent nature with metal atoms on the boundary, which in effect increase the boundary strength. Hondros and Seah [57], recorded a grain boundary enrichment ratio for boron in nickel of about 10,000, suggesting that there is a very strong driving force for segregation to surfaces and boundaries. It is believed that grain boundary boron improves the high temperature strength of nickel base alloys by reducing the grain boundary sliding. It is generally held that for optimum properties, boron should be present at a level, which fully saturates the grain boundaries but does not allow the formation of boride particles.

2.10 Mechanical Properties of Brazed Joint

One of the significant situations in which high temperature brazing has come into its own is that where structural component is required to meet high standards in terms of strength and ductility combined with high corrosion

resistance, while thermal influences on the base materials need to be comparatively slight. Nickel base brazing alloys comes into play in such situations. However they tend to precipitate hard phases, which have an embrittling effect on the joint's strength. Recent systematic research carried out on Ni base brazing alloys with austenitic base materials, has provided better understanding of the diffusion - based bonding mechanisms and also helped to optimize the strength properties of brazed joint of this type. It was demonstrated that by strictly adhering to optimize brazing parameters (temperature, time and gap width), it is possible to obtain joints that are free of hard phases and exhibit similar strength as the base material. On the basis of this optimization it is always necessary to investigate the ductility behaviour of high temperature brazed joints.

The work done to date on analysing ductility properties comprises various studies that use different specimen shapes and sizes in diverse testing techniques. As a result there is a limit to which such results can be compared with each other. One of the method involve conducting twisting test on brazed T – shaped specimens, which involves taking the twist angle to the point at which the joint fractures to provide a measure of toughness. Lugscheider et al. [58] used notch-bend impact tests (semicircular and V notch) to access the ductility properties of high-temperature brazed joints. They reported that semicircular – notch specimens gave more reliable results over the V – notch specimens. More recent work on the subject [59] involved applying scanning electron microscopy to fractured surfaces to explain various fracture mechanisms and obtain information about the ductility of diffusion brazed joint. Other various mechanical

tests that are currently in use for evaluating brazed gap integrity include, high temperature tensile test, creep rupture test and tensile shear test.

2.11 Scope of the Present Investigation

In the preceding introduction and literature review, it was shown that diffusion brazing has evolved as a viable alternative joining technique for difficult to weld nickel base superalloys like IN-738 alloy. However it was noted that explicit consideration of the bonding parameters; temperature, time and gap width, is paramount to producing a joint with properties consistent to that of base alloy. Quite a number of diffusion models have been developed and proposed for TLP bonding process, aimed at understanding the conditions essential for producing brazed gap free of deleterious phases that are known to fraught conventional brazing process. In contrast to commercial practise, most of these models are based on binary filler alloy system and furthermore, there are few detailed publications found in open literature about the diffusion brazing of IN-738, with ternary and multi component brazing alloys.

It was then, the objective of the present study to gain a comprehensive understanding of the influence of gap size, bonding temperature & time on the microstructure and, in effect, mechanical properties of brazed joint in IN-738 alloy with commercial brazing alloys. The study was conducted using Nicrobraz 150 and Amdry DF3 nickel based filler materials with narrow and variable gap. The primary focus of the investigation was a thorough microstructural characterization of the various brazed joint using optical, scanning electron & transmission

electron microscopy along with microhardness and high temperature tensile tests. The result of the study is expected to provide an understanding of the various phases that are formed in diffusion-brazed gap of IN-738 and their effects on the joint's high temperate properties.

Chapter 3

EXPERIMENTAL TECHNIQUES

3.1 Material

As-cast Inconel 738 in the form of 160mm x 30mm x 6mm plates, provided by Hitchiner Manufacturing Co. Inc., were used in this investigation as the base alloy. The average composition from the supplier is given in Table 3.1. The material was used in as-received condition without any heat treatment. TLP brazing was performed using powdered Amdry DF3 "DF3" and amorphous foil of Nicrobraz 150 "NB 150" as the braze alloys, and their chemical compositions are shown in Table 3.2.

3.2 Sample Preparation and Diffusion Brazing

Two categories of samples were used in the investigation, viz., industry and laboratory processed. In the case of industry processed samples, an assembly of two samples with the gap size between them varying from0 – 125μm was prepared by tack welding. These test pieces with variable gap size were sub-contracted to Ti Coating Inc. through Standard Aero Ltd for fluoride ion cleaning. Subsequent to surface cleaning, the samples were vacuum brazed at Standard Aero Ltd, Winnipeg. In addition to variable gap specimens, samples with fixed gap (75μm) were likewise fluoride ion cleaned and vacuum brazed. Laboratory prepared samples were initially polished to 600 grade, to remove deformed surface produced by machining operation.

Table 3.1 Composition of IN-738 Base Alloy

Elements	Wt%
Aluminium (Al)	3.46
Boron	0.012
Carbon (C)	0.11
Chromium (Cr)	15.84
Cobalt (Co)	8.50
Iron (Fe)	0.07
Manganese (Mn)	0.01
Molybdenum (Mo)	1.88
Niobium (Nb)	0.92
Silicon (Si)	0.01
Sulfur (S)	0.001
Tantalum (Ta)	1.69
Titanium (Ti)	3.47
Tungsten (W)	2.48
Zirconium (Zr)	0.04
Nickel (Ni)	REM

Table 3.2 Filler Alloys Nominal Composition

Filler Alloy	Composition Wt%	Solidus °C	Liquidus °C
Nicrobraz 150	B – 3.5, Cr – 15, C – 0.03, Ni – Bal	1055	1055
DF3	B – 3.0, Cr – 20, Co – 20, Ta – 3.0, La – 0.05, Ni - Bal	1045	1200

They were then ultrasonically cleaned using acetone, and wrapped in stainless steel foil with "NB 150" foil pre-placed between the mating surfaces. The samples (15mm x 7mm x 7mm) were sealed in vycor capsules backfilled with 160 torr of commercial argon and then placed in a horizontal tube furnace for brazing at different temperatures and holding times. Brazed samples were sectioned by electro-discharge machining due to the brittle nature of the brazement for metallographic examination.

3.3 Optical and Scanning Electron Microscopy

Standard metallographic techniques were used to prepare samples (both polished & etched) for optical and scanning electron microscopy. Cross sections of brazed joints were etched using a solution of 10g $CuCl_2$ + 40 ml HCl + 60 ml methanol. For general assessment of the joint microstructure, optical metallograhic examinations were performed using Nikon EPIPHOT – TME inverted optical microscope with a magnification range of 50 to 1000X and Nikon 35 mm Polaroid camera attachment. Polished samples were used in examining the nature and level of pores and micropores formed during the bonding process.

Microstructural examination (using secondary & backscatter electron imaging) and compositional analysis of brazement were conducted on a JEOL 5900 scanning electron microscope equipped with Oxford electron dispersive spectrometry (EDS) system with INCA standardless correction software. The average width of the centreline eutectic structure in the bonded region was measured by evaluating the cross – section area of the eutectic structure at a

magnification of 500X. An average of 30 measurements over a distance of 5mm at the mid section of the TLP bonded area were taken from each sample. X-ray mapping and line scan by the EDS system with INCA standarless correction software, were utilized in examining the distribution of the major alloying elements of the base and filler metal across the bonded region.

3.4 Transmission Electron Microscopy (TEM)

Transmission electron microscopy was used to investigate the nature of small globular precipitates found distributed within the base alloy grains adjacent to the base metal – joint interface, in brazed specimens. A JEOL 2000 FX Transmission electron microscope and Tracor Northern Model TN 5400 EDS system were used to analyse the precipitates extracted by Carbon extraction technique. Carbon extraction replicas were made using a mounted, polished and etched samples, which were subsequently carbon coated in Edwards Auto36 vacuum coater, under a vacuum of about 1x 10^{-5} torr. The deposited carbon film was scored into squares using a sharp edge before electroetching in a solution of 10% HCl + 90% methanol at a d.c voltage of 20 volts for 12 secs. The carbon film was floated off in distilled water by lowering the sample slowly into the water at a shallow angle. Water surface tension pulled off the carbon film, which were gathered and dried on 3mm diameter, 200 mesh, copper grid disks for the succeeding TEM examination. Effort was made to prepare thin foil from brazed joint using twin jet electropolishing technique. Due to the different nature of phases in the joint, several off centre holes were produced with no area thin

enough for TEM examination. Bright and dark field imaging along with selected area diffraction approach were used in the analysis of extracted precipitates. Chemical composition was measured using a high purity Si (Li) detector of the EDS attached to TEM.

3.5 Hardness Measurement

Microhardness of the brazed joint was determined using a 25-gram load on a Lietz microhardness tester. 20 measurements were taken per sample to compute the average values. Using a polished sample, it was possible to measure the hardness of the centreline eutectic phase, precipitated second phases and solid solution phase. As a result it was possible to compare the hardness of these phases to that of the base metal.

3.6 Mechanical Test

The tensile properties of the brazed joints were evaluated at 980°C. The high temperature tests were carried out using specimens with butt joint configuration, shown in figure 3.1, on an Instron 1137 tensile machine using 10^{-3}/s strain rate. All mechanical property results are an average of 3 samples of each condition.

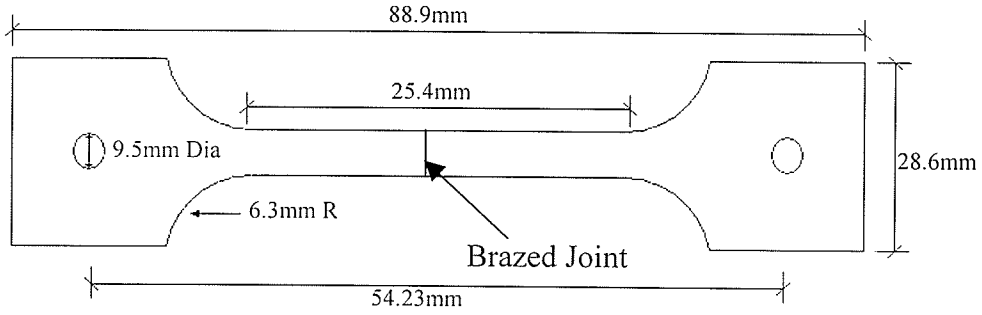

Material Thickness: 2.54mm

Figure 3.1 Tensile coupon for High Temperature Tensile Test

Chapter 4

RESULTS AND DISCUSSION

4.1 Microstructure of As – Received IN-738 Base Alloy

An optical micrograph of a polished as-received cast IN-738 sample is shown in figure 4.1. A small volume fraction of casting micropores is observed mainly within the large grains of the alloy. These apparently do not appear to be detrimental to the mechanical properties since the mechanical properties were found to be within the specification. Optical and scanning micrographs of etched samples are shown in figures 4.2 & 4.3. The microstructure consists of polygonal grains of an average size of 750μm with cellular dendritic precipitation of primary MC carbide particles, which was observed by EDS-SEM analysis. However within the resolution capability of the EDS-SEM system, secondary $M_{23}C_6$ carbides could not be detected along the grain boundaries. 12ml H_3P0_4 + 40ml$HN0_3$ + 48ml H_2SO_4 etched samples revealed an extensive intragranular precipitation of unimodal shapes particles, which SEM and TEM composition and diffraction analysis demonstrated to be γ' phase, the principal strengthening phase of the base alloy, as shown in figure 4.4.

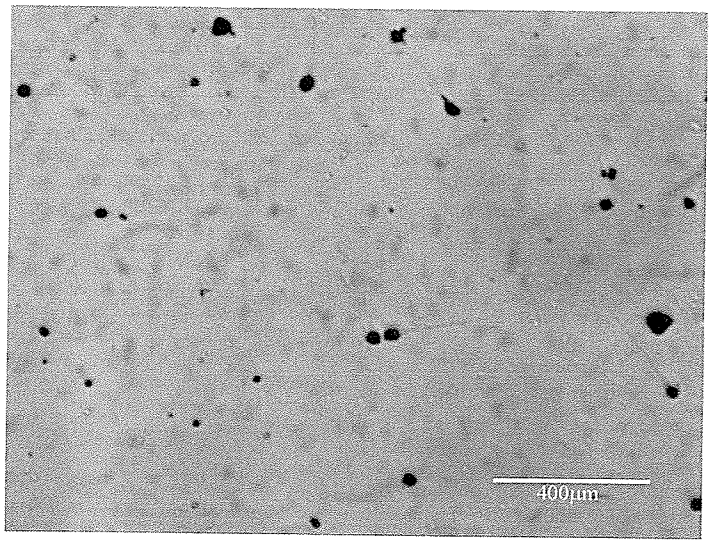

Figure 4.1 Optical Micrograph of Polished As-Received IN-738, Showing Micropores at 50X.

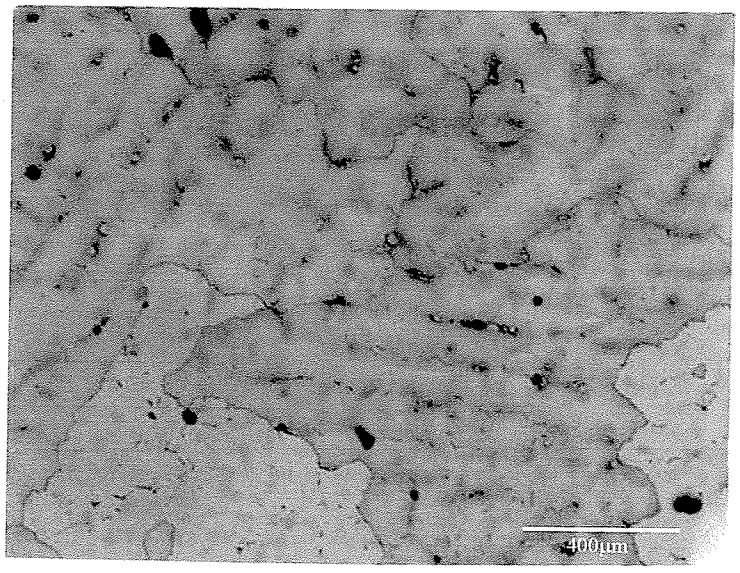

Figure 4.2 Optical Micrograph of Etched As-Received IN-738, Showing Cellular Dendritic Structure at 50X.

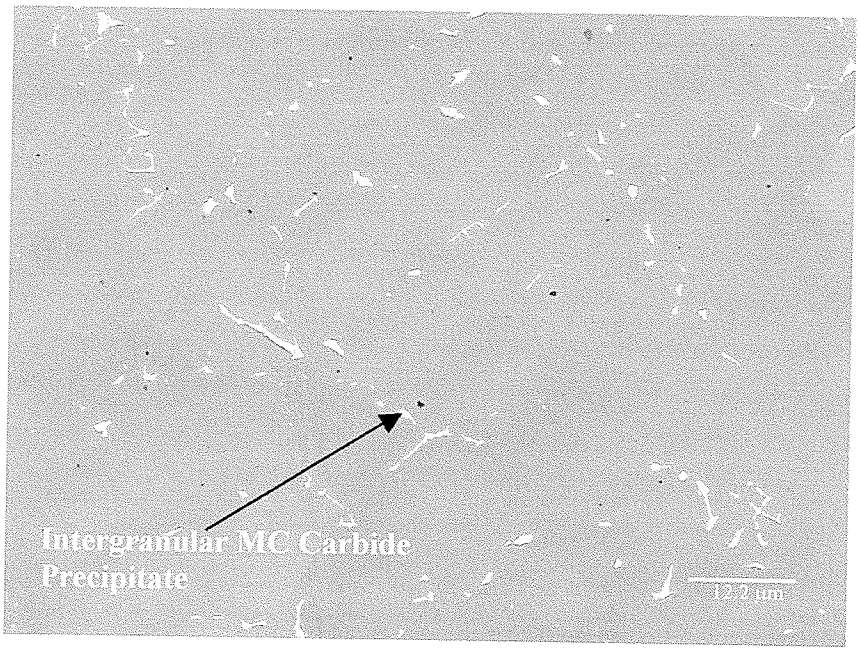

Figure 4.3 SEM Back Scatter Electron Image of As-Received IN-738, showing Grain Boundary Precipitation of MC Carbide.

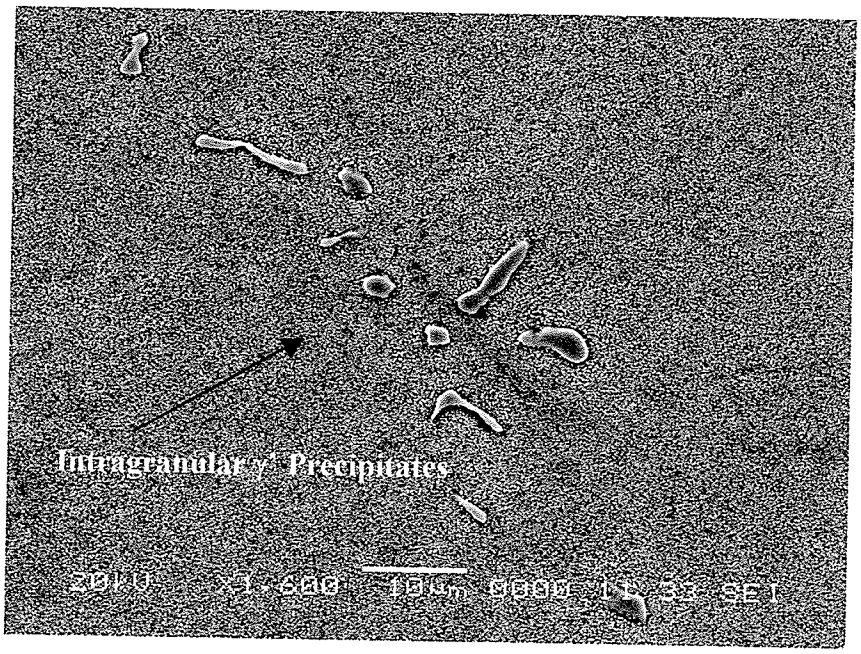

a

Figure 4.4 (a) SEM Micrograph showing Intragranular distributed γ' Phase.

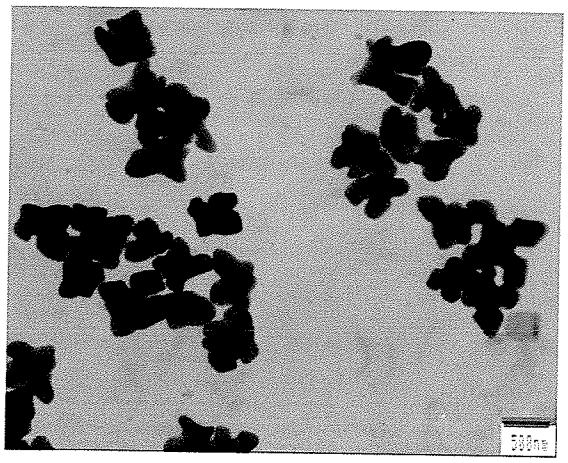

b

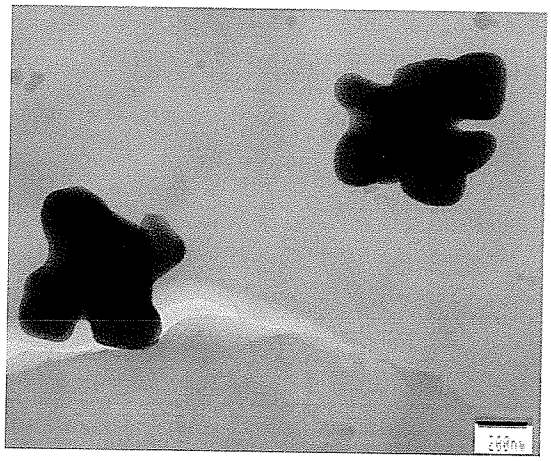

c

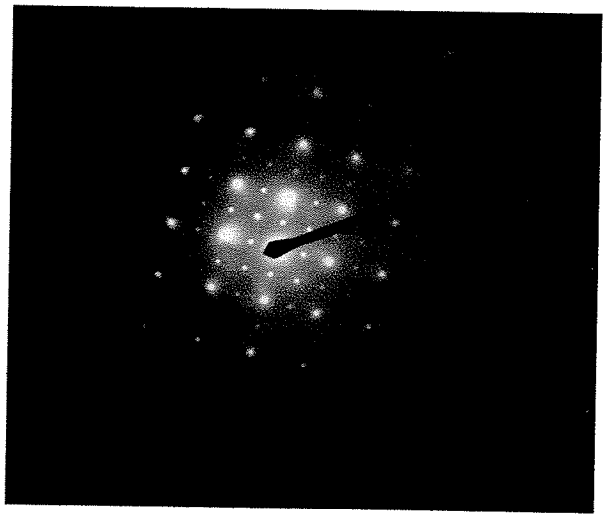

d

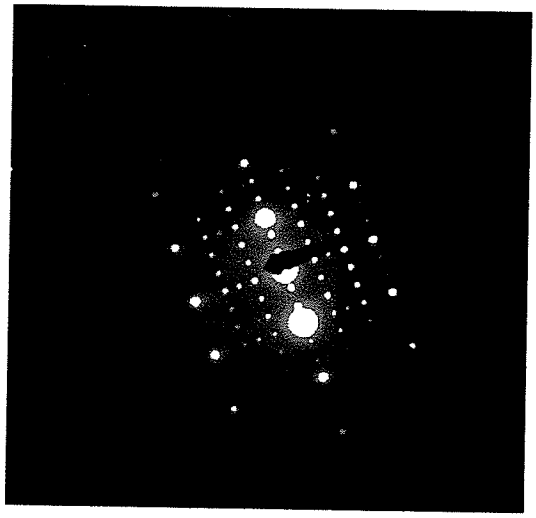

e

Figure 4.4 TEM Micrograph showing the Morphology of γ' in As-Received Sample (b) at 15KX, (c) higher magnification micrograph of precipitates at 40KX, (d) SADP from γ' Phase at [011] and (e) at [112] Zone Axis

4.2 Microstructural Analysis of "NB 150" Brazement

To study the effect of gap size on joint microstructure, a variable gap width (0 - 100μm) assembly of IN-738 base alloy was vacuum brazed with "NB 150" filler at 1120°C for 15 minutes and diffused at 1065°C for 4 hrs. The microstructure of the sample at three different gap widths, obtained by SEM in secondary electron mode is shown in figure 4.5. Between 0 - 50μm initial gap width, the microstructure consists predominantly of γ solid solution phase. As the gap increased above this critical size at the brazing conditions, a centreline eutectic phase was observed to form across the joint layer, which became wider, denser and continuous with further increase in the gap width. The hardness of the solid solution and eutectic phase were measured by microhardness tester.

Figure 4.6 illustrates variation in the average hardness of the centre region along the brazement. The hardness value was found to increase with increase in gap width, with the only exception observed between 25μm and 50μm where it decreased. This can be explained by the fact the strength of the γ solid solution phase is mainly dependent on solid solution strengthening by alloying elements diffused into the joint during the bonding process. At the end of the process, the quantity of these strengthening elements in the joint is expected to decrease with increase in the joint size, causing a drop in hardness. However the increase in hardness across the joint above 50μm is apparently a result of formation of centreline eutectic phase, which grew wider and denser with gap size. The average hardness of the eutectic phase was found to be 720VHv, which is far higher than that of the base alloy. This, coupled with the fact that it formed in a

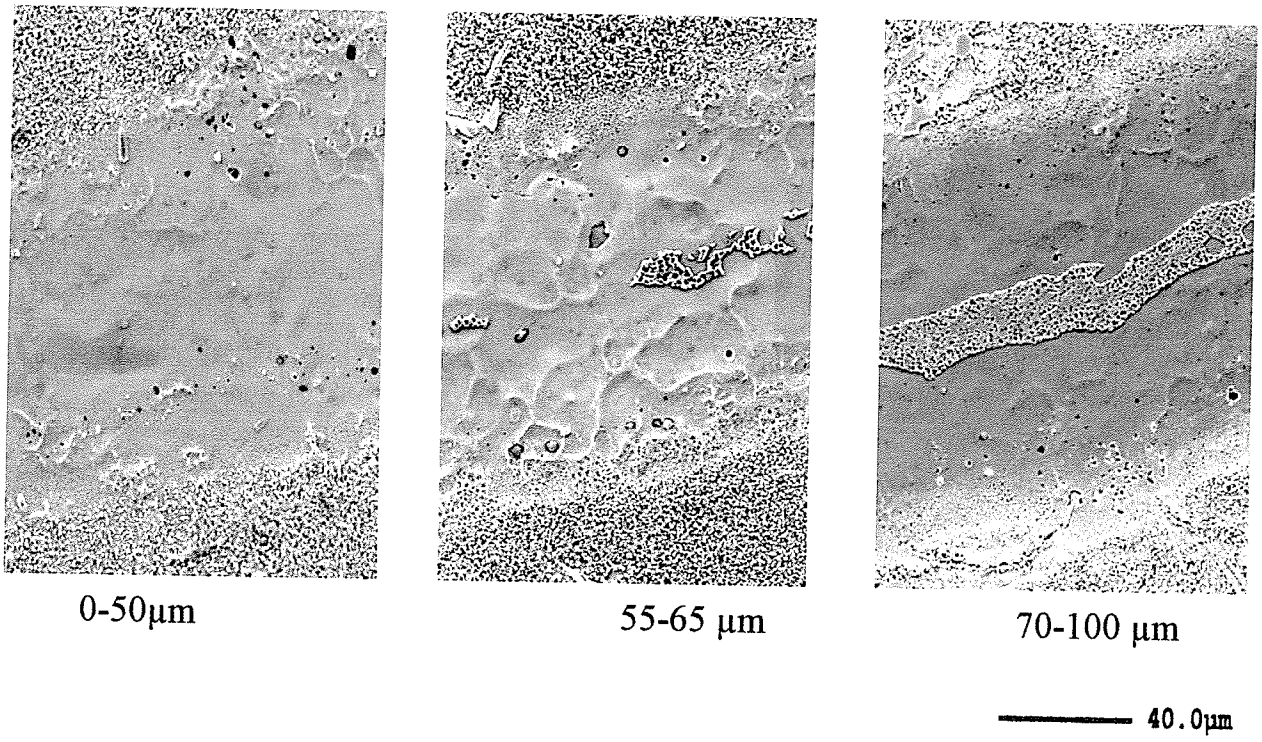

Figure 4.5 SEM Micrograph showing Variation of Microstructure of "NB 150" Brazement with Gap Size.

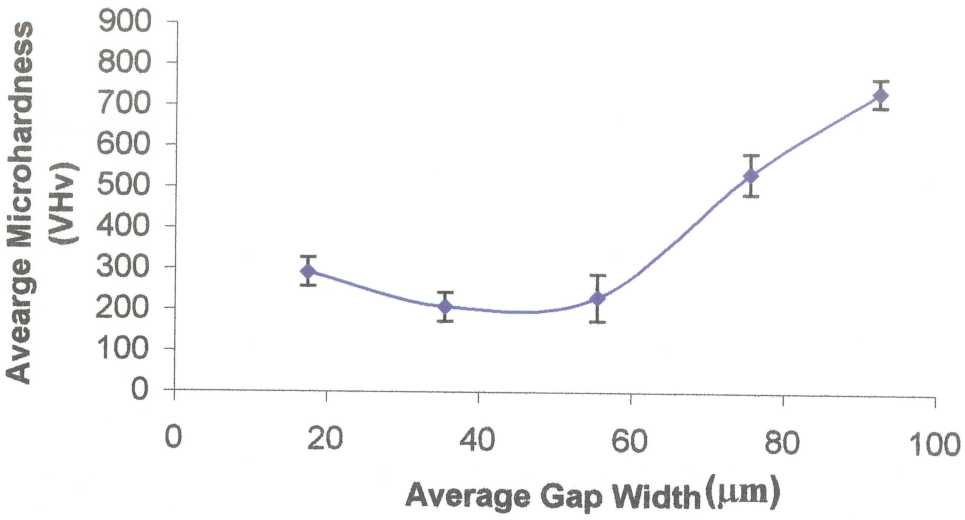

Figure 4.6 Variation of "NB 150" Brazement Centre-Area Microhardness with Gap Width.

continuous fashion above 65μm gap size, suggests its embrittling effect detrimental to the joint properties.

4.2.1 Microstructure of 30μm and 60μm Gap "NB 150" Brazement

In order to further investigate the effect of gap size on microstructure of "NB 150" brazement, 30μm and 60μm fixed gap assemblies were brazed at 1100°C for 1 hr. Figure 4.7 shows the microstructure of the joints. At the end of 1 hr hold time at this temperature, isothermal solidification of the liquid metal was observed to be complete in the 30μm sample, and the resulting microstructure comprised of equiaxed grains of γ solid solution phase. In comparison, a centreline eutectic phase was observed in the 60μm gap sample as a result of insufficient hold time for isothermal solidification of the liquid metal. On cooling, the residual liquid subsequently transformed into eutectic composition phase.

4.2.2 Effect of Brazing Temperature and Time on Joint Microstructure

The brazing temperature and time are known to have a profound effect on diffusion brazing. To study the effect of these brazing parameters on microstructure in IN-738 joint, 75μm fixed gap samples were vacuum brazed with "NB 150" at three different temperatures: 1070°C, 1100°C and 1130°C for 10mins, 20mins, 40 mins and 60 mins.

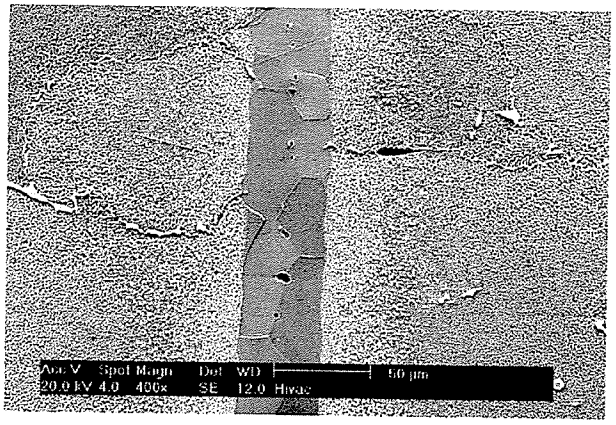

a

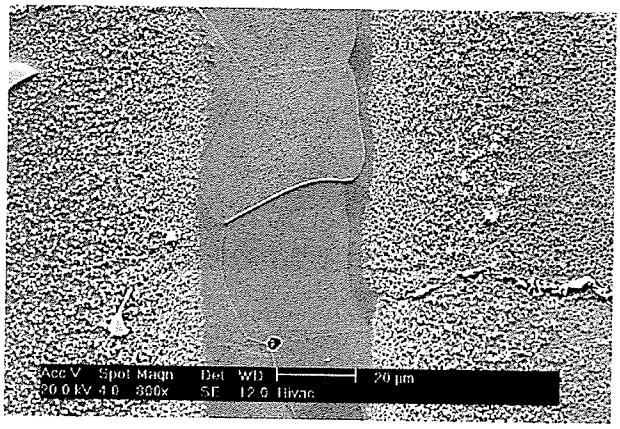

b

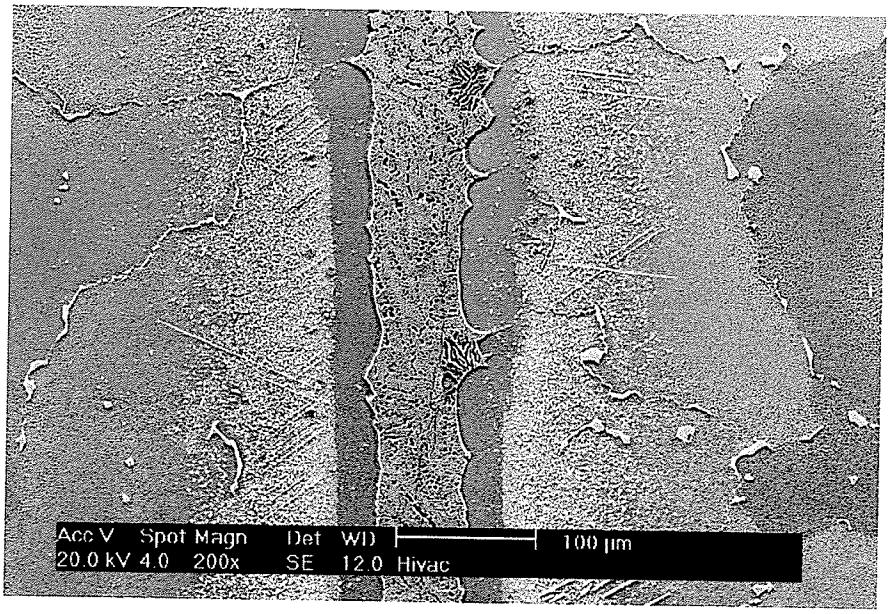

c

Figure 4.7 Microstructure of 30μm (a), (b) and 60μm (c) fixed gaps Brazed at 1100°C for lhr.

4.2.2.1 Microstructure of Joint Brazed at 1070°C

Braze microstructures developed in samples joined at this temperature comprised of centreline ternary eutectic phase bordered by pro-eutectic Ni solid solution phase that formed by the interdiffusion induced compositional change resulting in isothermal solidification of the liquid interlayer. The eutectic width however decreased with increase in holding time. In addition, a region of angular and spherical precipitates were noticed on the braze side of the original substrate – liquid interface figure 4.8 (a) & (b). The particles grew in size as bonding time increased from 10mins to 60 mins. EDS point analysis and line scan of precipitates formed after 60 mins holding, revealed them to be Nickel and Chromium rich borides figure 4.8 {(c), (d), (e) & (f)}.

4.2.2.2 Microstructure of Joint Brazed at 1100°C

Increasing the bonding temperature to 1100°C, it is expected that diffusion rate of the melting point suppressing element (boron in this case) into the base alloy will rise, reducing the time needed for liquid inserts to solidify. It was observed from the microstructures of the brazed joints, that despite the fact that eutectic width decreased with bonding time and condensed in size compared to the 1070°C brazing (figure 4.8 and 4.9), more than 60 mins of holding is still required to complete the isothermal solidification. It is worthy of note however, that in the 1100°C joint, the line of boride precipitates that were observed in 1070°C prepared samples, consisted largely of globular particles. Compositional analysis revealed them to be Chromium rich boride (figure 4.10).

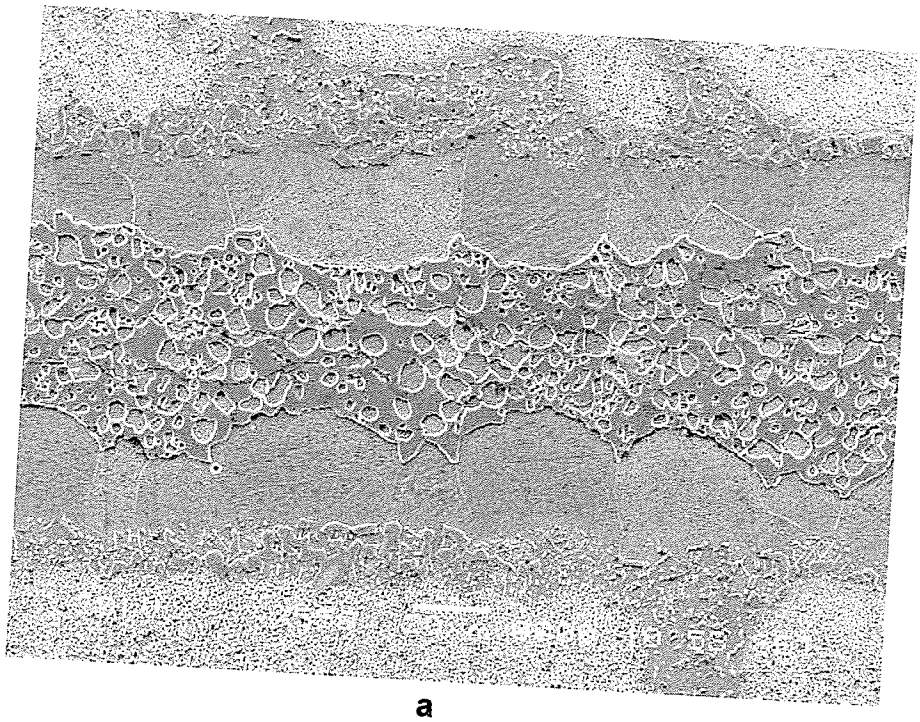

a

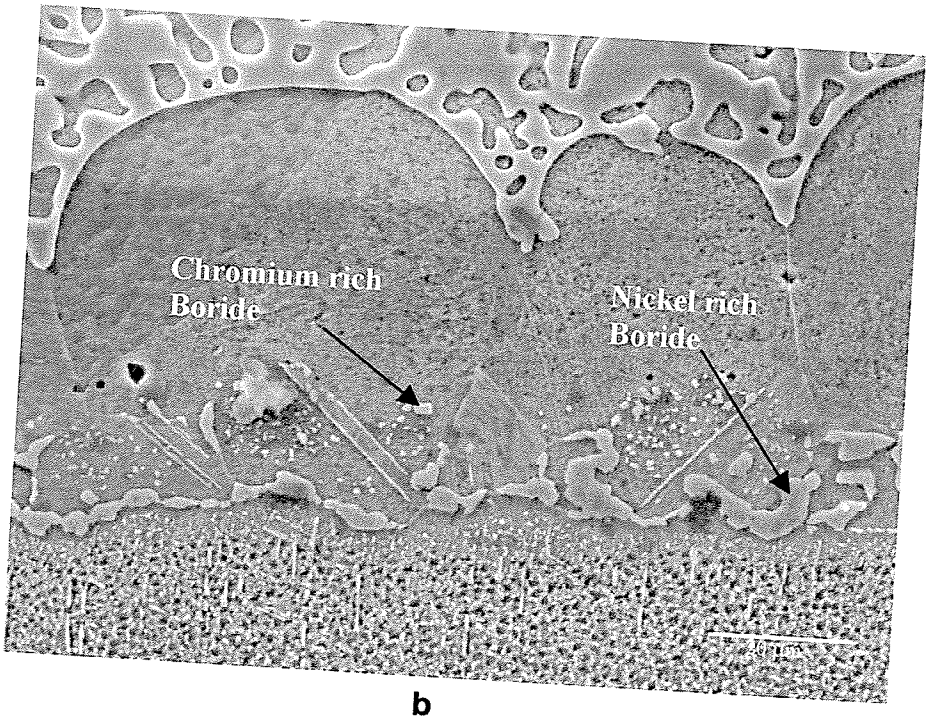

b

Figure 4. 8 (a & b) Microstructure of 1070°C Brazed 75μm Gap for 60 mins showing Nickel and Chromium rich Borides at the Substrate- Braze Interface.

Element	Atomic %
Al	1.94
Ti	5.18
Cr	8.63
Co	5.78
Ni	76.48
Nb	0.67
Mo	0.57
W	0.75

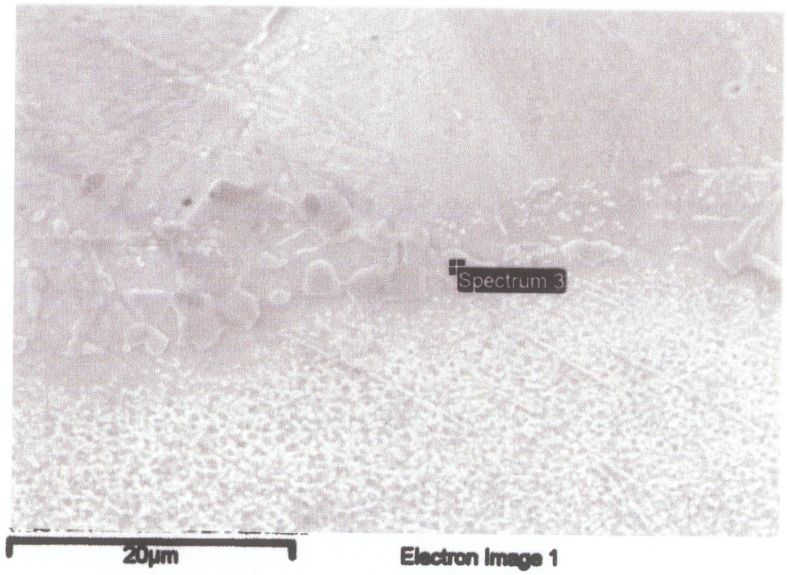

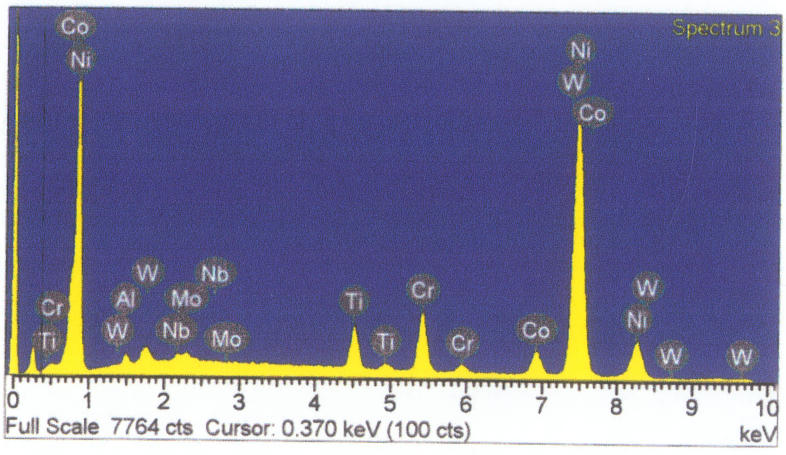

c

Figure 4.8 (cont...)

Element	Atomic %
Cr	82.52
Co	2.87
Ni	8.59
Mo	3.85
W	2.16

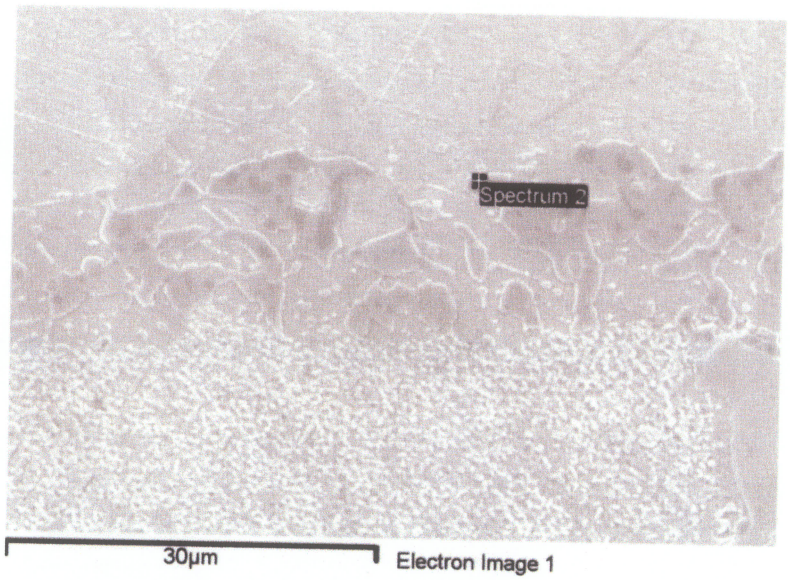

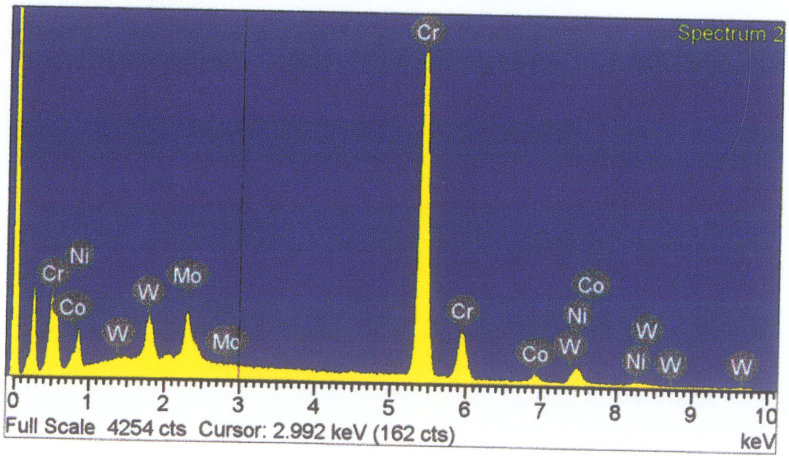

d

Figure 4.8 (cont...)

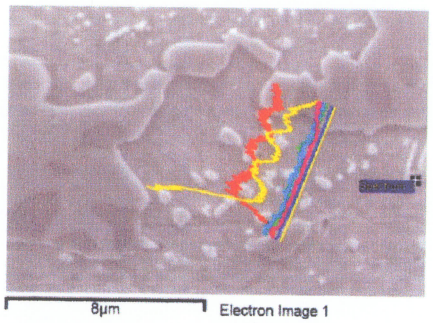

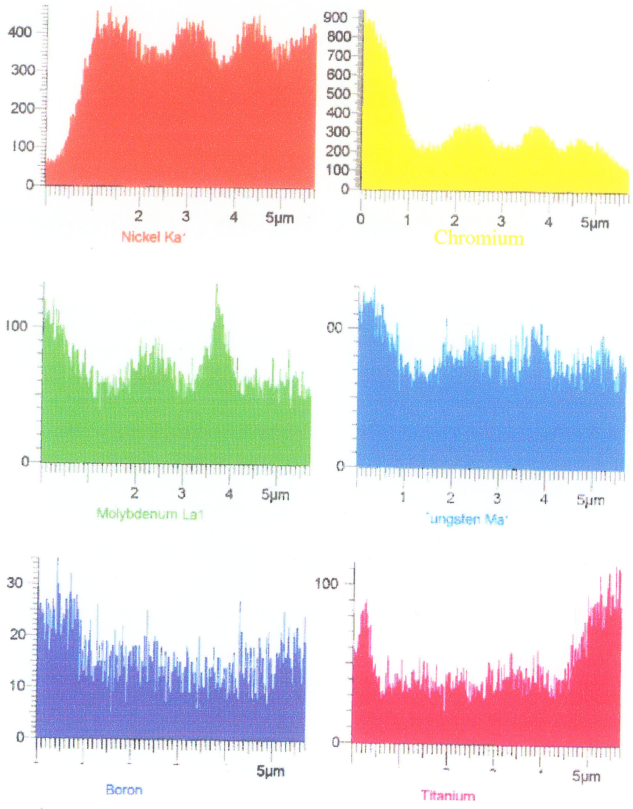

e

Figure 4.8 (cont…)

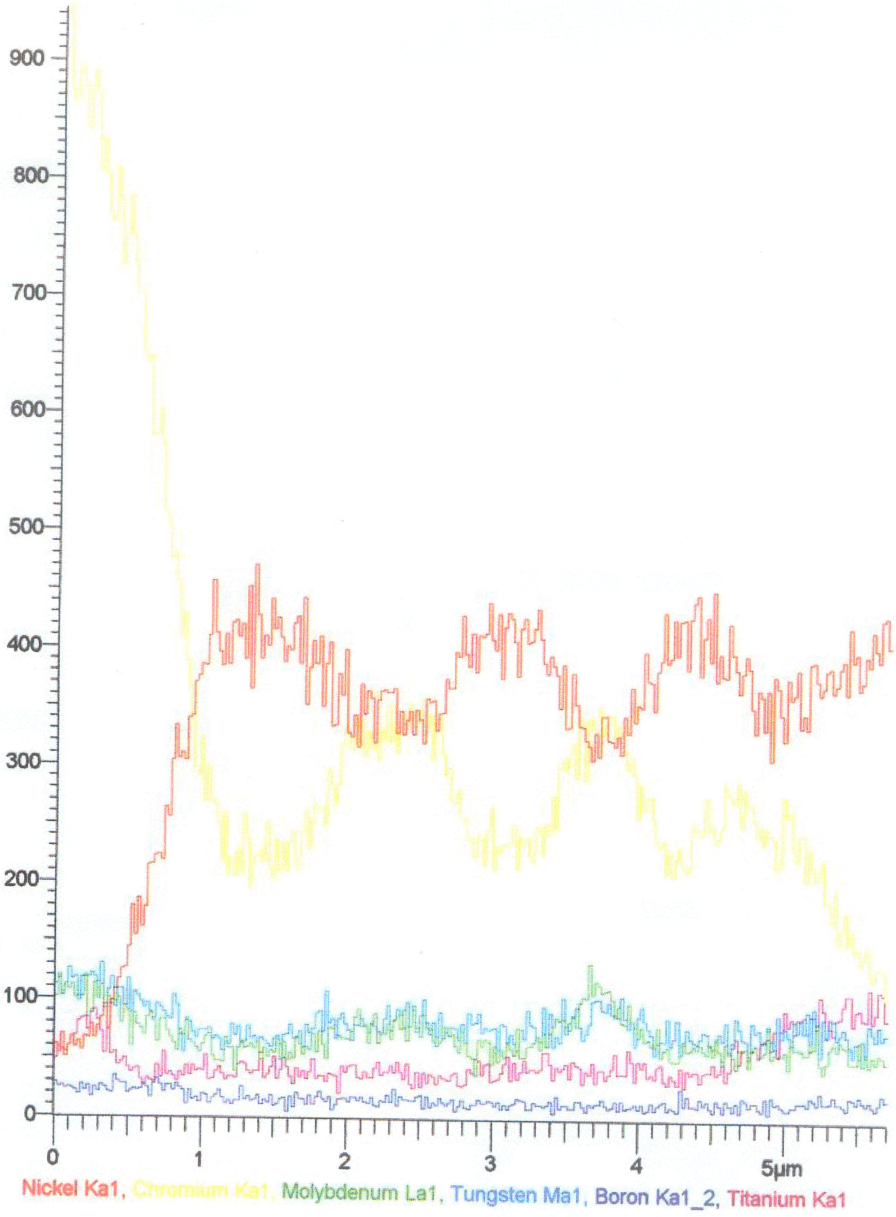

f

Figure 4. 8 (c & d) EDS point analysis and (e & f) Line scan of boride phases observed at the Substrate- Braze Interface of 1070°C Brazed 75µm Joint.

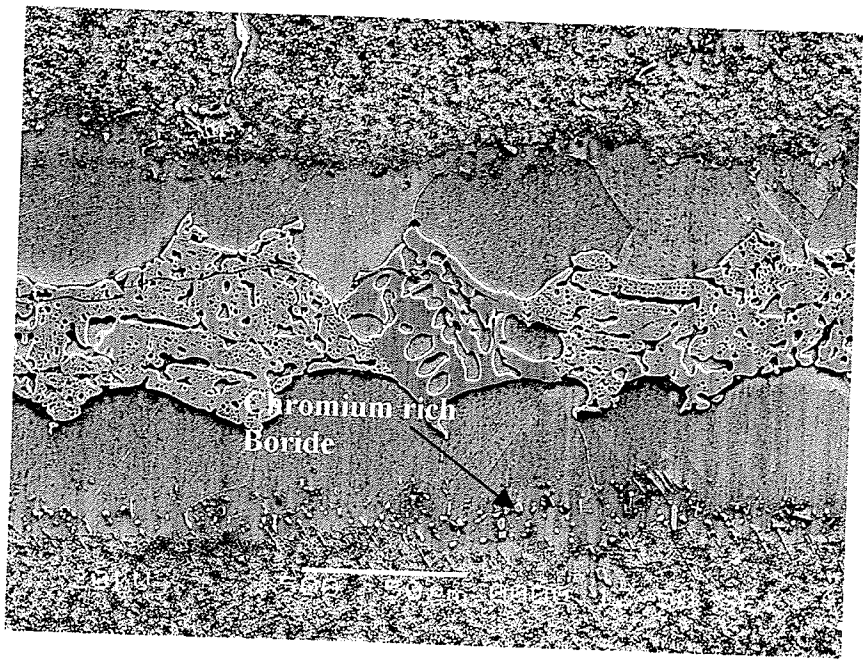

Figure 4. 9 Microstructure of 1100°C brazed Joint.

Element	Atomic %
Ti	0.25
Cr	83.76
Co	2.16
Ni	6.55
Mo	4.28
W	2.99

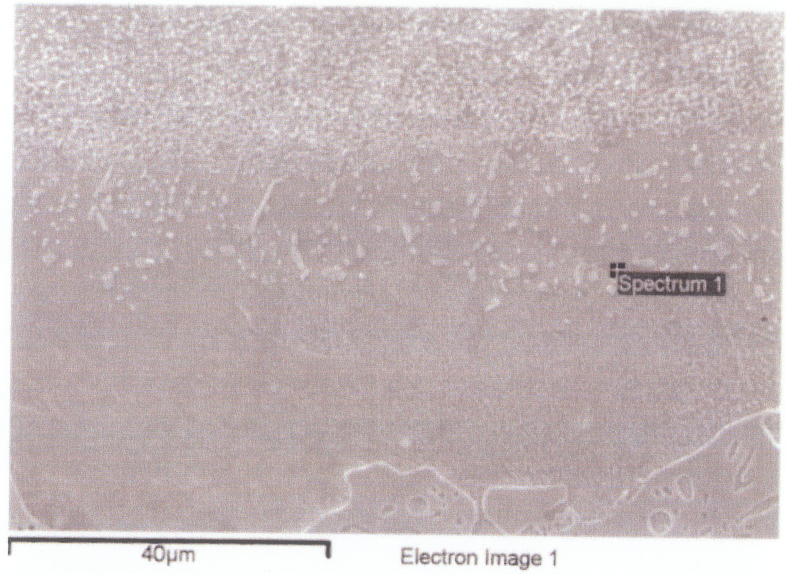

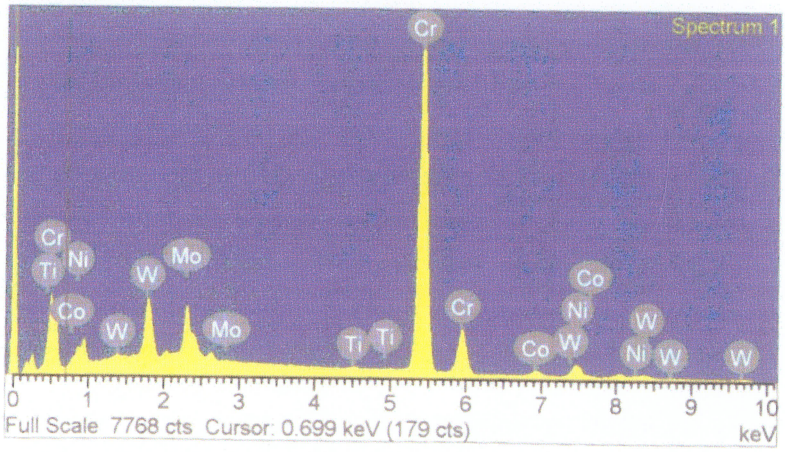

Figure 4.10 EDS analysis of precipitates observed at the melt zone of 1100°C 75µm brazed joint.

4.2.2.3 Microstructure of Joint Brazed at 1130°C

Microstructures of joints fabricated at 1130°C, differed substantially from those observed after bonding at 1070°C and 1100°C. The size of residual liquid eutectic width was least at this bonding temperature, affirming highest diffusion rate. Nevertheless, as shown in figure 4.11 (a), it is evident that 60 mins holding time is insuffient to solidify the liquid interlayer isothermally, even as the eutectic width decreased more rapidly with brazing time. The most striking difference was the absence of angular nickel rich boride precipitates as markedly observed in 1070°C bonds. Globular chromium rich boride deposits were observed along base alloy grain boundaries adjacent to the initial substrate - liquid interface, as well within the melt-back zone of the braze seam shown in figure 4.11 (a). EDS composition analysis comparison of this phase and the surrounding austenitic γ solid solution phase confirmed a relatively higher concentration of Boron in the Chromium rich phase as shown in figure 4.12.

4.2.3 Analysis of Centreline Eutectic Phase of "NB 150" Brazement

Ohsasa et al [60] in their experiment on numerical modelling of transient liquid phase bonding of Nickel using Ni – B – Cr ternary filler metal calculated using Scheil simulation, the solidification behaviour of the residual liquid during cooling stage. They reported that a ternary invariant centreline eutectic phase consisting of Ni base FCC solid solution phase, Ni boride (Ni_3B) and Cr boride (CrB) formed at 1097°C.

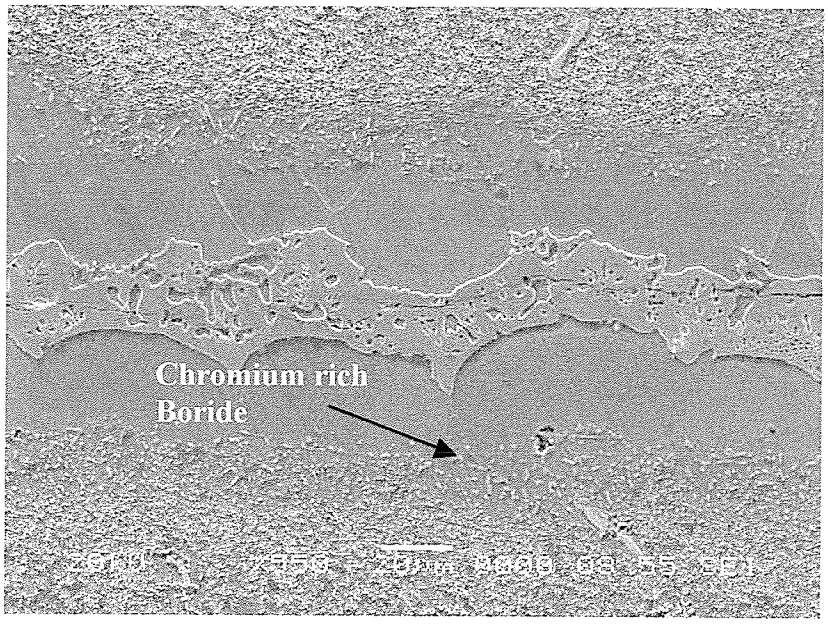

a

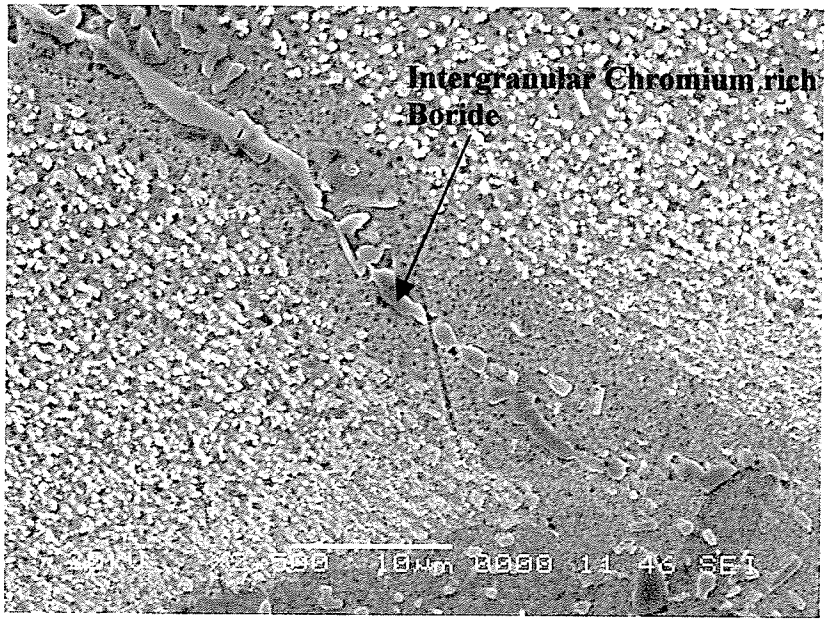

b

Figure 4.11 (a) Microstructure of 1130°C Brazed 75μm Gap for 60 mins showing Chromium rich Borides at the Melt-Back Zone and (b) along the Base Alloy Grain Boundary.

Element	Atomic %
Ti	1.07
Cr	74.47
Co	2.50
Ni	6.13
Mo	8.60
W	7.23

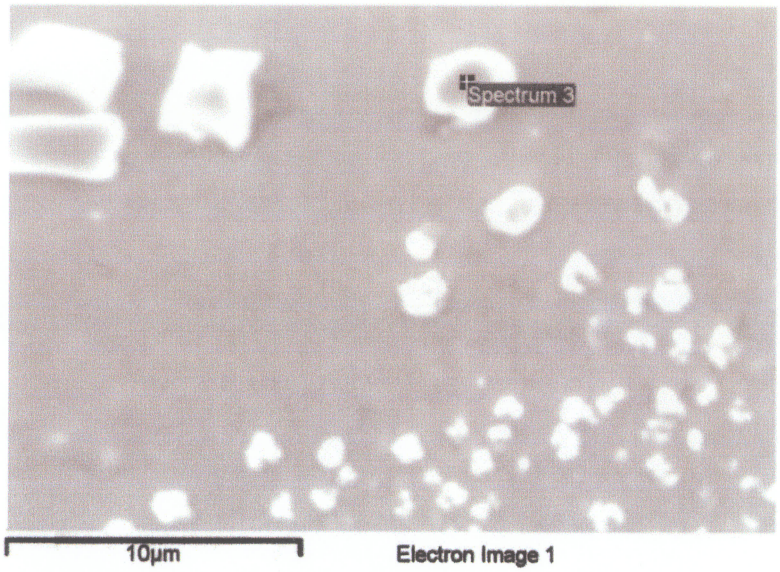

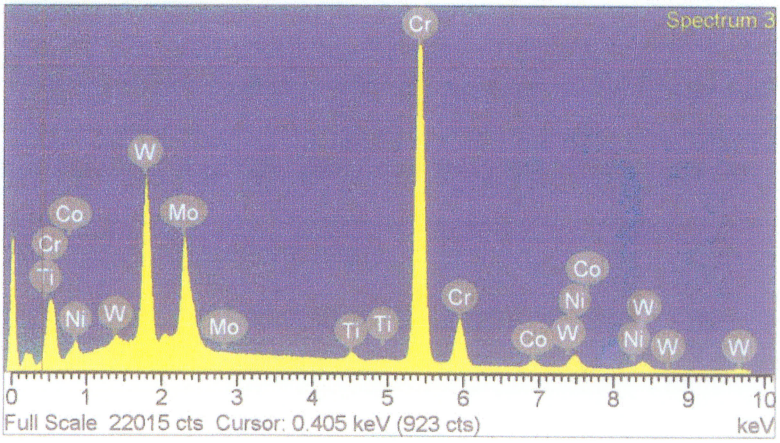

a

Figure 4.12 (cont…)

Element	Atomic %
Al	7.09
Ti	3.27
Cr	16.43
Co	9.26
Ni	61.27
Nb	0.34
Mo	0.81
Ta	0.45
W	1.08

b

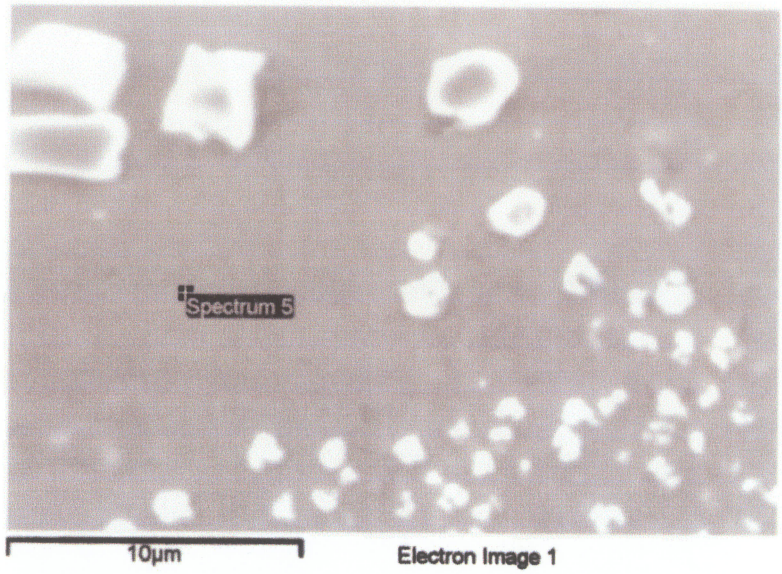

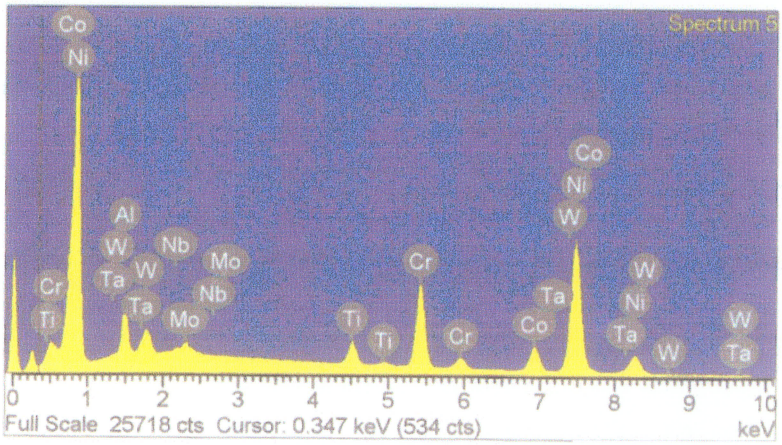

Figure 4.12 (cont...)

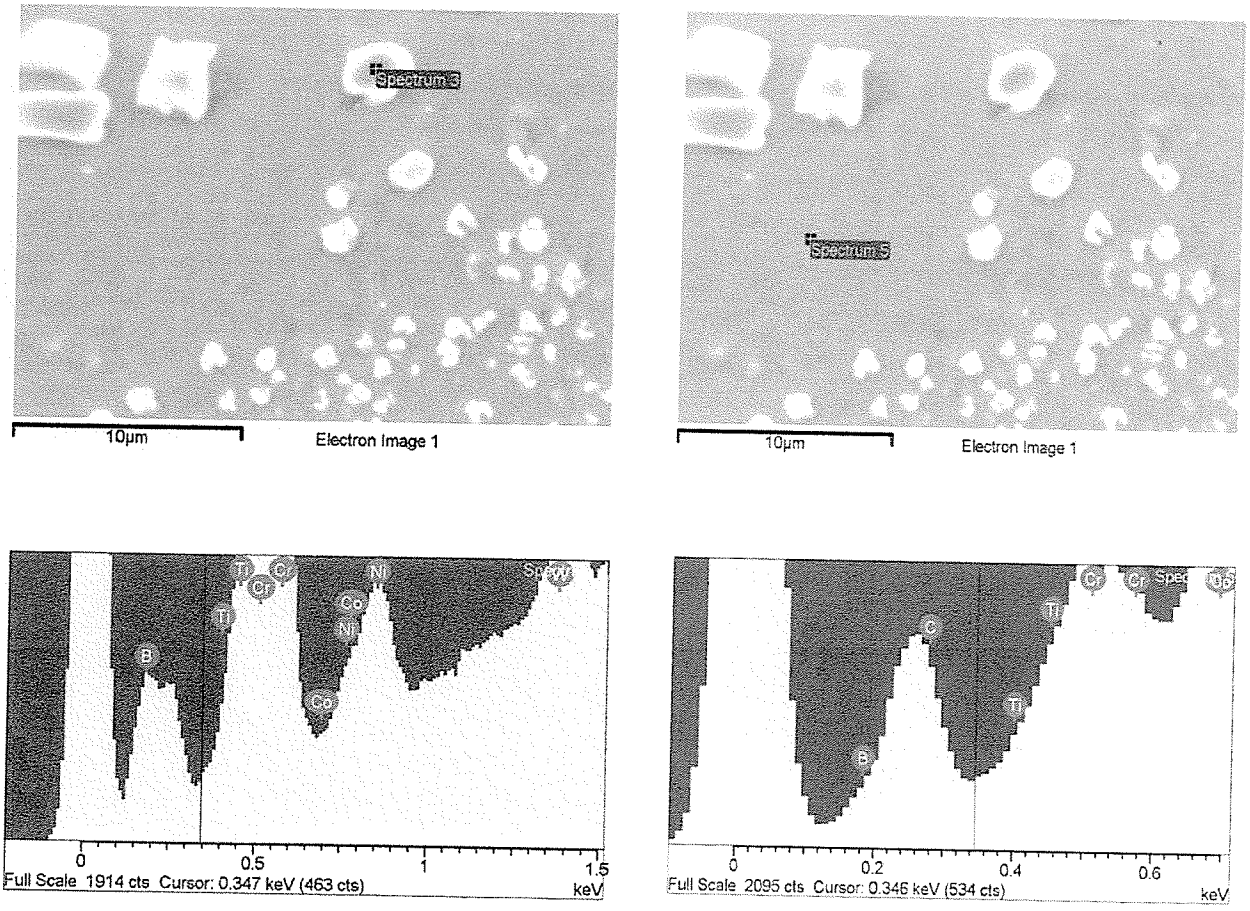

Figure 4.12 { (a), (b), (c) & (d) } EDS Analysis Comparison of Boride Phase and Braze Austenistic Solid Solution Phase confirming segregation of Boron into Second Phase during Bonding.

The numerical modeling was performed by combining thermodynamic calculations with thermo-calc software and diffusion analysis by a finite difference method. Simulation showed that during the solidification of residual liquid in a sample held at 1100°C, Ni rich FCC phase formed as the primary phase, followed by eutectic reaction $L \rightarrow FCC + Ni_3B$ at 1042°C. Solidification was reported to be complete with a ternary eutectic reaction $L \rightarrow FCC + Ni_3B + CrB$ at 997°C. Figure 4.13 [60] shows the calculated Ni-rich corner of the Isothermal section of the Ni-Cr-B ternary system at 1100°C and 1070°C. Experimental results were in good agreement with the predicted structure.

In the present work, the centreline eutectic phase resulting from solidification of the residual liquid insert during cooling was examined by SEM operating in secondary and backscatter electron mode, X-ray mapping and EDS composition analysis. The analysis, as demonstrated in figure 4.14, revealed a ternary eutectic phase comprising of: Nickel base solid solution phase, (similar to pro-eutectic solid solution phase formed from isothermal solidification of the liquid insert), nickel rich boride and chromium rich boride phases. The average hardness of the eutectic phase, measured by microhardness tester, was 720VHv. This is a hard and brittle phase and as stated earlier, is likely to have a profoundly detrimental influence on joint properties. This is demonstrated in figure 4.15 where the phase is seen to offer a preferred low resistance path to crack propagation. Besides, it was observed to be selectively etched by 10g $CuCl_2$ + 40 ml HCl + 60 ml methanol solution (figure 4.16) which indicates its degrading impact on corrosion resistance of the brazed joint.

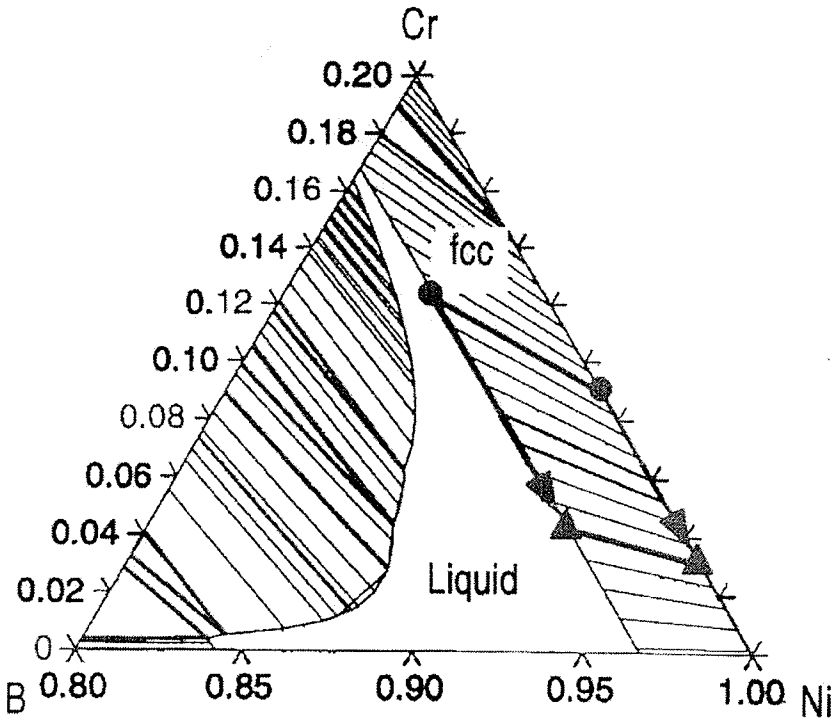

a)

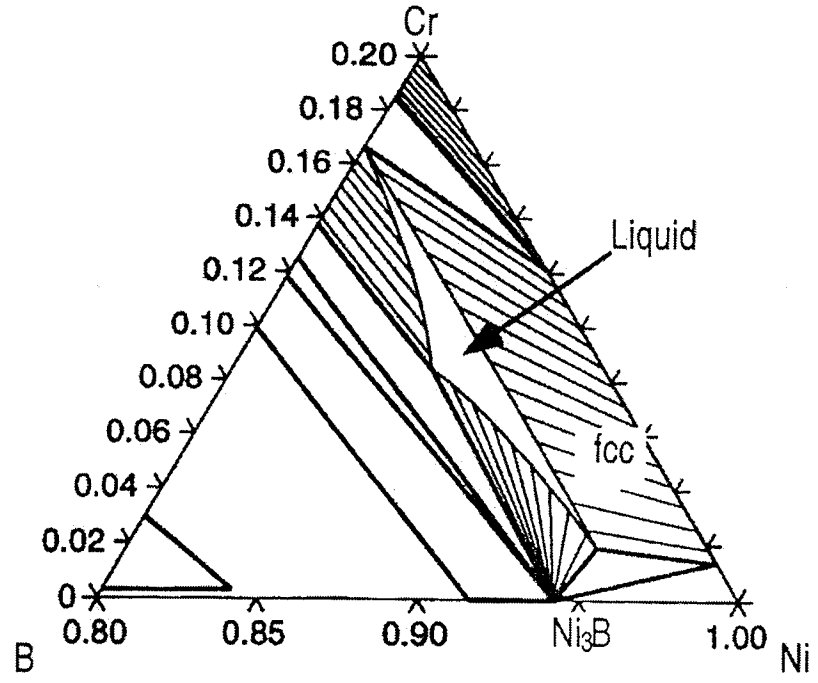

b)

Figure 4.13 Isothermal cross sections of Ni-Cr-B ternary Phase Diagram at (a) 1100°C & (b) 1070°C [60].

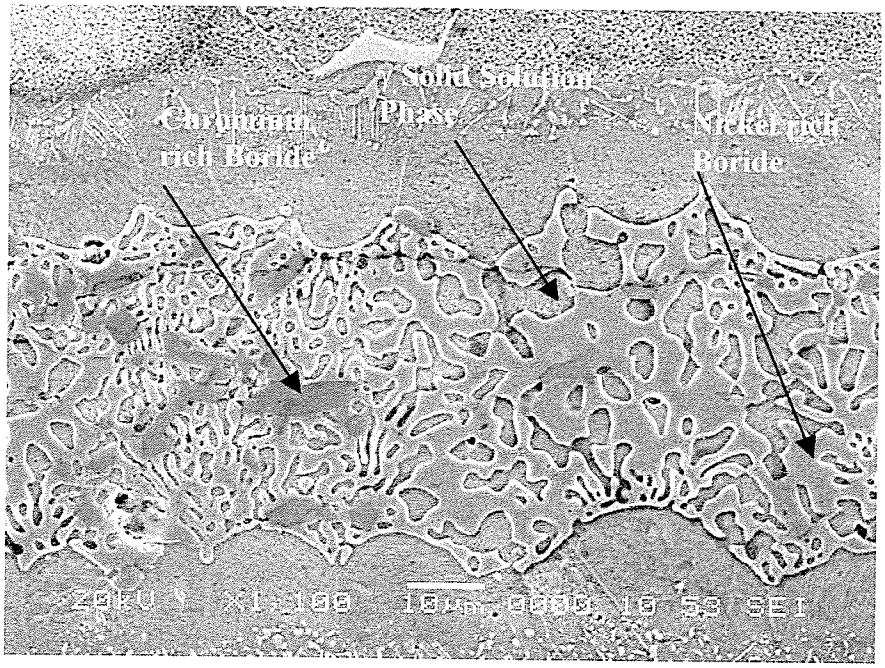

a

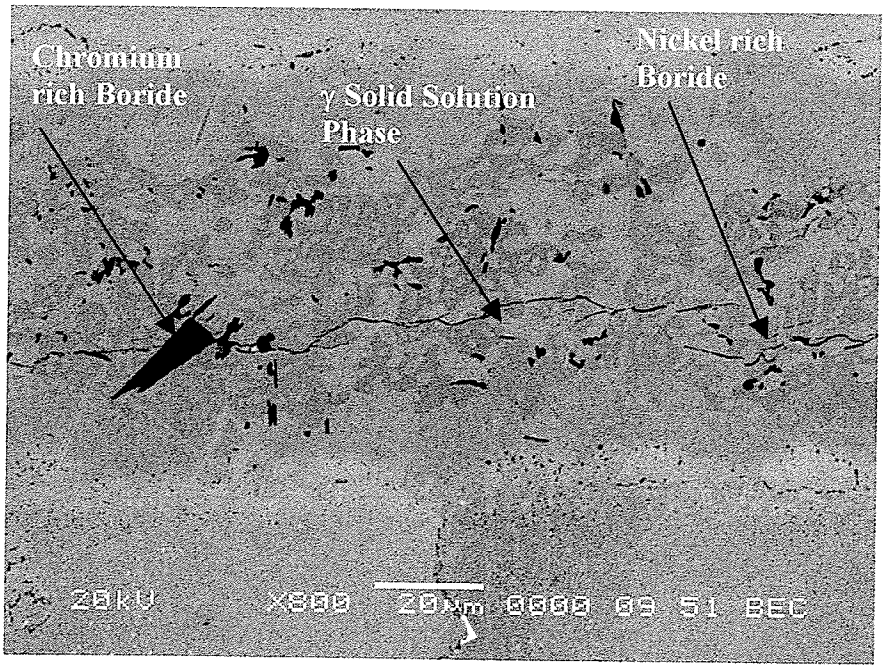

b

Figure 4.14 SEM (a) Secondary Electron Image (b) Back Scatter Electron Image of Centreline Ternary Eutectic Phase in "NB 150" Brazement.

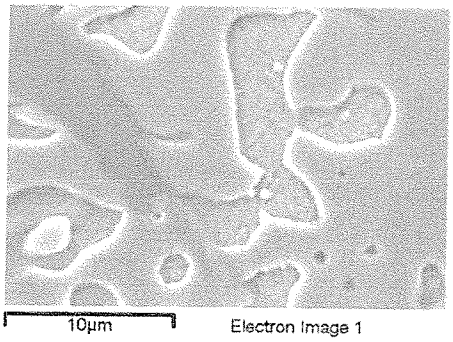

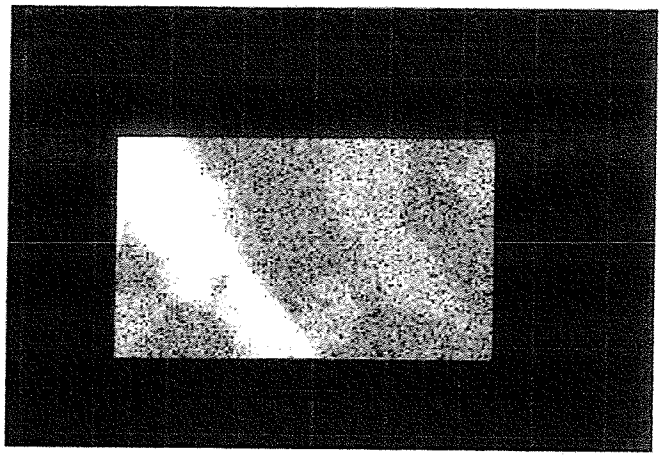
Chromium Ka1

Figure 4.14 (c) X-ray mapping of centerline ternary eutectic showing distribution of Chromium and Nickel.

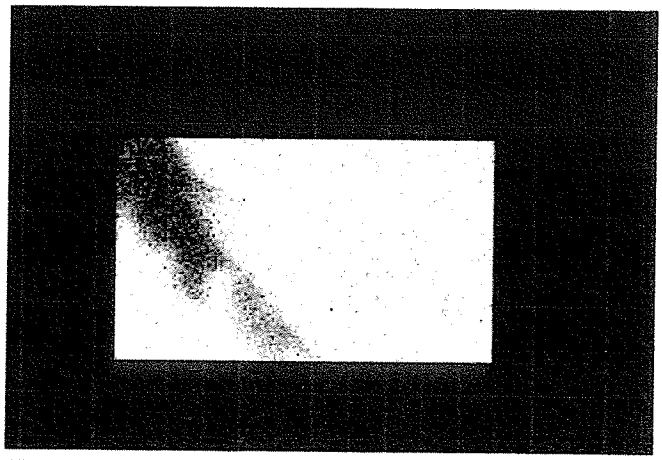
Nickel Ka1

Element	Atomic %
Al	0.04
Ti	0.08
Cr	93.98
Co	0.41
Ni	1.88
Mo	2.32
W	1.29

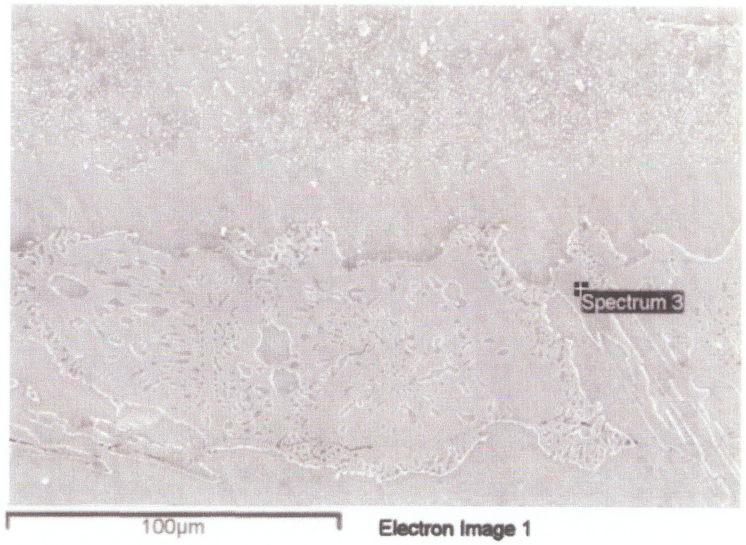

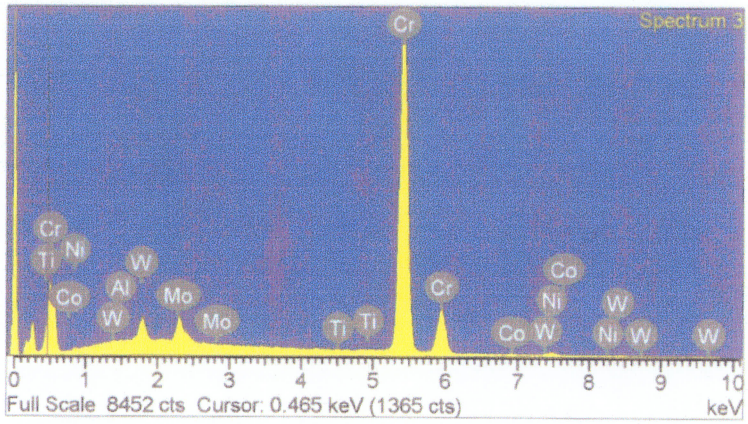

d

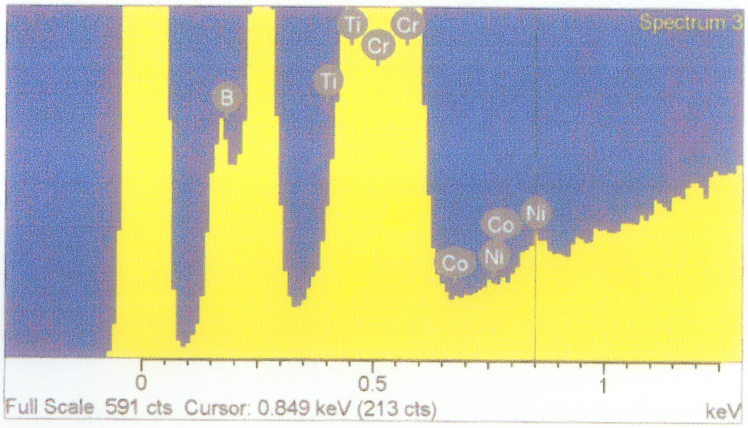

Figure 4.14 (cont…)

Element	Atomic %
Al	0.81
Ti	1.63
Cr	11.40
Co	2.68
Ni	82.02
Nb	0.41
Mo	0.27
Ta	0.47
W	0.29

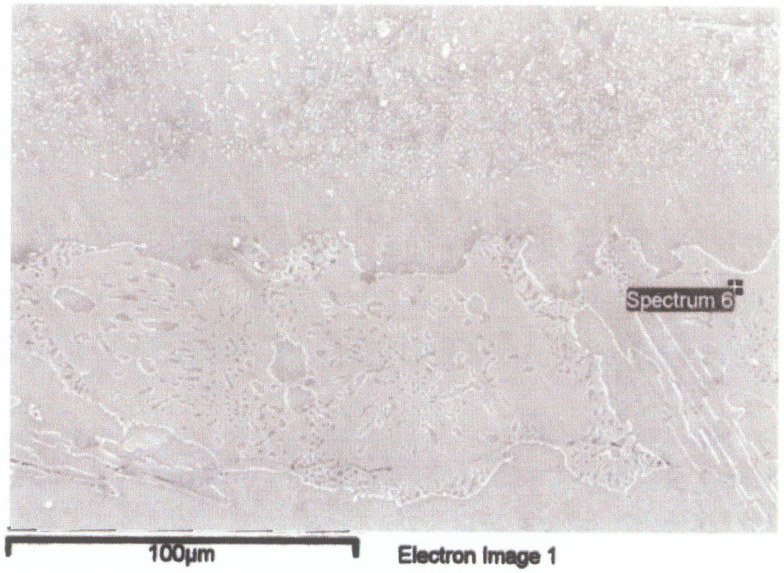

e

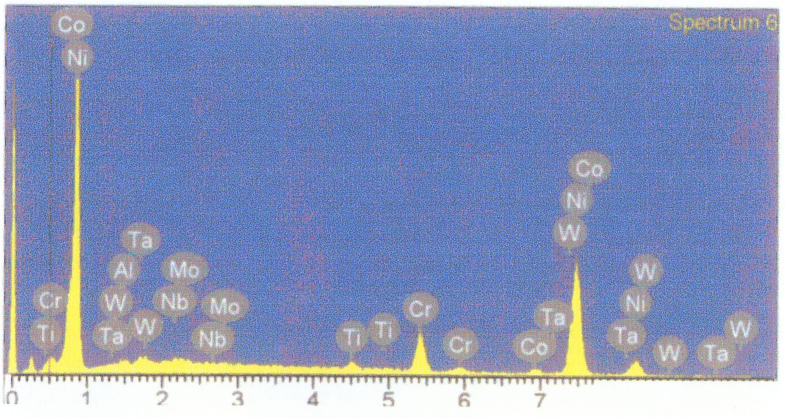

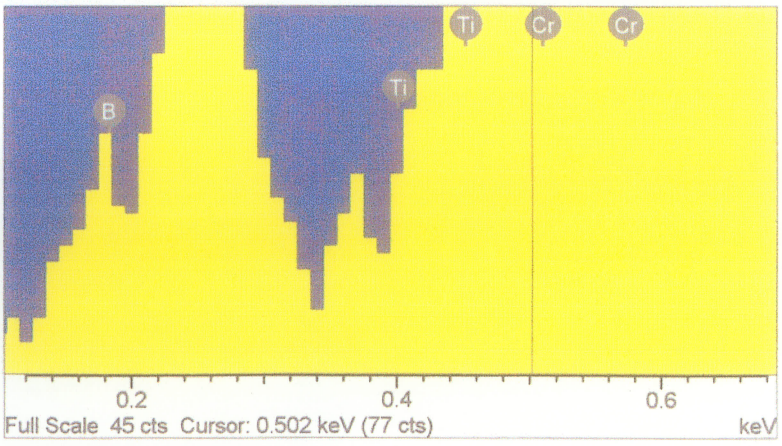

Figure 4.14 (cont…)

Element	Atomic %
Al	1.34
Ti	0.38
Cr	18.54
Co	2.39
Ni	76.50
Mo	0.30
W	0.54

f

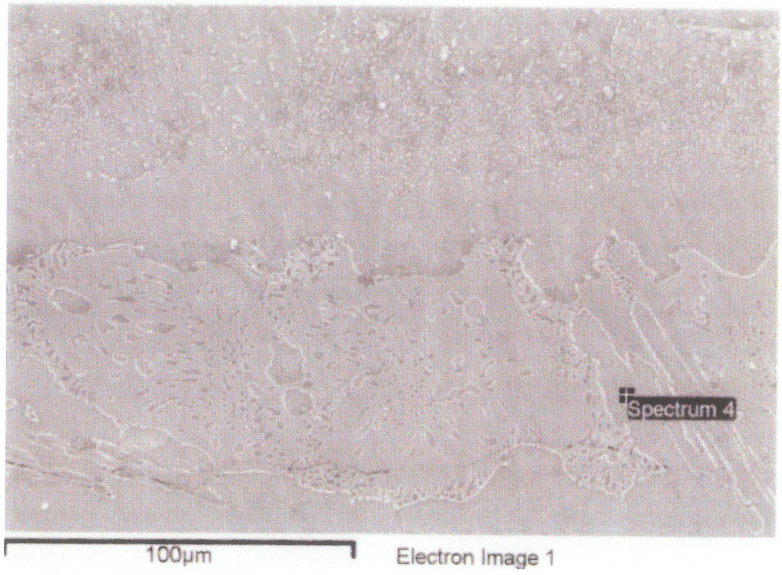

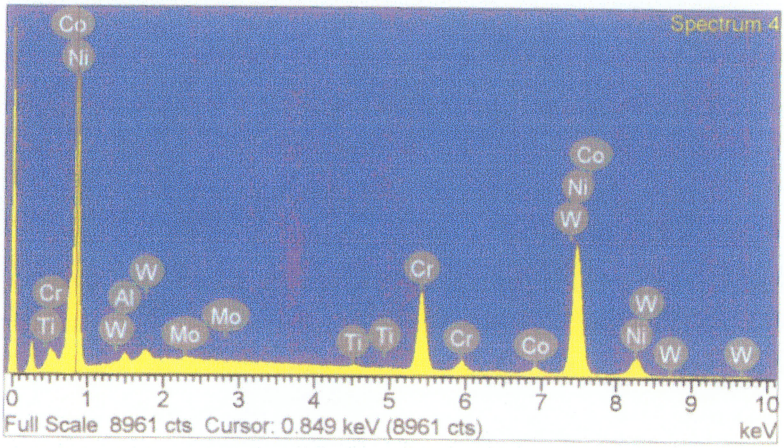

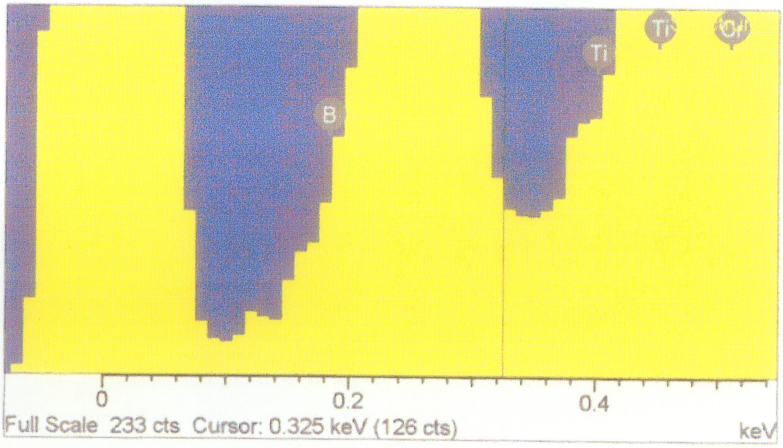

Figure 4.14 (d), (e) & (f) EDS Composition Analysis of the Centreline Ternary Eutectic Phase in "NB 150" Brazement.

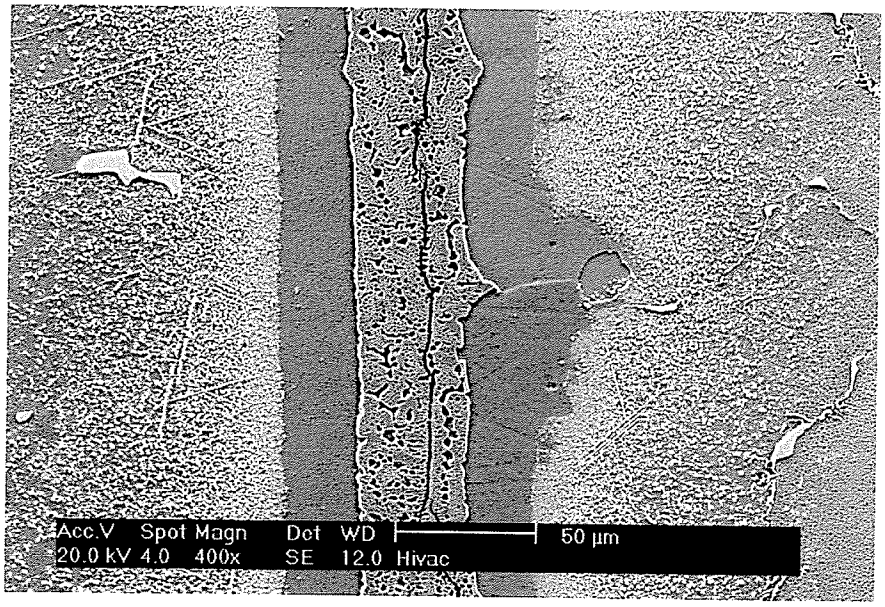

Figure 4.15 The Centreline Eutectic of "NB 150" Brazement Serving as Low Resistance Path for Crack Propagation.

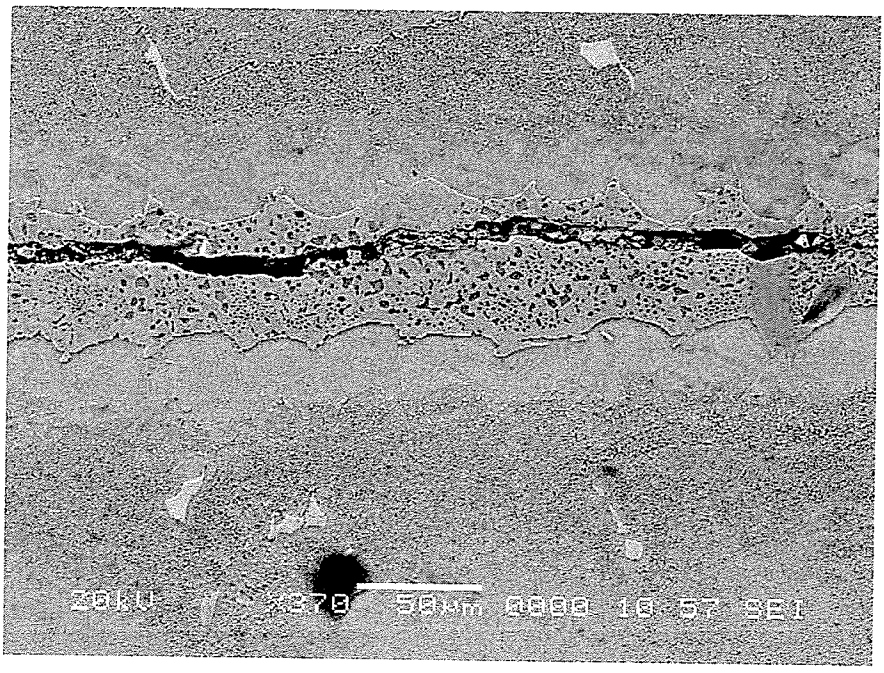

Figure 4.16 Selective Etching of "NB 150" Brazement Eutectic Phase.

4.2.4 Effect of Brazing Temperature on Boride Formation

Gale et al [32] in their research work compared the formation of Ni_3B phase above and below the Ni-B binary eutectic temperature. Using a ternary Ni-Si-B insert, in pure Nickel substrate bonding, marked precipitation of Ni_3B was observed in the vicinity of original position of substrate – insert interface, and separated from the eutectic mixture by primary pro-eutectic Nickel solid solution phase was reported.

In this work, using "NB 150" filler, boride formation at two brazing temperatures 1065°C & 1150°C were investigated since they are clearly below and above the range of quoted Ni-B eutectic temperature in the literature (1080°C - 1140°C). In addition to centreline ternary eutectic phase, bands of irregular shaped Nickel rich borides were observed on the braze side of the substrate-braze interface in 1065°C joint (figure 4.17). There was a significant difference in 1150°C bond as such a boride precipitation was not observed in the microstructure (figure 4.18).

In the Cr-B and Ni-B phase diagrams, shown in figure 4.19 [61], the lowest Cr-B eutectic temperature is observed to be 1500°C while in Ni-B the highest eutectic temperature is 1111°C. Consequently, at 1150°C only chromium rich boride is likely to form since the operating temperature is higher than the temperature at which a Nickel boride could precipitate. This correlates very well with the observed result, that nickel rich boride was not observed in 1150°C joint (figure 4.18).

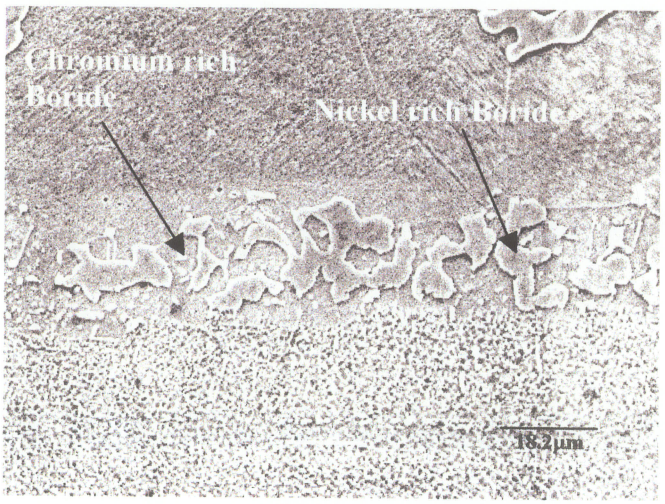

a

Element	Atomic %
Al	1.81
Ti	5.88
Cr	10.32
Co	7.33
Ni	73.58
Mo	0.02
W	1.06

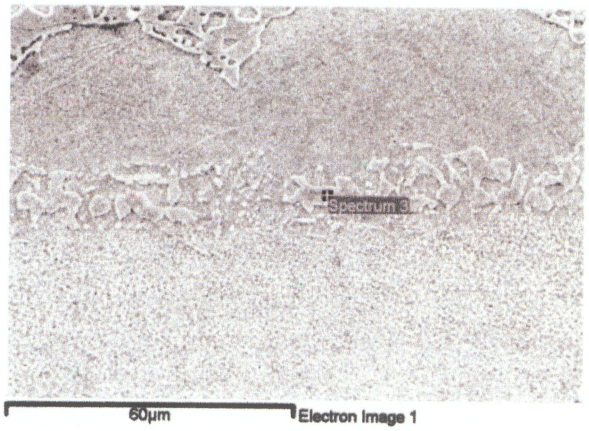

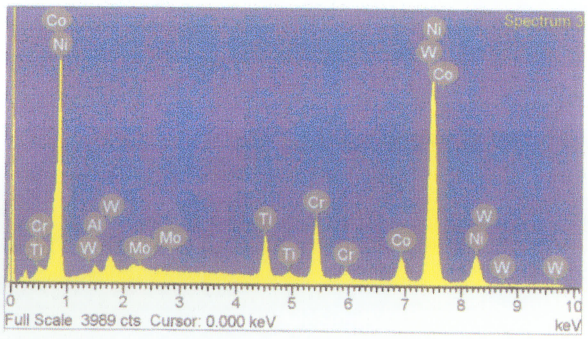

b

Figure 4.17 (a) Microstructure and (b) EDS Analysis of 1065°CBrazed 60µm Gap showing Precipitated Angular Nickel rich Boride.

Figure 4.18 Microstructure of 1150°C Brazed 60µm Gap showing absence of Nickel rich Boride Phase.

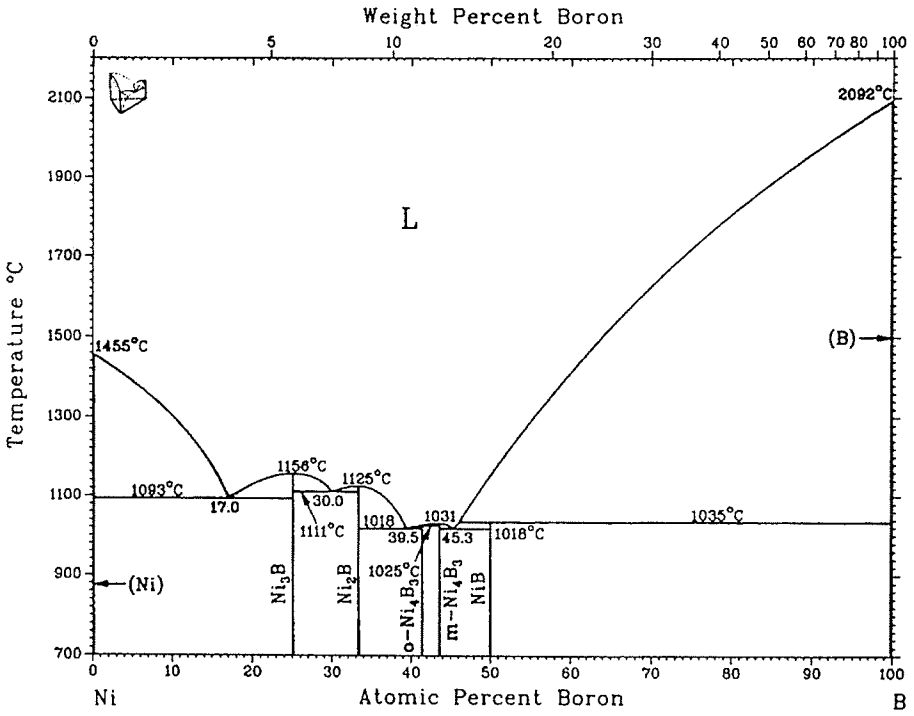

a

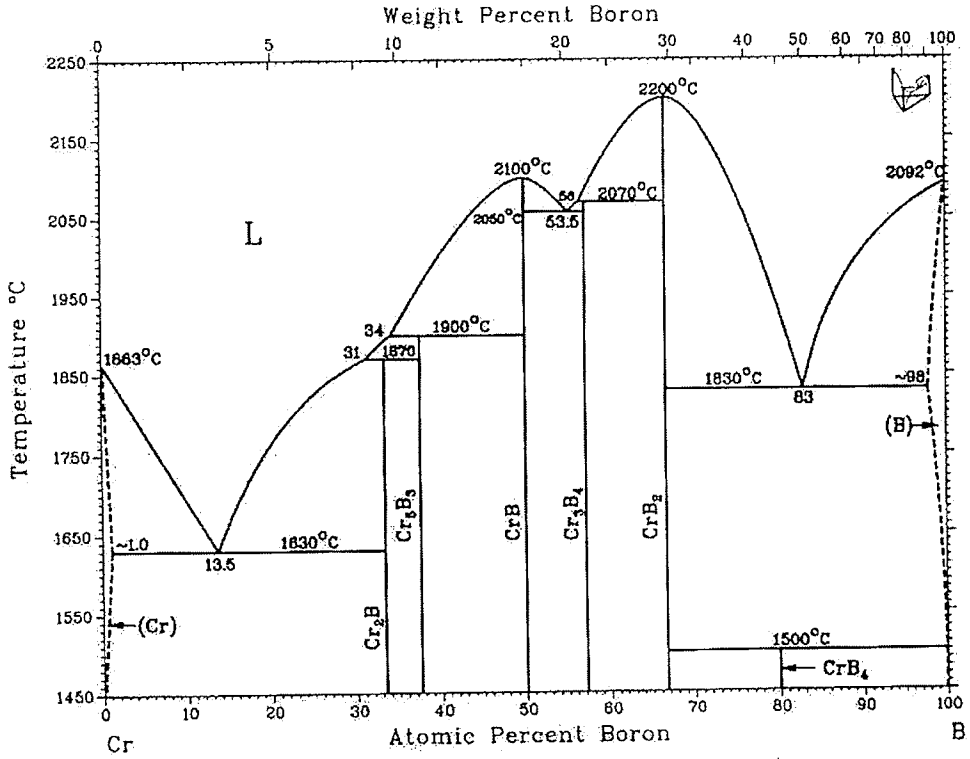

b

Figure 4.19 Binary Phase Diagram for (a) Ni - B, (b) Cr- B Systems [61].

Any tendency to form such boride phases during holding at the bonding temperature is of a significant importance as their formation is not predicted by standard TLP bonding models and could be deleterious to the bond properties. Presence of Nickel rich boride along the base alloy grain boundaries and at the substrate-joint interface could reduce the service temperature of bonded material, considering the eutectic temperature range (1018°C - 1111°C) of Ni-B phase diagram (figure 4.19 [61]). More so in this case as the boride phase is a more complex boride (containing other alloying element) with possibly a further reduced melting temperature, which is potentially detrimental to the joint's creep properties.

4.2.5 Diffusion of Base Alloying Elements into Brazed Joint

Diffusion of major strengthening base alloy elements into braze seam during bonding is fundamental to producing high strength joint capable of withstanding elevated temperature service conditions. Diffusion of Al, Ti and Co were investigated at brazing temperatures 1070°C, 1100°C, & 1130°C for 10 mins, 20 mins, 30 mins & 60 mins holding time. Al and Ti were chosen because these are the key elements in γ' (Ni_3 Al, Ti) which is the principal strengthening phase of the base alloy, and Co, because it is a solid solution strengthening element. Their diffusion into the joint is crucial for high temperature applications, considering the fact that the filler alloy initially does not contain any of these vital alloying elements.

The atomic composition of the elements in the pro-eutectic phase of "NB 150" brazement were measured by EDS-SEM and plotted against holding time at each bonding temperature, as shown in figure 4.20 (a, b & c). It is apparent from the plot that diffusion of the elements increased with operating temperature and longer the holding time the more quantity diffused. At all the bonding temperatures, Co had the highest amount of diffused, followed by Al and then Ti. This can be explained by the higher chemical potential of Co and its atomic size is (125 pm) almost the same as that of Ni (124 pm). Furthermore Ti solute atoms are 34% larger than the Al atoms, therefore Al diffuses faster than Ti. Also demonstrated in the plot, is the marked effect of holding time on quantity diffused with increased temperature. However too high a bonding temperature is undesirable, as it is both uneconomical and potentially detrimental to the base alloy properties (e.g. induced grain growth).

4.3 Microstructural analysis of "DF3" Brazement

The SEM micrograph shown in figure 4.21 demonstrates the effect of gap size on microstructural features of a variable gap (0 – 125μm) joint brazed with "DF3" alloy at 1195°C for 20 minutes and diffused at 1065°C for 4hrs. Between the initial gap size of 0 - 25μm, the microstructure consists mainly of γ solid solution phase. As the gap size increased above 25μm size, second phase precipitates formed within the austenitic gamma matrix along the joint, with their volume fraction increasing with gap width.

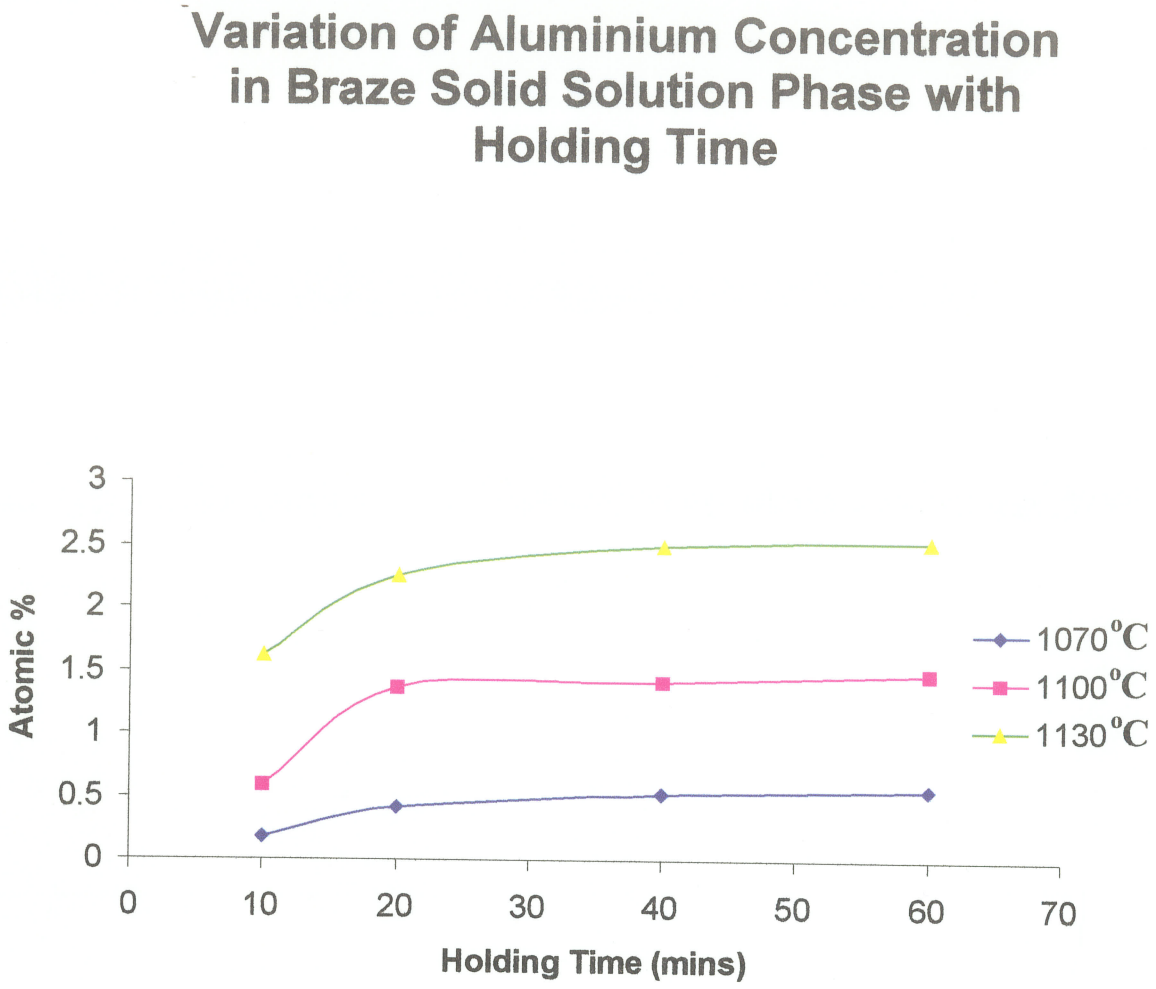
Variation of Aluminium Concentration in Braze Solid Solution Phase with Holding Time
Atomic %
3
2.5
2
1.5
1
0.5
0
0
10
20
30
40
50
60
70
Holding Time (mins)
1070°C
1100°C
1130°C

Figure 4.20 (a)

Variation of Titanium Concentration in Braze Solid Solution Phase with Holding Time

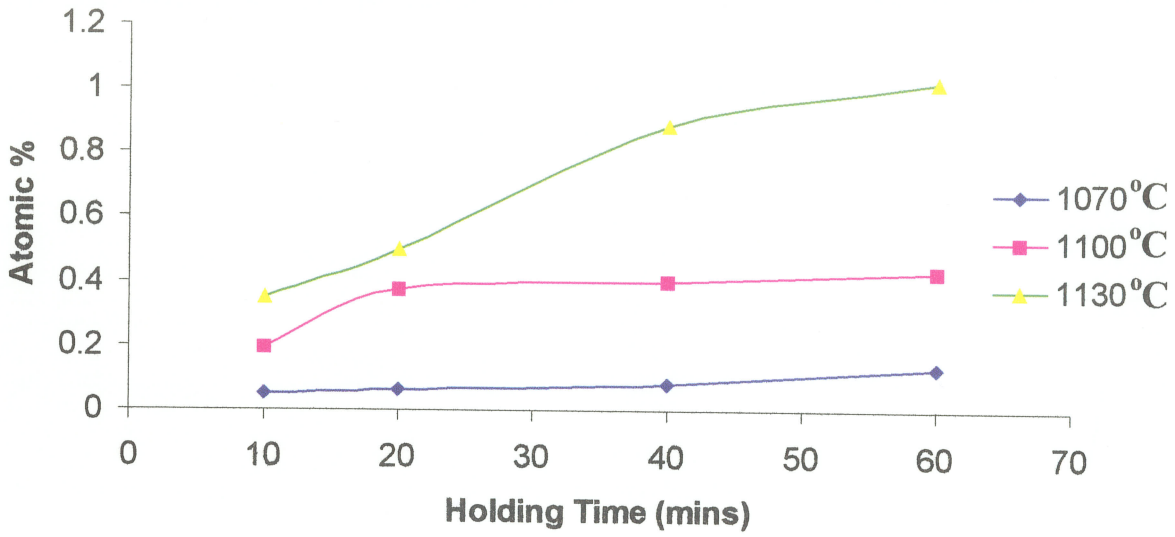

Figure 4.20 (b)

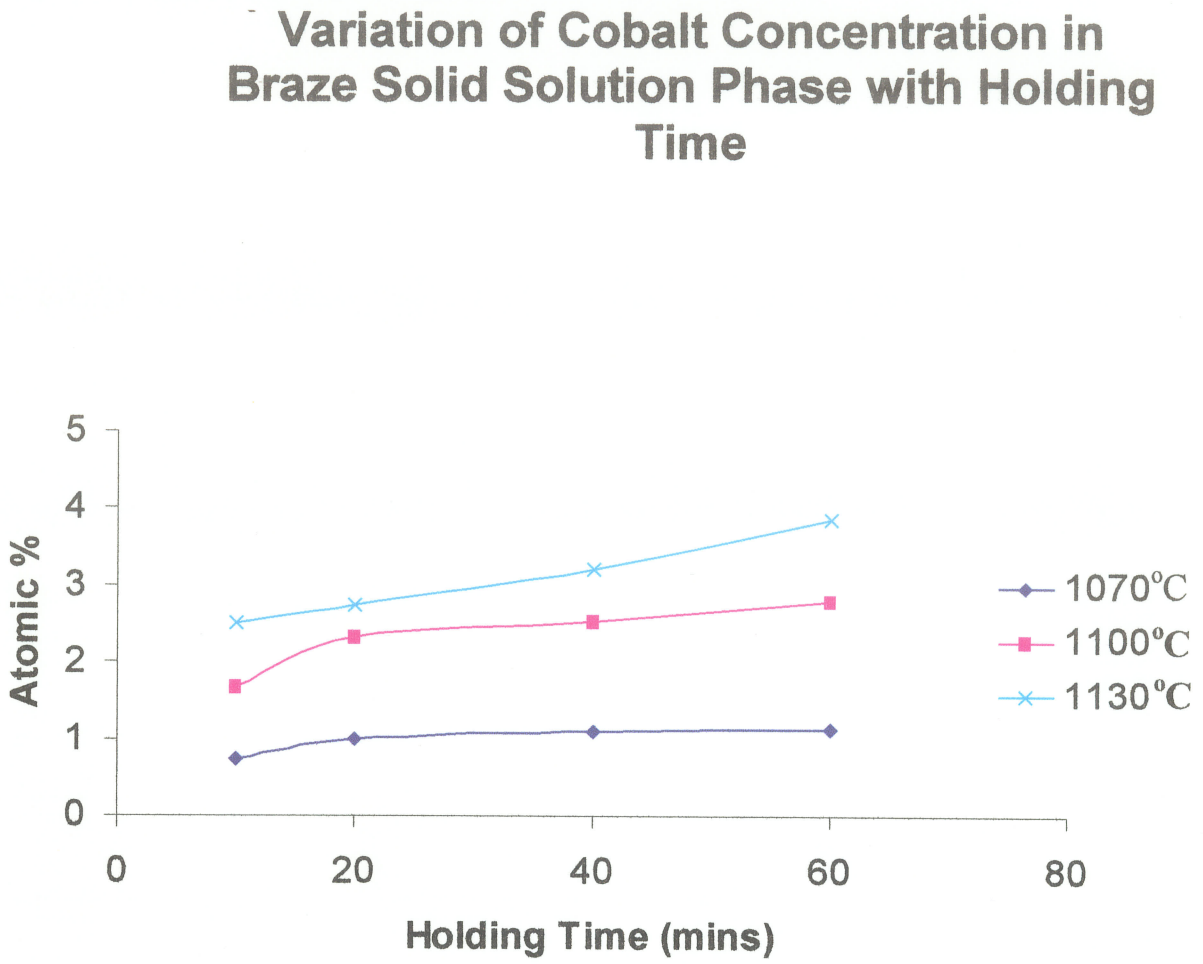
Variation of Cobalt Concentration in Braze Solid Solution Phase with Holding Time
Atomic %
0
1
2
3
4
5
0
20
40
60
80
Holding Time (mins)
1070°C
1100°C
1130°C

Figure 4.20 (c)

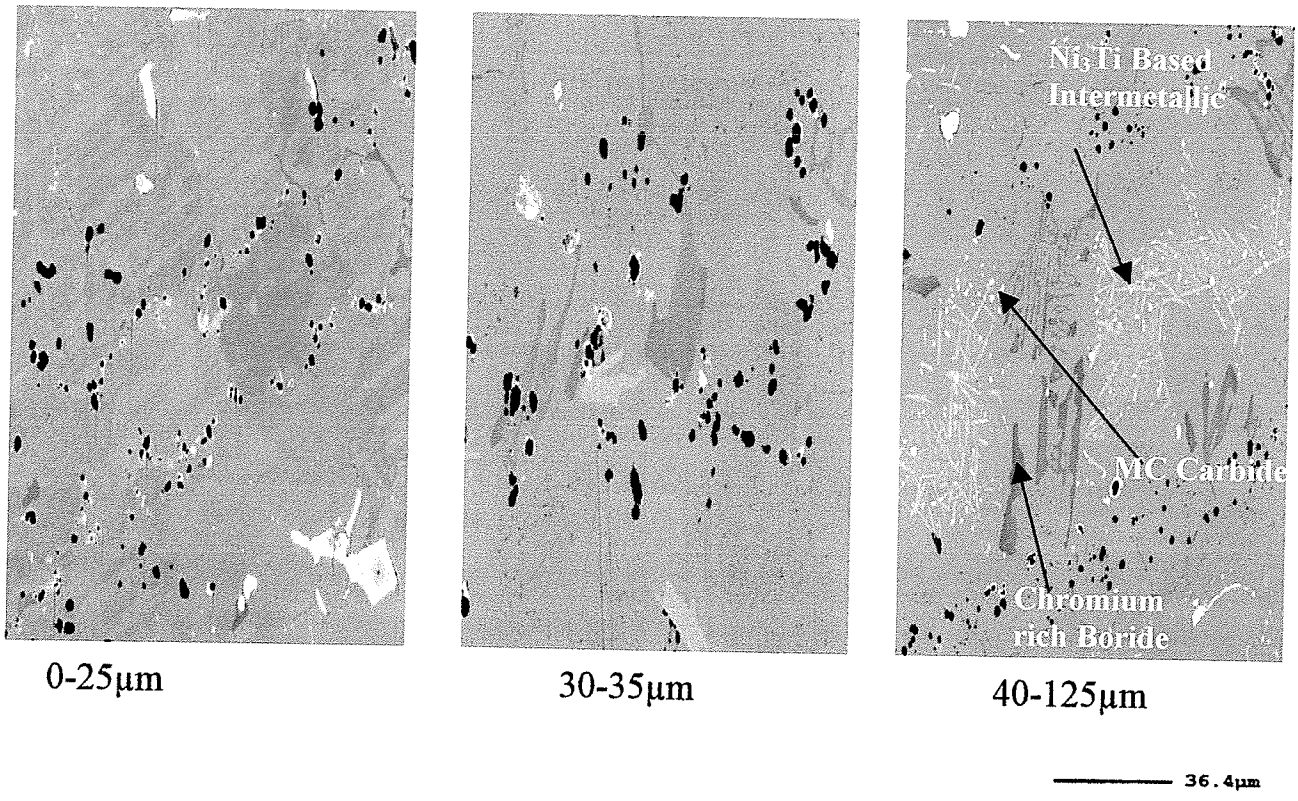

Figure 4.21 SEM Micrograph showing Variation of Microstructure of "DF3" Brazement with Gap Size.

Quantitative chemical analysis by EDS-SEM revealed three different types of precipitates. They were MC carbides, chromium base boride and elongated Ni_3Ti based intermetallic phase.

The hardness of central area of the brazement was measured using microhardness tester on polished samples. Figure 4.22 shows the variation in average centre region hardness with gap width. It is evident from the plot that average hardness increased with increase in gap width, which is a reflection of the presence of second phases transversely across the centre area of the joint. Notably, the hardness of the solid solution phase in the "DF3" brazement was found to be higher than that observed in "NB 150" brazed joint. This can be explained by the fact that the strength of a single phase depends on the amount of solid solution strengthening - elements it contains, and since "DF3" alloy, initially contained significant amount of these elements (Co – 20%, Cr – 20% & Ta 3%), its solid solution phase is thus, expected to exhibit higher hardness. The average hardness of the second phases was found to be more than 200% of the base alloy.

4.3.1 Analysis of Second Phase Precipitates of "DF3" Brazement

Compared to "NB 150" filler, residual "DF3" liquid transformed into three different precipitates (MC carbide, Chromium rich boride and Ni_3Ti based intermetallic phase) along the joints centreline γ austenitic matrix (figure 4.23). The MC carbide particles that formed in the joint area were found to have composition that was similar to those present at the base alloy grain boundaries.

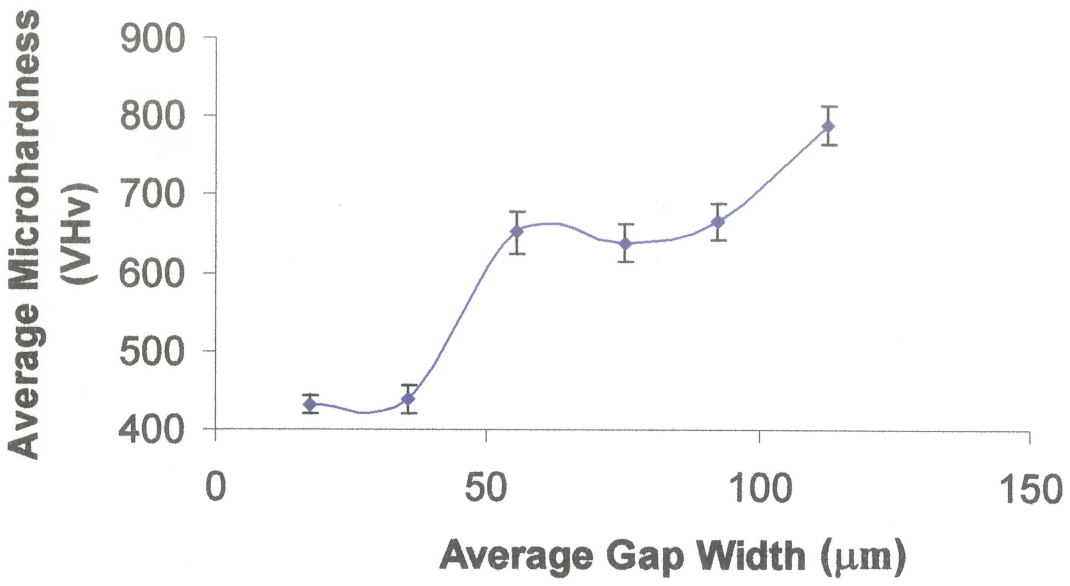

Figure 4.22 Variation of "DF3" Brazement Centre-Area Microhardness with Gap Width.

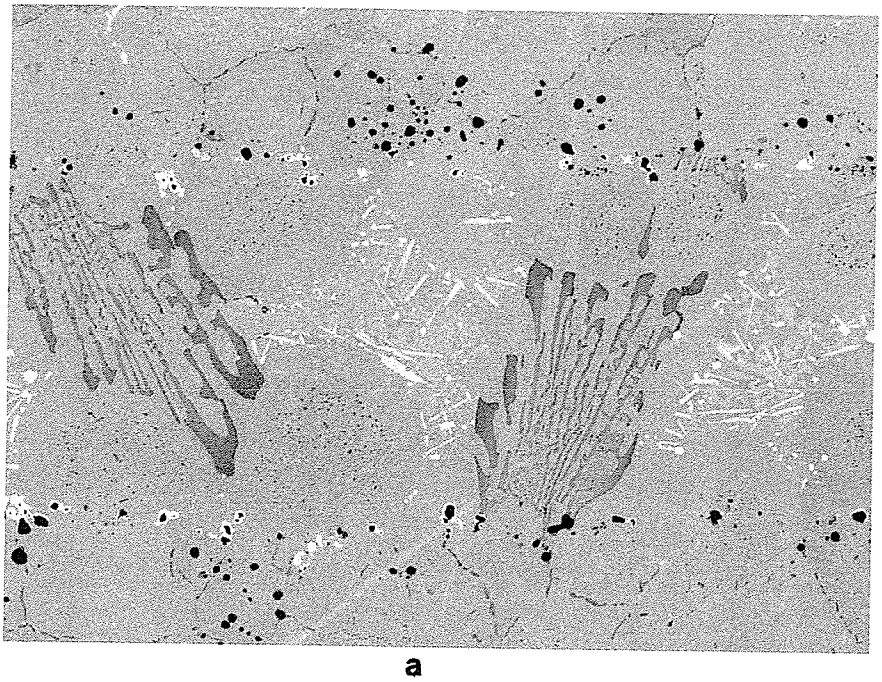

a

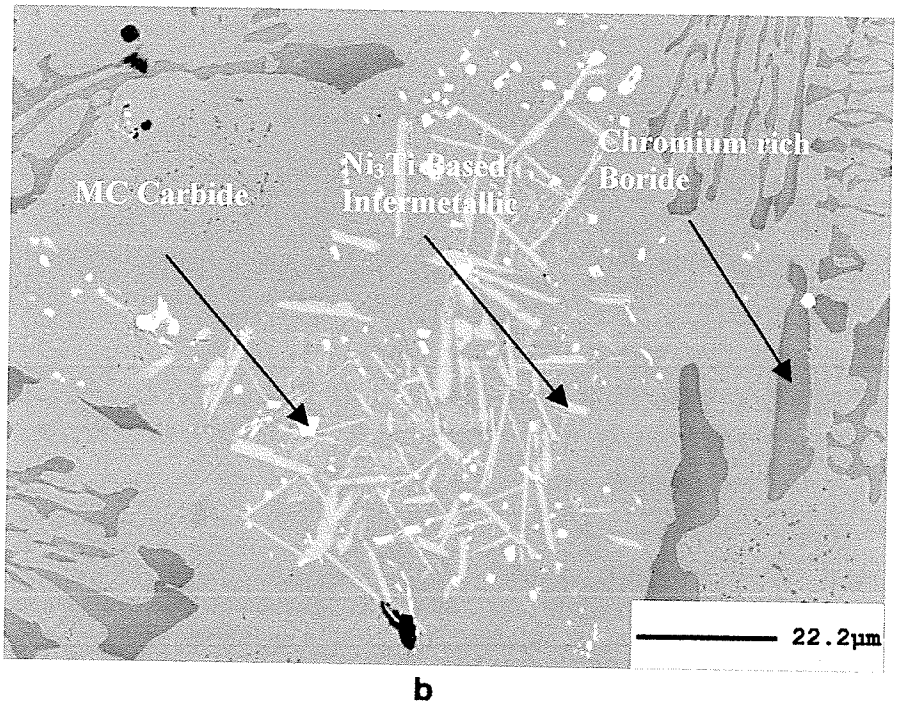

b

Figure 4.23 (a) & (b) Microstructure of "DF3" Brazement showing Second Phase Precipitates from Residual Liquid Braze.

MC Carbide in the Brazement								
Element	Ti	Cr	Co	Ni	Nb	Mo	Ta	W
Atomic %	42.41	2.29	1.77	6.22	14.56	1.23	28.02	2.58
MC Carbide in the Base Alloy								
Element	Ti	Cr	Co	Ni	Nb	Mo	Ta	W
Atomic %	47.87	1.29	0.14	2.95	21.04	2.62	20.06	4.03

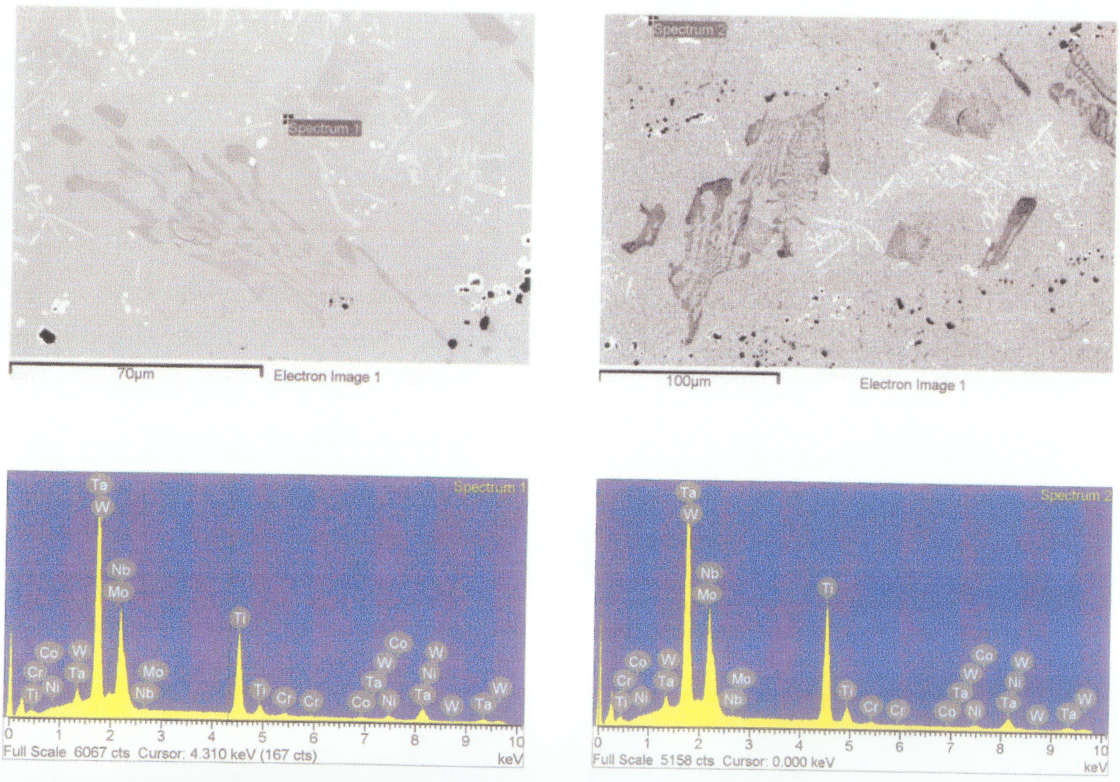

c

Figure 4.23 (cont…)

Element	Atomic %
Al	3.27
Ti	12.55
Cr	3.48
Co	9.22
Ni	65.64
Nb	2.46
Mo	0.39
Ta	2.61
W	0.39

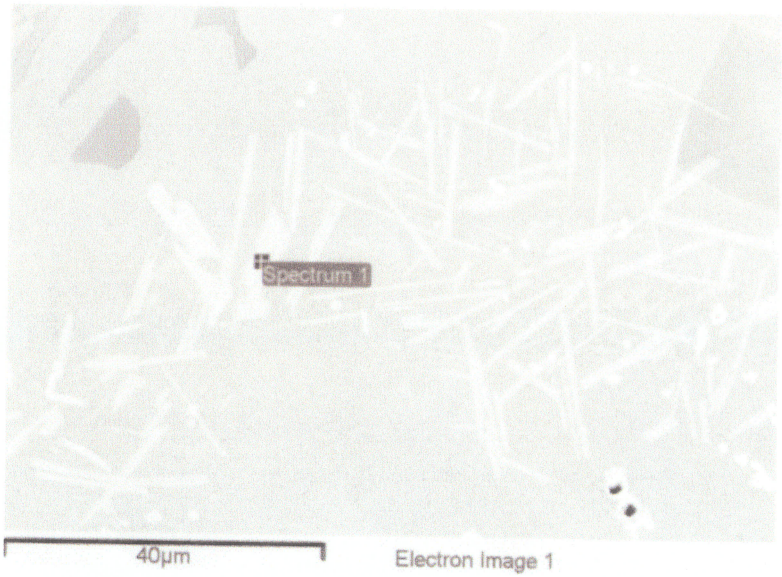

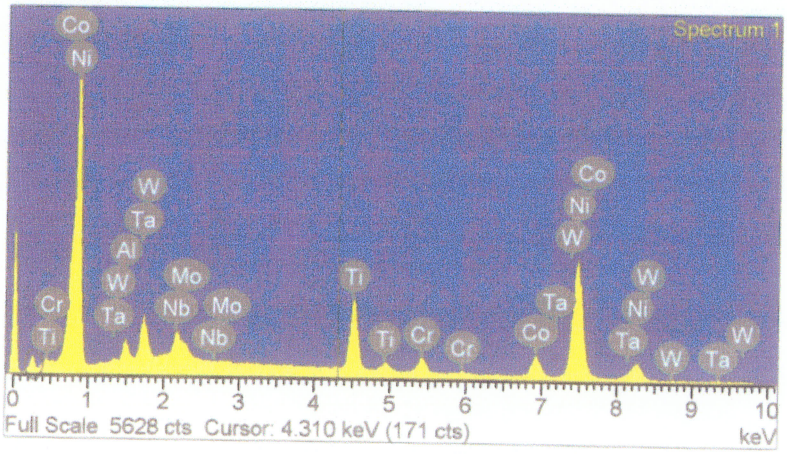

d

Figure 4.23 (cont…)

Element	Atomic %
Ti	0.41
Cr	83.13
Co	4.20
Ni	4.13
Mo	5.73
W	2.40

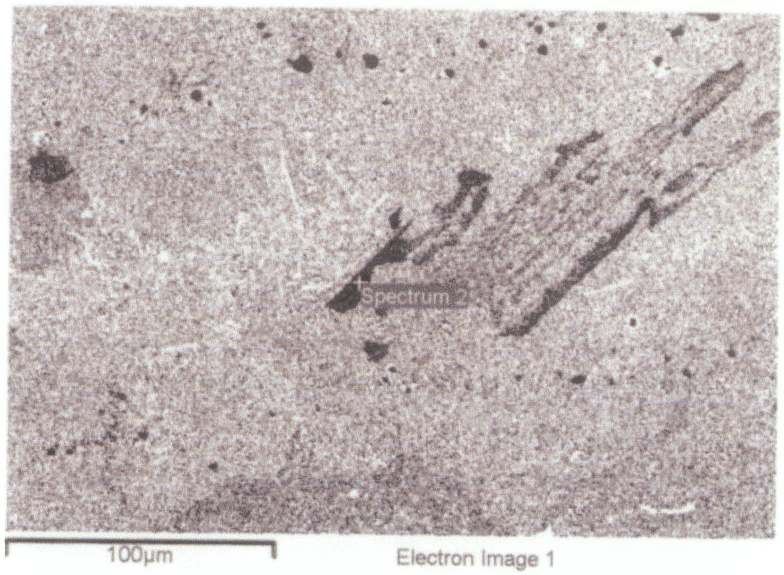

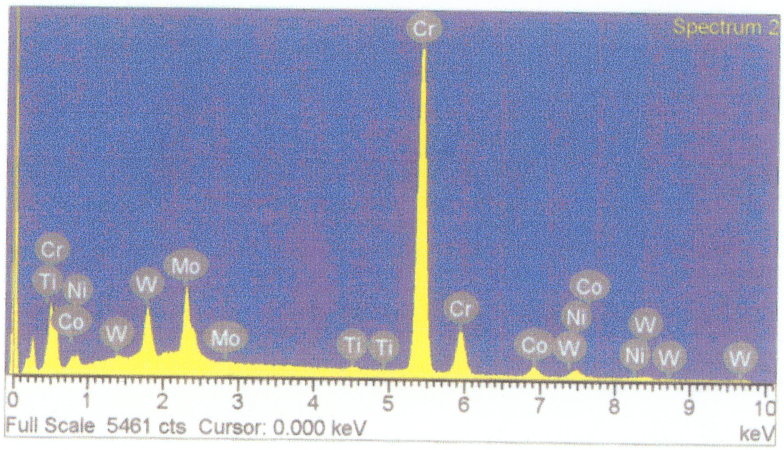

e

Figure 4.23 (c), (d) & (e) EDS Analysis of the Second Phase Precipitates in "DF3" Brazement.

The microstructural difference can be explained on the basis of initial compositional difference between the two fillers, which is further reflected in the higher hardness of "DF3" alloy. In addition, the presence of La is known to assist in suppressing boride chain formation and contribute to structural spheroidization. The chromium boride of "DF3" braze was found to be similar to that of "NB 150" in that both contained a relatively high amount of molybdenum and tungsten.

4.4 Base Alloy Intragranular Diffusion Induced Precipitates

Extensively distributed fine globular precipitates within the base metal grains adjacent to substrate – braze interface, were observed in all the samples brazed at different temperatures and holding time. The volume fraction of the precipitates declined in a gradual fashion with increasing distance from the bond line {figure 4.24(a)}. The particles were found to be too small for EDS point composition analysis in the SEM. Preliminary EDS line scan {figure 4.24(b)}, however suggests chromium rich boride. This suggestion was confirmed by TEM- EDS analysis (Fig. 4.24) performed on carbon-extracted precipitates in order to remove the effect of the surrounding matrix; a representative TEM-EDS spectrum produced by point analysis of the precipitate is shown in figure 4.25(e). Selected area diffraction patterns {figure 4.25(c) & (d)} from the precipitates indicate that the particles are neither tetragonal nor hexagonal crystal but most likely orthorhombic crystal structure.

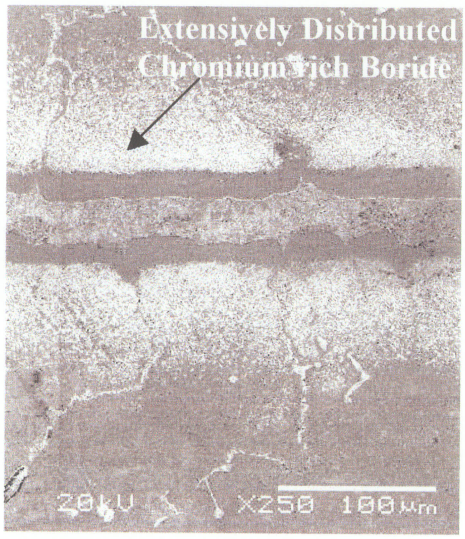

a

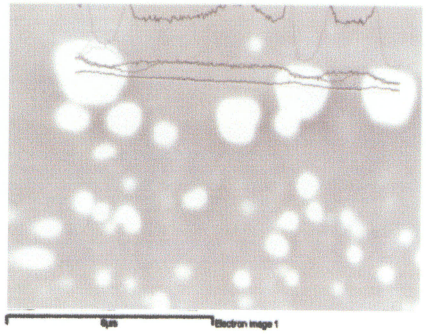

b

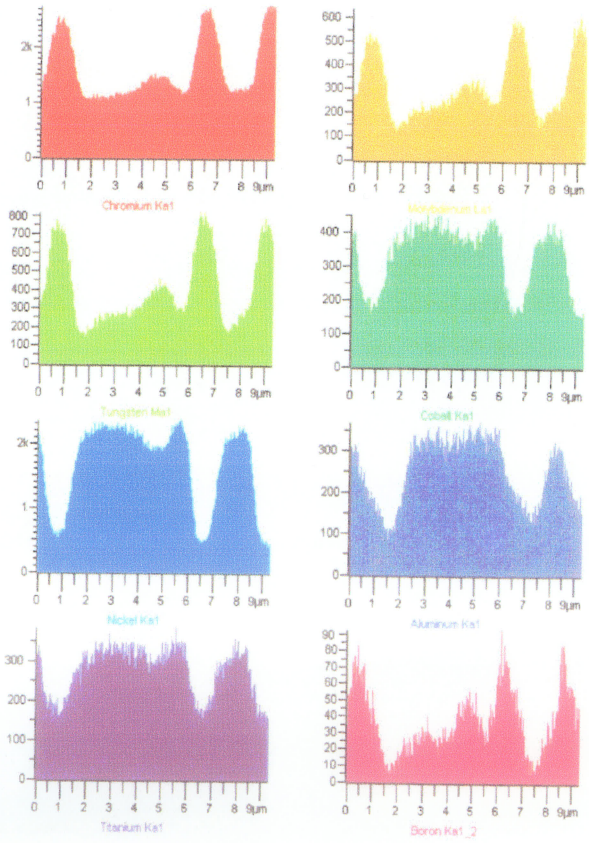

Figure 4.24 (cont…)

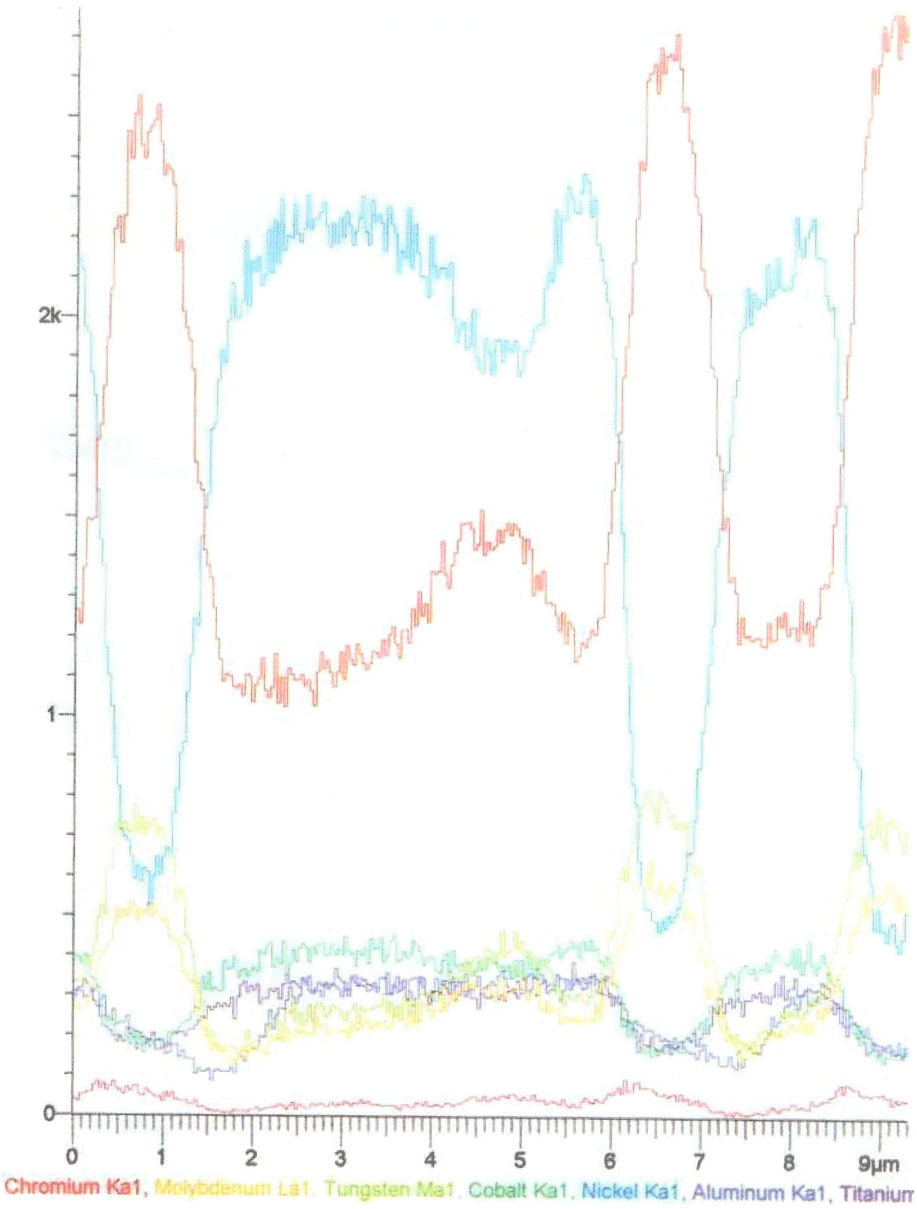

c

Figure 4.24 (a) SCM Micrograph, (b) & (c) Line Scan of Extensive Intraganular Distributed Chromium rich Boride, within the Base Alloy grains.

a

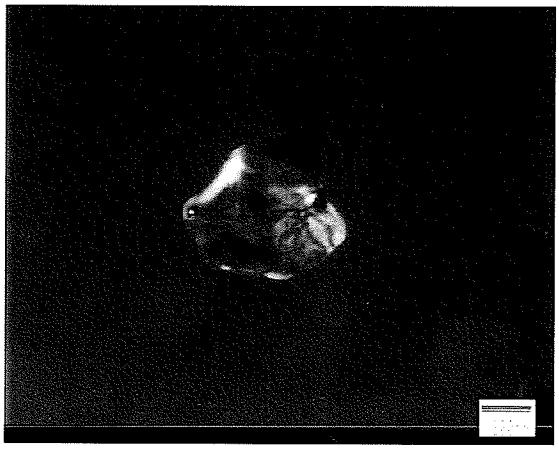

b

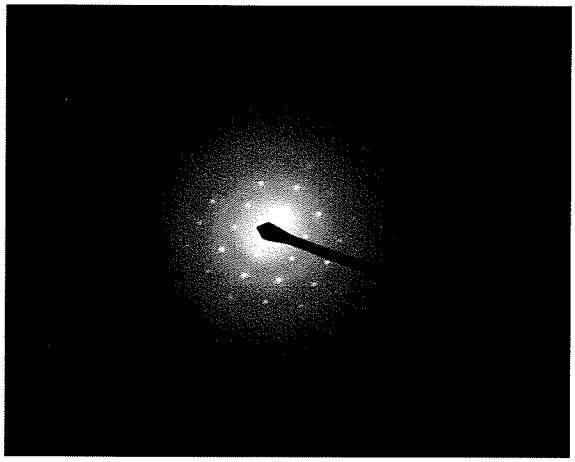

c

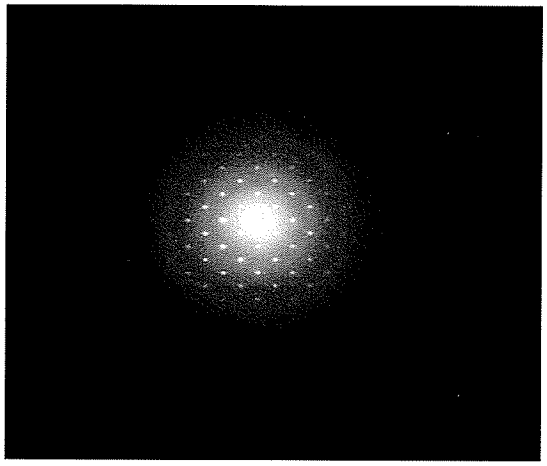

d

Figure 4.25 (cont...)

Element	Cr	Mo	W	Ti	Ni	Co
Atomic %	84.16	8.53	3.07	0.58	1.84	1.82

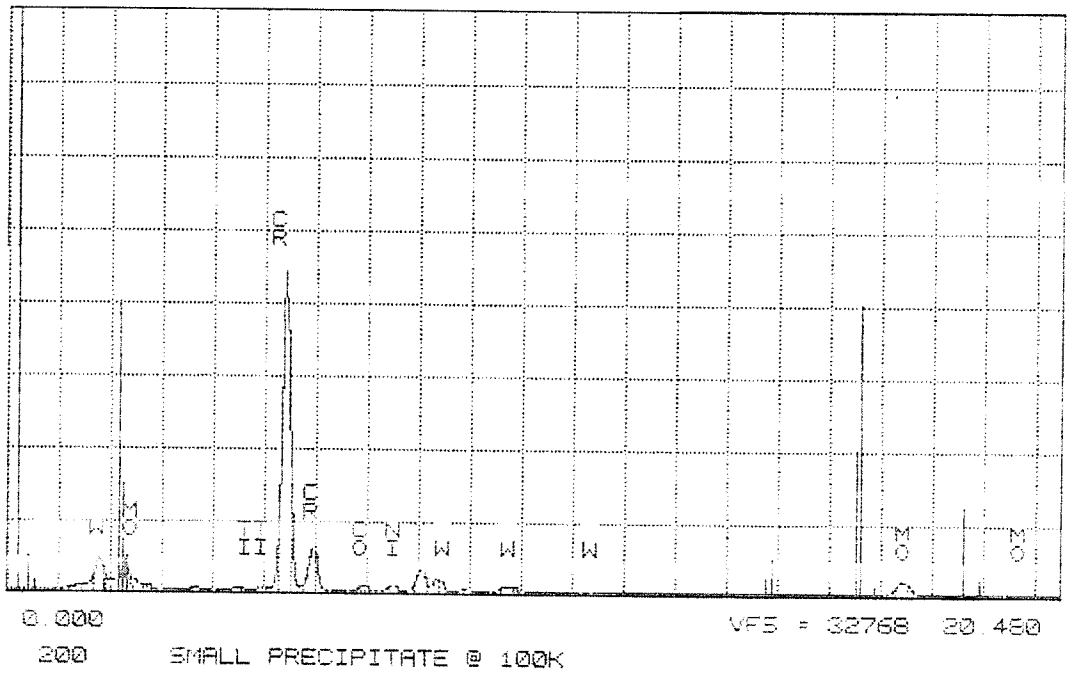

e

Figure 4.25 TEM Micrograph of the Carbon Extracted Chromium rich Boride Precipitate (a) Bright Field (b) Dark Field, (c) & (d) SADP and (e) TEM-EDS Spectrum from the Boride Phase.

This then suggests that the precipitates are possibly Cr_2B, CrB_4 or CrB, as opposed to Cr_5B_3 and CrB_2 that are tetragonal and hexagonal. From the EDS semi-quantitative analysis (demonstrating high chromium content), literature [62] and Cr-B phase diagram {figure 4.19(b) [61]} they are more likely to be Cr_2B. TEM bright and dark field micrographs of one of these precipitates are shown in figure 4.21(a) & (b).

The boride precipitation, however, is in contrast to conventional TLP bonding models, which assumes rapid equilibration of the solid and liquid phases to their respective solidus and liquidus compositions upon complete interlayer melting. This is followed by solid state diffusion of the melting point depressant in the base alloy, resulting in gradual isothermal solidification of the insert without the precipitation of second phases. Conversely, it appears from the experimental results that the chromium boride precipitates formed as a result of diffusion of boron exceeding the solubility limit at the bonding temperature (before solid-liquid equilibration) during the initial stages of joint formation. It is generally held that for optimum properties, boron should be present at a level, which fully saturates the grain boundaries in superalloy but does not allow the formation of boride particles. Jena and Charturvedi [52] had suggested that grain boundary borides in superalloy could be harmful to its properties.

Considering the high chromium content and extensiveness of the precipitation, this could lead to a significant depletion of chromium around this region of the substrate, resulting in a dramatic decrease in the corrosion resistance. Such a situation in which corrosion resistance depended essentially

on the chromium content in intergranular regions controlled by Cr_5B_3 and CrB precipitation has been previously reported [63].

4.5 Modelling of TLP Bonding Process

An imperative experimental parameter in the consideration of TLP bonding process for commercial applications is the holding time necessary to complete the isothermal solidification process and, hence, prevent the formation of the brittle phases. Models of the isothermal solidification process have been proposed and described in the literature [31,47,48,49,50]. In this work, the rapid diffusion of boron (rather than the slower diffusion of Cr) is considered to be the rate controlling of TLP bonding with ternary Ni-Cr-B filler. This is because it is the low solid solubility of boron in Nickel that maintains the liquid layer and results in the formation of the eutectic.

The model developed by Nakao et al [48] was selected and applied to microstructures of "NB 150" joints prepared at temperatures 1070°C, 1100°C, & 1130°C for 10 mins, 20 mins, 30 mins & 60 mins. The centreline eutectic average width was measured by SEM and plotted against the square root of holding time, as shown in figure 4.26. The eutectic width decreased linearly with increase in the square root of holding time at the bonding temperatures. Isothermal solidification rate apparently increased as the operating temperature was raised. The slope of each curve in figure 4.26 was evaluated and plotted against the corresponding inverse absolute bonding temperatures (figure 4.27).

This relationship can be represented by the equation:

$$\ln m = A - Q / 2RT \ldots\ldots\ldots (4.1)$$

where m is the slope of the curve, Q, activation energy, T, bonding temperature, R, gas constant and A, constant. Accordingly, the apparent activation energy for diffusion of the melting point depressing element (boron in this work), was computed from the slope of curve in figure 4.27 to be 218KJ/mol. A Similar approach was used by Ramirez, et al. [64] to estimate activation energy for boron diffusion in pure Nickel. The result obtained in this work is in close agreement with those reported for Nickel base polycrystals superalloys [48] such as IN-713 (211KJ/Mol), IN-600 (209KJ/Mol), Mar-M-247 (199KJ/Mol) and MM007 (219KJ/Mol).

The time required to complete the isothermal solidification process can consequently be obtained from the expression [48]:

$$t_f^{1/2} = J (2h / D^{1/2}) \ldots\ldots\ldots (4.2)$$

D being the diffusion coefficient of boron in the base alloy at the bonding temperature, 2h, the maximum width of braze seam (following liquid homogenisation) and J a constant. Extrapolating t_f (time at which the eutectic width equals zero) at each bonding temperature from figure 4.25, and plotting this against $2h/D^{1/2}$ (figure 4.28), J, the slope of the curve was thus found to be 32.05. Previous derivations for isothermal solidification completion time are of similar forms to equation...(4.2) above, with different values of J and representation [31,47,49,50,64]. Calculated time from Tuah-Poku et al expression [31] was however found to be strongly overestimated.

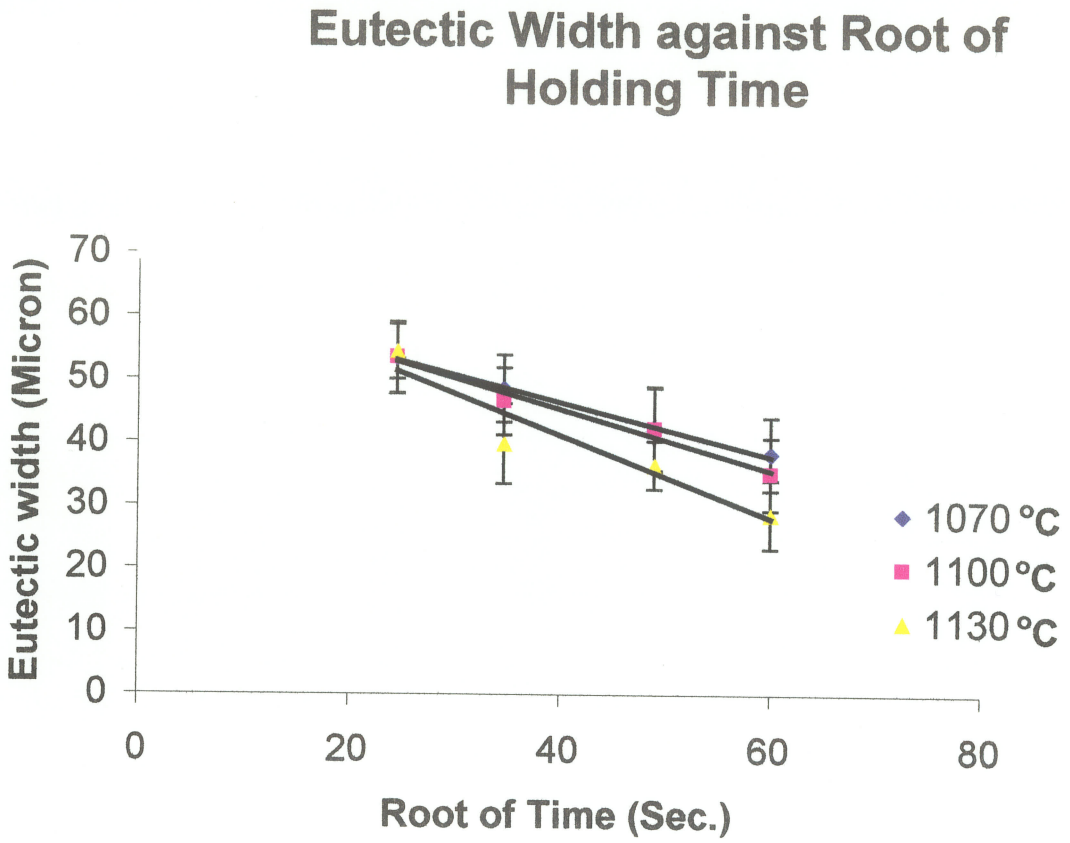
Eutectic Width against Root of Holding Time
Eutectic width (Micron)
70
60
50
40
30
20
10
0
0
20
40
60
80
Root of Time (Sec.)
1070 °C
1100 °C
1130 °C

Figure 4.26

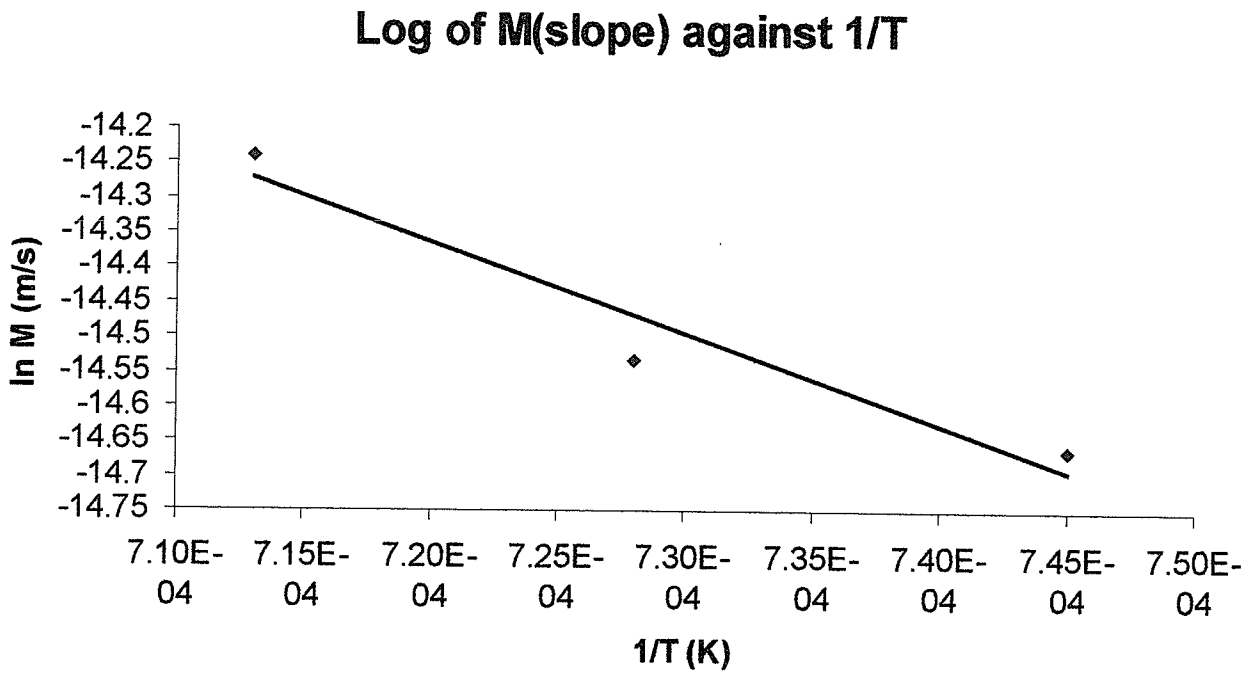
Log of M(slope) against 1/T
ln M (m/s)
-14.2
-14.25
-14.3
-14.35
-14.4
-14.45
-14.5
-14.55
-14.6
-14.65
-14.7
-14.75
7.10E-04
7.15E-04
7.20E-04
7.25E-04
7.30E-04
7.35E-04
7.40E-04
7.45E-04
7.50E-04
1/T (K)

Figure 4.27

The expression was modified by incorporation of a dimensionless parameter γ_s by Ramirez, et al. [64], and the use of a K factor in the solution of Liu, et al. [47]. In the present work, actual experimental values of 2h were used to compute the value of J as opposed to the use of mass balance by Tuah-Poku et al [31].

In this connection, using the above expression for t_f and evaluated J value (32.05); isothermal solidification completion time in the present work can thus be predicted at a given bonding temperature and gap size. Predicted times were compared with experimental completion times for 50μm & 30μm gaps, brazed at 1065°C and 1100°C for 3.5 hrs and 30 mins respectively. At the end of these holding times isothermal solidification was observed to be completed without formation of the deleterious eutectic phase. Model developed here predicted the completion times for the above conditions to be 3.72 hrs and 48 mins, which are reasonably close to the observed values, though isothermal solidification was actually completed ahead of estimated time.

The difference could possibly be attributed to the grain boundary regions acting as high-diffusivity paths and formation of borides during the initial stages of isothermal solidification. Nonetheless the expression is valuable in predicting the time within which isothermal solidification is expected to be completed at any given operating temperature and gap size. This is a vital consideration in designing repair procedure for commercial purpose.

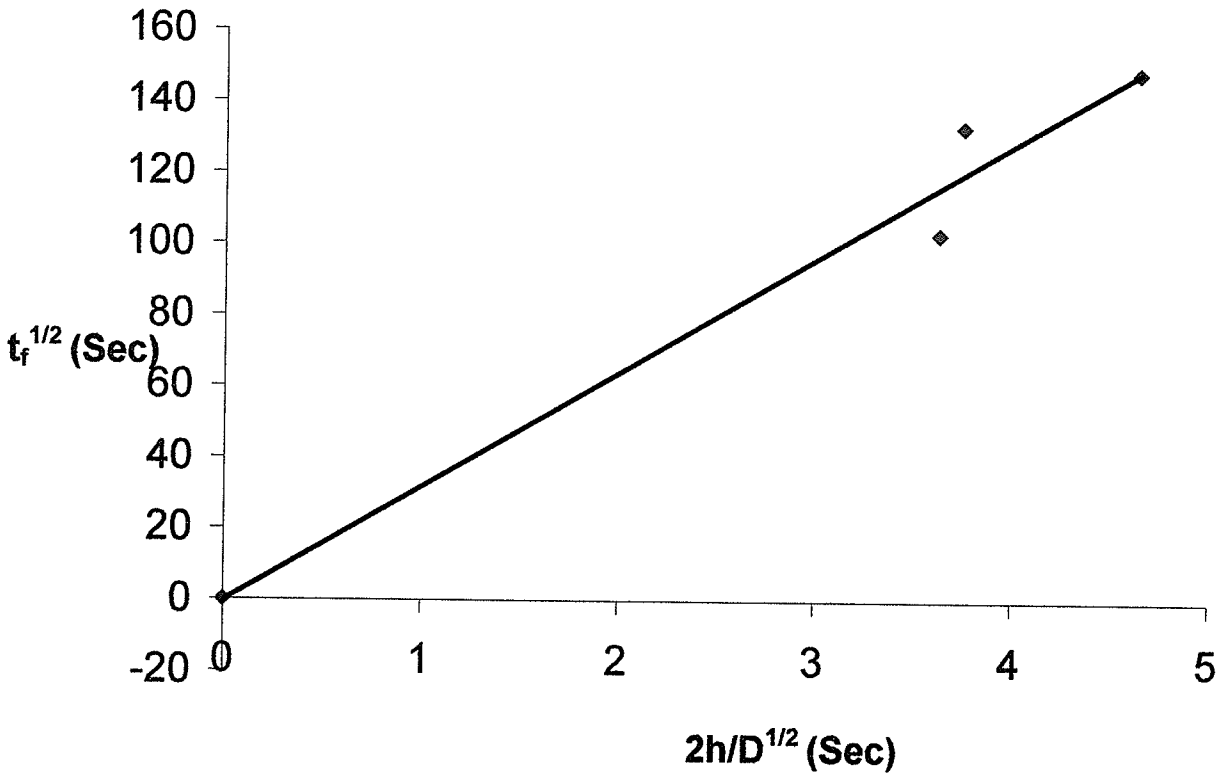
Root of Isothermal Solidification Time (t_f) against $2h/D^{1/2}$
160
140
120
100
80
60
40
20
0
-20
0
1
2
3
4
5
$t_f^{1/2}$ (Sec)
$2h/D^{1/2}$ (Sec)

Figure 4.28

4.6 Joint Defects

Notable defects that were observed in laboratory prepared joints were porosity and voids as shown in figure 4.29. Much of the observed porosities were probably due to insufficient bonding pressure and solidification shrinkage of the filler metal - in the case of centreline voids. These defects appeared to be more prominent in large gap samples brazed at lower temperatures (1065°C & 1070°C) at which the braze viscosity is low. Porosity caused by poor joint assembly is not really a metallurgical problem, and can be overcome by greater care or better approach in preparing the braze assembly. Aluminium fluoride particles were observed at the original substrate – filler interface in first set of industry prepared samples figure 4.30. These were found to be residue from fluoride ion cleaning, which were not properly scrubbed and neutralized. Subsequent samples were free of these particles as the suggestion of sufficient scrubbing and neutralizing was apparently heeded.

Figure 4.29 Microstructure of 1065°C Brazed 30µm Gap Showing typical defects – Void and Pores observed in Laboratory prepared samples.

Element	Atomic %
F	69.95
Al	28.60
Ti	0.11
Cr	0.39
Co	0.18
Ni	0.76

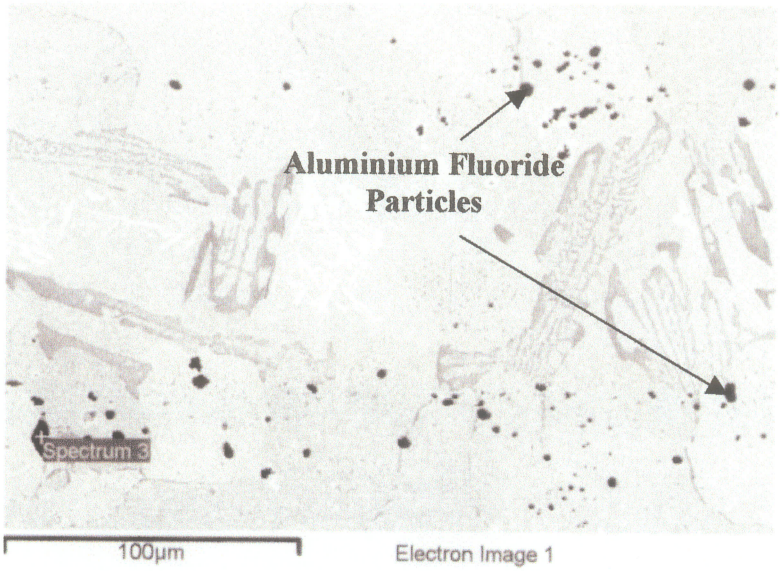

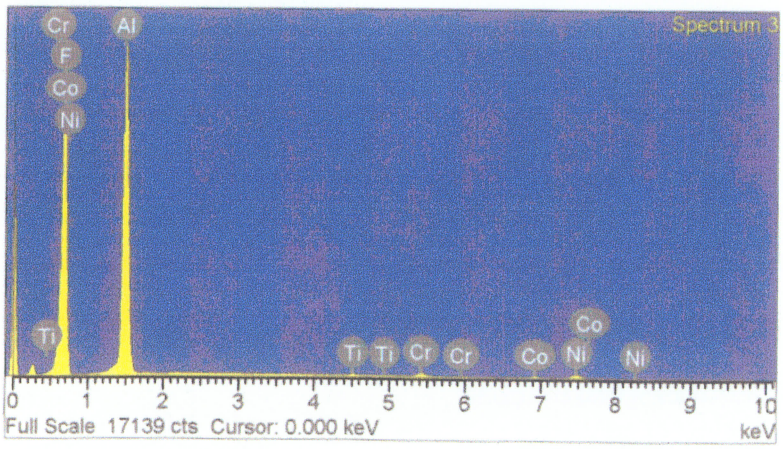

Figure 4.30 EDS Analysis of Fluoride Ion Cleaning Residue Observed at Substrate – Braze Interface.

4.7 Mechanical Properties

High temperature tensile tests at 980°C were conducted on "DF3" and "NB 150" brazed samples. The tests were aimed at investigating the effect of precipitated second phases on the elevated temperature strength and ductility of brazed material. As was previously stated, precipitation of the second phases along "DF3" and "NB 150" brazement were found to increase with increase in gap width at a given bonding temperature and time. Based on this fact, samples were brazed according to the brazing schedules given in table 4.1.

4.7.1 "NB 150" Brazed Samples

Microstructural examination of "NB 150" brazed joint under the same brazing condition as the one used for the tensile test revealed that below 65μm joint width, the brazement consisted mainly of solid solution phase while above it, a centreline eutectic phase formed along the brazed joint which became wider, denser and continuous with further increase in gap size. The tensile test results (Table 4.2, figure 4.31) show that the ultimate tensile strength, 0.2% yield strength and percentage elongation of "NB 150" brazed specimens at 980°C decreased with increase in the joint width from 25μm -75μm-125μm.

This could be due to the formation of hard and brittle continuous centreline eutectic phase, which is a preferred low resistance path for crack propagation, reducing the strength and ductility of bonded samples. The highest strength and ductility of the tested specimens was exhibited by the 25μm gap

Table 4.1: Brazing Schedule for Brazed Tensile Test Specimens

"NB 150" Filler	
Gap Size (μm)	Braze Cycle
25	1120°C / 15 mins + 1065°C / 4 hrs
75	1120°C / 15 mins + 1065°C / 4 hrs
125	1120°C / 15 mins + 1065°C / 4 hrs
"DF3" Filler	
Gap Size (μm)	Braze Cycle
25	1190°C / 15 mins + 1065°C / 4 hrs
75	1190°C / 15 mins + 1065°C / 4 hrs
125	1190°C / 15 mins + 1065°C / 4 hrs

Table 4.2 : "NB 150" Brazed Samples Tensile Test Results

Gap Size (μm)	Ultimate Tensile Strength (MPa)	0.2% Yield Strength MPa)	Elongation (%)
25	317.48	282.96	2.7
75	278.32	262.24	2.61
125	265.96	260.82	0.86

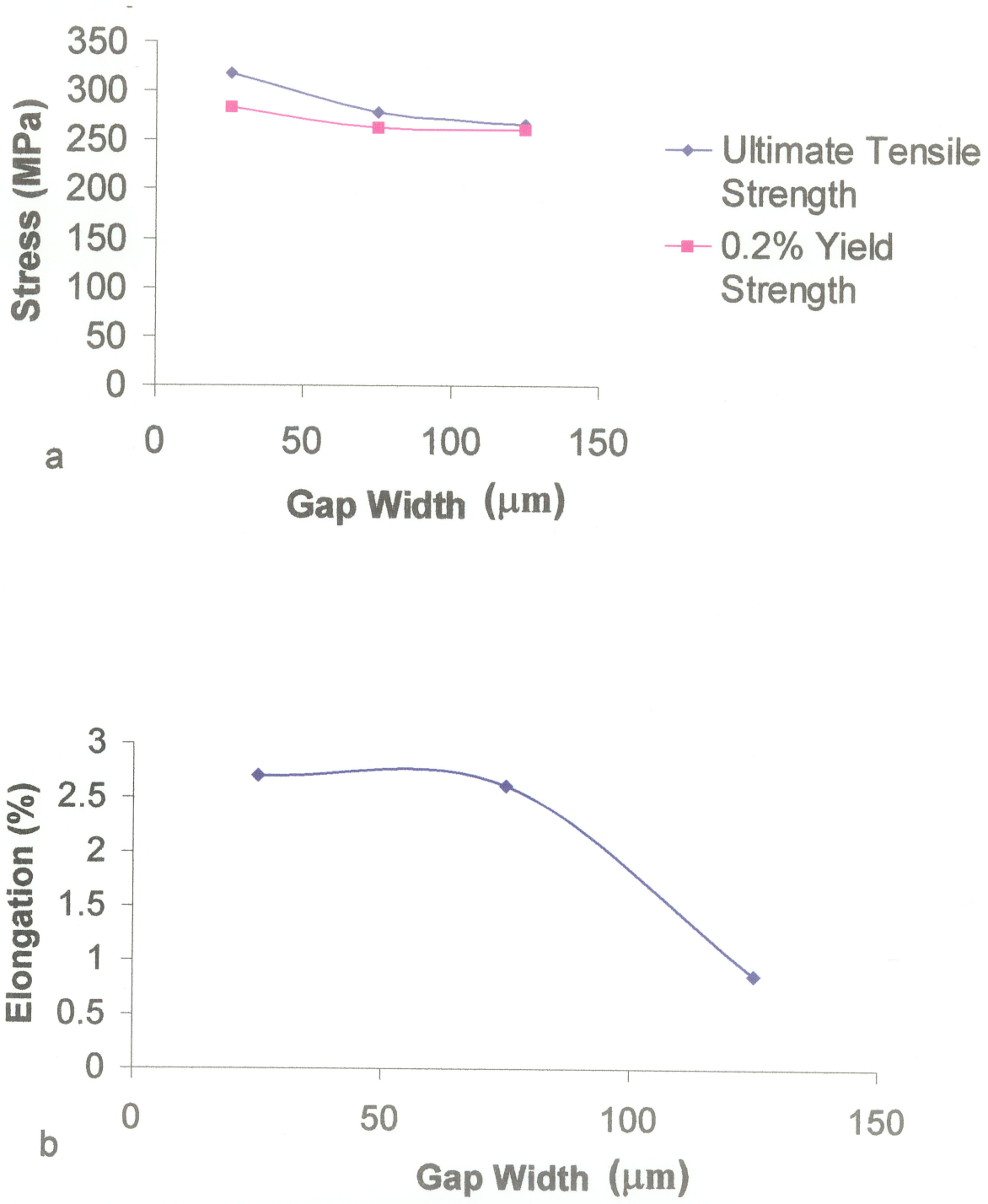

Figure 4.31 Variation of (a) Ultimate Tensile Strength and 0.2% Yield Strength & (b) Percent Elongation with Gap Width in "NB 150" Brazement.

sample, which was previously observed to microstructurally consist of mainly solid solution phase, and free of the eutectic phase. It can thus be deduced that the centreline eutectic phase is detrimental to both the high temperature tensile strength and ductility of brazed samples.

4.7.2 "DF3" Brazed Samples

As was stated in section 4.3, "DF3" brazed joint with joint width below 25μm gap at same brazing condition as used for the tensile test specimens, consisted mainly of solid solution phase, and as the gap size increased above 25μm three different dispersed intermetallic precipitates formed along the brazement, with their volume fraction increasing with increase in joint's size. The results of tensile test of "DF3" brazed specimens are shown in table 4.3 and figure 4.32.

The ultimate tensile strength and 0.2% yield strength followed the same pattern, by first decreasing with an increase in joint width from 25μm to 75μm and then increased with a further increase in joint width to 125μm. However while the subsequent increase in strength with joint width caused the ultimate strength of the 125μm joint to be higher than that of 25μm joint, its 0.2% yield strength remained below that of 25μm joint.

Table 4.3 "DF3" Brazed Samples Tensile Test Results

Gap Size (μm)	Ultimate Tensile Strength (MPa)	0.2% Yield Strength (MPa)	Elongation (%)
25	377.82	301.66	3.12
75	337.19	267.12	3.9
125	401.84	275.71	3.56

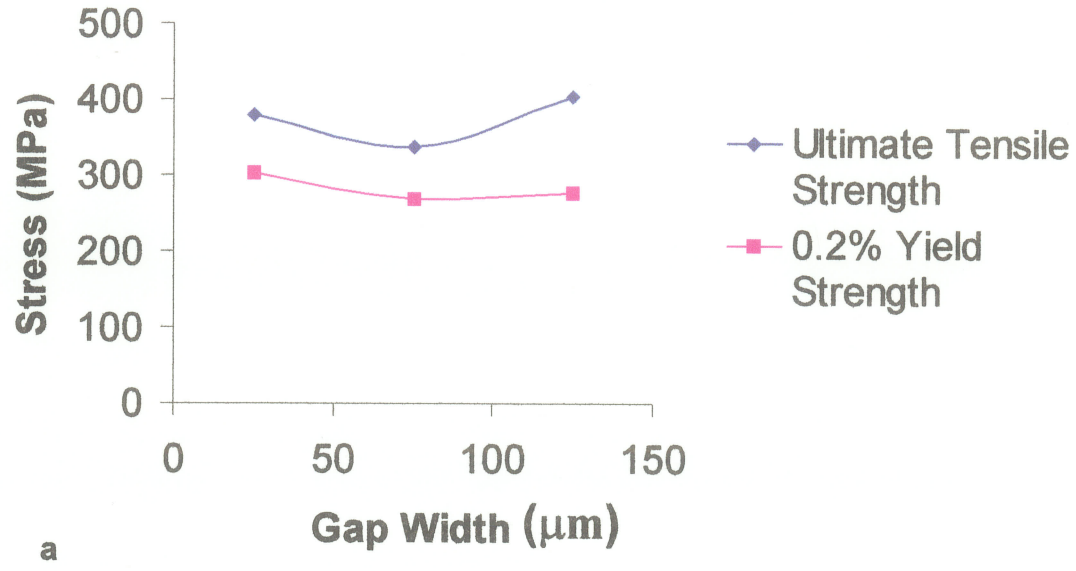

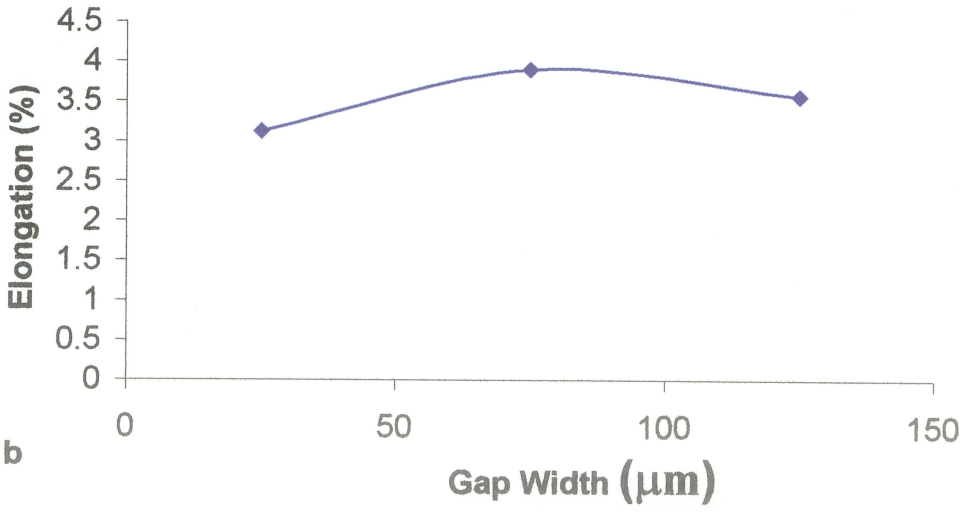

Figure 4.32 Variation of (a) Ultimate Tensile Strength and 0.2% Yield Strength & (b) Percent Elongation with Gap Width in "DF3" Brazement.

The percentage elongation on the other hand followed a direct opposite pattern. This observation could be due two factors that appear to be contributing to the joint's strength:

(1) Strengthening of the joint by base alloy elements diffused into the brazement during the bonding process.

(2) Strengthening due to the dispersed second phase precipitates along the brazed joint.

The strength of the 25μm brazed joint was obviously a result of alloy element strengthening since microstructural examination revealed the joint to be free of the precipitated second phases. As the gap size increased to 75μm, it is expected that the volume fraction of diffused base alloy strengthening elements in the joint will be lower than in 25μm joints as a result of increased gap size, causing a decrease in the joint's strength. An increase in the joint's strength when the gap size was increased from 75μm to 125μm is probably due to the compensating effect of strengthening from the higher volume fraction of dispersed second phase precipitates that formed along the joint.

4.7.3 Comparison of Tensile Properties of "NB 150" and "DF3" Brazed Joint

In general, all the tested specimens ("DF3" and "NB 150" brazed) failed at the brazed joint, with tensile properties; ultimate tensile strength, 0.2% yield strength and percentage elongation lower than those of the base alloy at 980°C,Table 2.2 [6]. Fractography of failed "NB 150" and "DF3" brazed joints

(figure 4.33) show predominantly low energy fracture mode. A comparison of the tensile test results of "DF3" and "NB150" brazed samples, revealed the effect of initial composition of filler alloy on the high temperature strength of brazed joint. The 25μm joint, brazed with "NB 150" (initially containing no cobalt) which consisted mainly of solid solution phase exhibit 70% of the base alloy strength, while "DF3" (initially containing 20% cobalt) 25μm brazed joint exhibit 83% of the IN-738 base alloy strength. In addition the dispersed nature of the second phase precipitates in "DF3" brazement as against the continuous centreline eutectic in "NB 150" brazement reduced the degrading effect of the second phase precipitates on the joint's high temperature strengths and ductility.

It is worthy of note however, that from the results of the tensile tests, reduction in the brazed samples strengths and ductility were not caused solely by the presence of second phase precipitates along the joint. This is clear by observing the properties of 25μm joint of both "NB 150" and "DF3" which are free of the precipitated second phases. The joints strengths were found to be below that of the base alloy, with their ductility drastically reduced (approximately 31% of the base alloy). There are possibly two notable contributing factors: (i) The closely spaced fine and hard globular chromium rich boride precipitates, that are distributed within the base alloy grains adjacent to the substrate-braze interface in all the bonded samples, could reduce the joint's ductility as it is a region of inhomogeniety (discontinuity) in brazed material. (ii) Insufficient diffusion of the base alloy elements into the

joint during bonding could also contribute to the reduced strengths and ductility.

It is thus evident that not only should a brazed joint be free of precipitated second phases, but also there is a need for both microstructural and chemical homogenisation treatment following isothermal solidification, in order to achieve a joint with comparable properties to that of the base alloy.

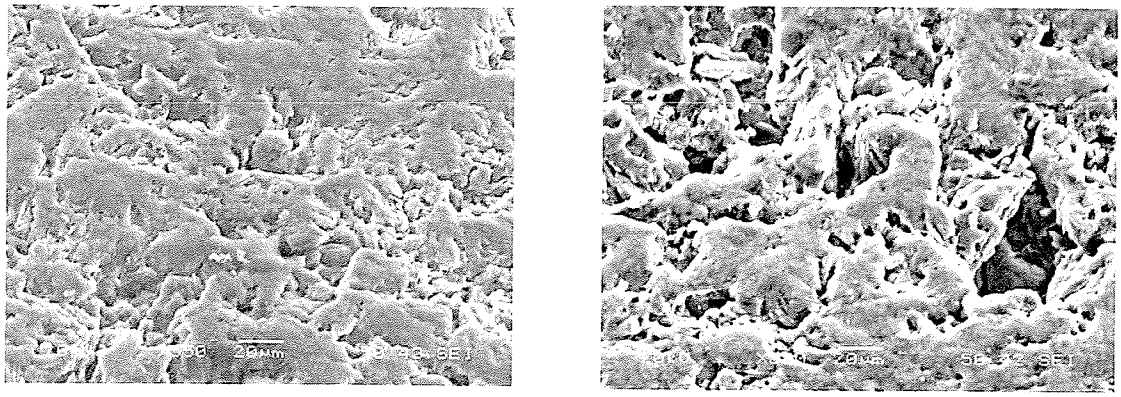

a b

Figure 4.33 Fractography of failed (a) "NB 150" and (b)"DF3" Brazed Joint showing low energy fracture mode.

Chapter 5

CONCLUSIONS

1) The base alloy cast IN-738 had a coarse grain size of about 750μm with a cellular dendritic microstructure, intergranular precipitation and alignment of primary MC carbide and, intragranular precipitation of unimodal distribution of cuboid shape γ' phase. It also contained a small volume fraction of casting micropores.

2) During diffusion brazing of this superalloy, using two commercial filler alloys, "NB 150" and "DF3", residual liquid present at the bonding temperatures transformed on cooling, into centreline ternary eutectic phase in "NB 150" brazement. The ternary phase consisted of Nickel rich boride, Chromium rich boride and γ austenitic solid solution phase. In "DF3" brazement, MC carbide, Ni_3Ti based intermetallic and Chromium rich boride were observed along the joint centre – area. Sufficient holding time was required for isothermal solidification of existing liquid phase at bonding temperature to prevent the formation of these precipitated phases.

3) Microhardness tests demonstrated that the second phase particles were very hard, much more than the base alloy. The average hardness of the centreline eutectic phase in "NB 150" brazement was 720 VHv and that of the second phases in "DF3" was 780 VHv. The tendency of formation of

the hard second phase precipitates at a given brazing temperature and time increased with increase in gap width in both "NB 150" and "DF3" braze.

4) Diffusion of major base alloy strengthening elements (Al, Ti & Co examined) into the brazed joint during bonding increased with operating temperature and holding time. A marked effect of holding time on the diffusion was observed with increase in bonding temperature. Al, being a smaller atom than Ti, diffused more into the braze at all the brazing temperatures. Co however had the highest quantity diffused being the one with the highest chemical potential and atomic size very close to that of the nickel matrix. Significant diffusion of these elements into the brazed joint is crucial for strengthening of the brazed joint, since the brazing alloys do not initially contain these vital strengthening elements.

5) Extensively distributed fine globular chromium rich borides not predicted by conventional TLP bonding models were observed within the base alloy grains adjacent to the substrate – braze interface in all brazed samples as well as along the grain boundaries. It is suggested that, considering the high chromium content and extensiveness of the precipitation, this could lead to a significant depletion of chromium around this region of the substrate, resulting in a remarkable decrease in the corrosion resistance.

6) Applying existing diffusion models to microstructures of "NB 150" brazement, the centreline eutectic width decreased with increase in the square root of holding time at the bonding temperatures and isothermal solidification apparently increased with operating temperature. The activation energy for boron diffusion in the base alloy, taken to be the controlling mechanism of the whole bonding process was estimated to be 218 KJ/Mole. This is in close agreement with those reported for Nickel base polycrystals superalloys such as IN-713, IN-600, Mar-M-247 and MM007. Using this activation energy value and the expression $t_f^{1/2} = J\ (2h / D^{1/2})$ where J was computed to be 32.05, the time required for isothermal solidification, which is imperative to preventing formation of deleterious centreline eutectic phase, could be estimated at a given bonding temperature and gap width. Experimental and predicted times were in reasonably close agreement.

7) Notable defects observed in laboratory prepared samples were voids and pores which are believed to be formed mainly as a result of solidification shrinkage of the braze. Aluminium fluoride particles were also observed at the substrate – braze interface in the first set of industry prepared samples and were considered to be residues from the fluoride ion cleaning. Subsequent samples were free of these particles as proper flushing and scrubbing following cleaning was effective in eliminating them.

8) High temperature tensile tests at 980°C of both "DF3" and "NB150" brazed samples revealed that the second phase precipitates that formed in the brazed joints during bonding, reduced the strengths and ductility of brazed samples. The wider and denser the eutectic phase in "NB 150" brazement, which is a function of the joint size, at a given brazing temperature and time, the more pronounced its detrimental effect. It was evident however, that apart from eliminating the deleterious second phase precipitates, both structural and chemical homogeneity is necessary in brazed joint in order to achieve properties comparable to that of the base alloy.

Chapter 6

SUGGESTIONS FOR FUTURE WORK

1. Base metal dissolution (melt- back) during diffusion brazing is of great concern when thin material is brazed or when brazed joint must withstand vibration or impact load. The effect of gap size, brazing temperature and time on base metal dissolution needs to be investigated for both brazing alloys "DF3" and "NB 150". It appeared from this work, that both fillers had different effect on base metal dissolution. This will be a factor in choosing between the two for minimum melt back application.

2. The effect of brazing temperature and holding time on the microstructure of "NB 150" brazement was studied in this work. It would be expedient to explore the influence of these two important brazing parameters on the microstructure of "DF3" brazed joint. This becomes even necessary from the fact that "DF3" alloy contains B and Ta, combination of which is known to depress the melting point of Nickel. It might be useful to determine the influence of Ta on boron diffusion in controlling isothermal solidification of the liquid phase and thus the prevention of second phase precipitation on cooling. Precipitation of second phases was found to start at lower gap size in "DF3" samples compared with "NB 150" samples diffused at same temperature and hold time.

3. In the model used to formulate an expression for estimating isothermal solidification completion time of the liquid phase in "NB 150" brazed samples, isothermal solidification was considered to be controlled by boron diffusion in the IN-738 substrate. Similar situations where isothermal solidification was actually controlled by diffusion of melting point depressant has been verified and reported by several workers. However, Ramirez et al [64] suggested that an increase with time in boron concentration of the base alloy at or near the liquid-solid interface, could in the long run markedly decrease the rate of isothermal solidification. In order to verify this suggestion, isothermal solidification in larger gap size samples than the one used in this experiment (75μm) should be investigated. This could aid in the determination of the range of gap size (narrow gap range for the alloy) above which boron diffusion ceases to control the process and thus becomes uneconomical to produce joint devoid of the deleterious eutectic phase.

4. Further work needs to be done to confirm the exact type of phases formed within "NB 150" and "DF3" brazed joints. X-ray diffraction analysis on large gap samples enough to be analyzed, is suggested, to determine the exact phases formed within the brazement. In addition, more TEM analysis need to be done to determine the nature of the phases formed at the diffusion zone of the substrate, adjacent to substrate-braze interface. Especially the

extensively distributed intragranular fine globular precipitates, found in this work to be chromium rich borides.

5. It was evident from this work that both chemical and microstructural homogenization subsequent to isothermal solidification is crucial to achieving high temperature mechanical properties comparable to the base alloy. The maximum hold time used in this work was 4 hrs. Effect of additional time at different temperatures on microstructure and properties of both "NB 150" and "DF3" brazed material needs to be examined.

6. In cases where it becomes uneconomical to form reliable strong joint in large gap samples (usually above 250μm), due to extremely long fabrication time and insufficient braze flow, activated diffusion brazing is usually employed. This involves the use of a mixture of superalloy powder and filler alloy powder as the brazing material. The influence of the brazing parameters studied in this work, on microstructure and properties of such brazed wide gap joint in IN-738, needs to be studied, using different proportion mixture of superalloy powder with "DF3" and "NB 150" fillers.

REFERENCES

[1] Bieber, G.C., and Mihalisin, R.J., 2nd International Conference on the Strength of Metals and Alloys, Asilomer, ASM Vol. IV, p. 1031.

[2] Fahrmann, M., et al., 1995, Acta Metall., Vol. 43, No. 3, p. 1007.

[3] Buschke, I., E. Lugscheider, Joining of Advanced and Specialty Materials, ASM International, Rosemont, IL, 1998, pp.51- 55.

[4] Martens, L., et al., J. Materials Processing Technology, Vol. 58, 1996, pp. 13-23.

[5] Schwartz, M. M., " Modern Joining Techniques", 1969, by John Wiley & Sons, Inc., p. 291.

[6] "Alloy IN-738: Technical Data" INCO, New York, p. 1- 11.

[7] Kattus, J. R., Non Ferrous Alloys, March 1984, p. 7.

[8] Koul, A.K. and Castillo, R., Metallurgical Trans., Vol. 19A, Aug. 1988, p. 2049.

[9] Garosshen, T.J and McCarty, G.P., Metallurgical Trans., Vol. 16A, 1985, p. 1213.

[10] Ardell, A. J., Metallurgical Trans., Vol. 16A, Dec. 1985, p. 2131.

[11] Footner, P.K and Richards, B.P., Journal of Material Science, Vol. 17, 1982, p. 1007.

[12] Thakur, A., M.Sc. Dissertation, University of Manitoba, 1997.

[13] Larson, J. M., Metallurgical Trans., Vol. 7A, 1976, p. 1497.

[14] Bradley, E. F., et al., "Superalloys: a Technical Guide" Metals Park, Ohio, ASM International, 1988, p. 58.

[15] Rong, Y. H., et al., Electron Microscopy 1986, Vol. 1[Proc. Conf.], Kyoto Japan, 1986, p.879.

[16] Duvall, S. D. and Owczarski, W. A., Welding Journal, 1967, 46, (9), p. 423s - 432s.

[17] Okerblom N., "Le Calcul Des Deformation Des Constructions Metalliques Soudees", Report No 807, Institut De Soudure, Paris, 1964.

[18] Hermanek, F. J. and Stern, M. J., "Turbine Component Restoration by Activated Diffusion Brazing", 84 Westec, Los Angeles, California, March 19 – 22, 1984, ASM 8407 –004.

[19] Brauny, P., et al., Materials Science and Technology, Vol. 1, Sep. 1985, p. 724.

[20] Galmiche, P., 'Thermo-chemical Techniques – Applications in the Aerospace Industry', Technical Paper No. 571, Office National d'Etudes et de Recherchés Aerospatiales, Paris, 1968.

[21] Chasteen, J., 'The UDRI fluocarbon cleaning process', University of Dayton, Research Institute, Ohio, 1979.

[22] Haafkens, M., 'High Temperature alloys for gas turbines', (ed. D. Coutsourdis et al.) 931; 1982, Amsterdam, Reidel.

[23] Duvall, S. D. and Owczarski, W. A., Welding Journal, 1974, pp. 203 – 214.

[24] Zhang, Y. and Ruan, Z., Acta Metallurgica Sinica, Vol. 26, 1990, pp. B119 – B 124.

[25] Kepniss, D., et al., Joining and Repair of Gas Turbine Components, ASM International, Indianapolis, IN, 1997, pp 95 – 98.

[26] Miller, F., Weld. J., August 1961, pp. 821 – 827.

[27] Spinat, R. and Honnorat Y., "High Temperature Alloys for Gas Turbines and Other Applications", eds. W. Betz et al., Reidel Publ. Corp. Dordrecht, Holland, 1986, pp. 151 – 174.

[28] Jahnke, B. and Dannhauser, G., "High Temperature Alloys for Gas Turbines and Other Applications", eds. W. Betz et al., Reidel Publ. Corp. Dordrecht, Holland, 1986, pp. 175 - 216.

[29] Nakao, Y., Nishimoto, K., Shinozaki, K. and Kang, C., "Transient Insert Metal Diffusion Bonding of Ni-Base Cast Superalloy MM007", International Institute for Welding, Abingdon, United Kingdom, Document No. IA-334-86-OE, 1986.

[30] Nakao, Y., Nishimoto, K., Shinozaki, K. and Kang, C., "Superalloys 1988", TMS-AIME, Warrendale, PA, 1989, pp. 775 – 783.

[31] Tuah-Poku, I., Dollar, M. and Massalski, T.B., Metall. Trans. A, 1988, Vol. 19A, pp. 675 – 686.

[32] Gale, W. F. and Wallach, E. R., Metall. Trans. A, Vol. 22A, Oct. 1991, pp. 2451 – 2457.

[33] MacDonald, W. D. and Eagar, T. W., Annu. Rev. Mater. Sci., 1992, Vol. 22, pp. 23 – 46.

[34] Nakagawa, H., et al., Metall. Trans., 1991, Vol. 22A, pp. 543 – 555.

[35] Zhou, Y., Gale, W. F. and North, T. H., Inter. Mater. Rev., 1995, Vol. 40, No 5, pp. 181 – 196.

[36] Niemann, J. T., and Garret, R. A., Weld. J., 1974, 52, pp. 175 – 184.

[37] Li, Z., Fearis, W. and North, T. H., Mater. Sci. Technol., 1995, Vol. 11, No 4, pp. 363 – 369.

[38] Moelwyn-Hughes, E. A., The Kinetics of Reaction in Solution, Clarredon Press, Oxford, 1947, p. 374.

[39] Ikeuchi, K., Zhou, Y., Kokawa, H. and North, T. H., Metall. Trans., 1993, Vol. 23A, No 10, pp. 2905 – 2915.

[40] Zhou, Y., PhD Dissertation, University of Toronto, 1994.

[41] Nakao, Y., Nishimoto, K., Shinozaki, K. and Kang, C., " Joining of Advanced Materials", (ed. North, T.H.) pp.129 – 144, 1990, London, Chapman and Hall.

[42] Ikawa, H. and Nakao, Y., Trans. Jpn. Weld. Soc., 1977, Vol. 8, pp. 3 – 8.

[43] Sekerka, R. F., Proc. Conf. "Physical Metallurgy of Metals Joining", (ed. Kossowsky, R. and Glicksman, M. E.), 1980, pp. 1 – 3, St. Louis, MO, TMS-AIME.

[44] Langer, J. S. and Sekerka, R. F., Acta Metall., 1975, Vol. 23, pp. 1225 – 1237.

[45] Crank, J., The Mathematics of Diffusion, 2nd ed., Oxford University Press, Oxford, United Kingdom, 1975, pp. 15.

[46] Nakao, Y., Nishimoto, K., Shinozaki, K. and Kang, C., Trans. Jpn. Weld. Soc., 1989, Vol. 20, pp. 60 – 65.

[47] Liu. S., et al., Weld. J. 1991, Vol. 70, pp. 207s – 215s.

[48] Nakao, Y., Nishimoto, K., Shinozaki, K. and Kang, C., Quart. J. Jpn. Weld. Soc., 1989, Vol. 7, No 2. p. 47.

[49] Ikawa, H., Nakao, Y. and Isai, T., Trans. Jpn. Weld. Soc., 1979, Vol. 10, pp. 24 – 29.

[50] Onzawa, T., Suzamura, A. and Kim, J. H., J. Jpn. Weld. Soc., 1990, Vol. 8, No 4, pp. 74 – 78.

[51] Holt, R. T. and Wallace, W., Inter. Metals Rev. 1976, No. 203, pp. 1 – 24.

[52] Jena, A. K. and Charturvedi, M. C., J. Mat. Sci., 1984, Vol. 19, pp. 3121-3139.

[53] Radavich, J.F. and Couts, W. H., ASM Trans. Quart., 1961, Vol. 54, pp. 591 – 597.

[54] Wallace, W., et al., Canad. Metall. Quart., 1974, Vol. 13, pp. 517- 527.

[55] Barbassat, M. H., et al., " High Temperature Alloys for Gas Turbine and other Applications", eds. Betz, W., et al., Reidel, D., Publ. Corp. Dordrecht, Holland, 1986, pp 897 – 905.

[56] Messmer, R. P. and Briant, C. L., Acta Metall., 1982, Vol. 30, pp. 457 – 467.

[57] Hondros, E. D. and Seah, M. P., Int. Met. Rev. No. 222, pp. 262 – 301.

[58] Lugscheider, E., et al., Schweissen Und Schneiden, 1984, Vol. 36 No. 3, pp. e102 – e104.

[59] Su, C. Y., Lih, W. C., Chou, C. P. and Tsai, C. H., J. Mater. Process. Tech. 2001, Vol. 115, pp. 326 – 332.

[60] Ohsasa, K., Shinmura, T. and Narita, T., J. Phase Equili., 1999, Vol. 20, No. 3, pp. 199 – 206.

[61] Liao, P. K. and Spear, K. E., Bull. Alloy Phase Diagrams, 1986,Vol. 7, No. 3.

[62] Markham, A. J., PhD Dissertation, University of Cambridge, 1988.

[63] Jahnke, B. and Demny, J., Inter. Conf. on Metallur. Coatings, San Diego, U.S.A., April 18 – 22, 1983, pp. 225 – 235.

[64] Ramirez, J. E. et al., Weld. J., 1992, Vol. 71, pp. 365s – 375s.